Provenance of the ballast stones from the Roman Republican ship Ilovik-Paržine 1: A hypothesis about its place of construction

François Fournier, Philippe Leonide, Lionel Marié, Frédéric Quillévéré, Jean-Pierre Margerel, Igor Miholjek, Pavle Dugonjić, Marie-Brigitte Carre, Laetitia Cavassa, Michele Morsilli, et al.

Provenance of the ballast stones from the Roman Republican ship Ilovik-Paržine 1: a hypothesis about its place of construction

François Fournier[1, *], Philippe Léonide[1], Lionel Marié[1], Frédéric Quillévéré[3], Jean-Pierre Margerel[1], Igor Miholjek[4], Pavle Dugonjić[4], Marie-Brigitte Carre[2], Laetitia Cavassa[2], Michele Morsilli[5], Giulia Boetto[2]

1 Aix Marseille University, CNRS, IRD, INRAE, CEREGE, Aix-en-Provence, France

2 CNRS, Aix Marseille University, Centre Camille Jullian, Aix-en-Provence, France

3 Univ Lyon, Université Claude Bernard Lyon 1, ENS de Lyon, CNRS, UMR CNRS 5276 LGL-TPE, F-69622, Villeurbanne, France

4 Croatian Conservation Institute, Zagreb, Croatia

5 University of Ferrara, UNIFE, Ferrara, Italy

*Corresponding author; email: fournier@cerege.fr

Abstract

A substantial quantity of ballast, primarily comprising blocks and pebbles of limestones and quartzose limestones, has been recovered in Paržine Bay (Ilovik Island, Croatia) in the stern section of a sailing vessel discovered in 2016, that wrecked between the second and the third quarter of the 2nd C. BC. This research introduces an integrated methodology for investigating the provenance of ballast stones. Both the skeletal assemblages and the siliciclastic content of the rocks suggest a common source for most of the ballast. Micropalaeontological analyses (benthic and planktic foraminifera) and Sr^{87}/Sr^{86} values indicate an age younger than 500 ka. Three main lithologies dominate the ballast rock assemblage: 1) tightly cemented quartzose grainstones and quartzarenites, 2) bioclastic quartzose grainstone with large mollusks and

rhodoliths and 3) weakly indurated and bioturbated quartzose grainstone. An extensive field survey and samples analysis conducted in the Quaternary mixed carbonate-siliciclastic successions along the Adriatic and Ionian coast of Italy, reveal a very high degree of similarity between the ballast stones and the Middle to Upper Pleistocene terrace deposits of the region of Brindisi (Apulia, Italy). These similarities encompass palaeontological assemblages, age, lithofacies and microfacies associations, mineralogical composition, quartz grain morphology, sedimentary and diagenetic features, stable carbon and oxygen isotope compositions, as well as the morphology and alteration features of pebbles. Given the uniformity of the ballast of the Romano-Republican Ilovik-Paržine 1 wreck, the study suggests, with a reasonable degree of certainty, that it was loaded in a single operation near *Brundisium*, one of the major ports of the Apulian coast (Italy). The results also suggest two additional hypotheses: 1) the ballast could have served as permanent ballast transported to balance the ship after it was launched; 2) the provenance of the ballast may provide insights into the location where the ship was constructed.

Key words: Adriatic Sea, ballast, *Brundisium***,** carbonate, provenance, Romano Republican ship

1. Introduction

1.1. The Ilovik-Paržine 1 Wreck

Ilovik is a small (5.8 km^2) island of the Kvarner Gulf in northern Dalmatia, Croatia. Located at the south of the island of Lošinj, it forms a small archipelago with the islet of St. Peter. In addition to the well-preserved remains of a Venetian post dating from the late Middle Ages, the islet of St. Peter is home to the remains of a large Roman maritime villa and those of a Benedictine and later Franciscan monastery, housed in a vast early Christian Basilica (Bully

and Čaušević-Bully 2012). On Ilovik, the church of St. Andrew is the only remain of a hypothetical fortress which would have been built in the Justinian period (Starac 2011). Two fragments of a 2nd century AD inscription mentioning a high-ranked city official of Aquileia, Gaius Cornelius, have been reused in a wall of the church. The inscription belongs to a tombstone, which was probably on the island of St Peter, as there is no evidence to date of a Roman settlement on Ilovik mostly due to lack of research (Serventi 2012; Kurilić and Serventi 2013/2014). The inscription directly links the islands of Ilovik and St. Peter to Aquileia (Kurilić and Serventi 2013/2014: 239), and points the importance of these islands on the trade and maritime routes along the eastern Adriatic coastline (Orlić, 1986; Jurišić 2000: 53; Kozličić 2012).

The island of Ilovik is mainly composed of highly karstified Cretaceous and Paleogene limestones (Fuček *et al*., 2018). In the Paržine Bay, which is situated on the south-eastern coast of the island and where the Ilovik-Paržine 1 wreck was discovered in 2016 (**Fig. 1A**), Cenomanian calcisphere-rich limestones (Belej Formation) and Cenomanian to Coniacian rudist floatstones (Liski Formation) crop out along the eastern and western sides of the bay, respectively, while the northern shore exhibits Eocene foraminiferal limestones (Fuček *et al*., 2018) (**Fig. 1C**).

The Ilovik-Paržine 1 wreck has been systematically excavated from 2018 to 2022 as part of a collaboration between the Department of Underwater Archaeology of the Croatian Conservation Institute and the Centre Camille Jullian UMR 7299 (Boetto *et al*., forthcoming). The research was co-directed by I. Miholjek and G. Boetto. Oriented NE-SW, the shipwreck lies on a sandy seabed about 30 meters from the beach, at a maximum depth of 4 m below the sea level (**Fig. 1B**). The shipwreck site comprises two main deposits which are separated by a distance of approximately 20 meters (**Fig 1D**). The north-eastern deposit was excavated in 2018 and 2019. The trench of an area of 58 m^2 revealed the fore part of the bow structure preserved

for 9.76 meters in length, and composed of the axial carpentry with part of the strakes attached by mortise-and-tenons joints. To the north, a significant amount of intertwined wood, detached pieces of the ship's structure, a few fragmented amphoras and several other artefacts were discovered. The south-western deposit, excavated from 2020 to 2022, covered an area of around 70 m^2 (**Fig. 2**). As the ship rested on the port side, this side was covered by the ballast stones that preserved the ship's structure for a length of 12.75 m and a maximum width of 4 m.

As evidenced by the shipwreck site, a considerable portion of the ship's structure has deteriorated over time, particularly in the last decades by natural and anthropogenic factors. The shallow nature of the site, coupled with coastal erosion and the cyclical movement of sandbanks that cover and uncover the hull structure, has contributed to this deterioration. Additionally, a large number of pleasure boats anchor in the bay during the summer months. Furthermore, given the shallow depth and proximity to the coast, the cargo has probably been salvaged in ancient times or looted later (**Fig. 1D**).

The ship, of an evaluated length of 21.5 meters and a beam of 6.5 meters, was transporting a cargo of logs and wine contained in amphoras. Most of them were found fragmented and scattered in the north-eastern deposit. The analysis of their diagnostic parts showed that they belonged to the Adriatic Greco-Italic type (**Fig. 3**) (Carre, 2022), wine amphora which was produced, at least, between the 3rd century BC and the end of the 2nd century BC when the form evolved into the Lamboglia 2 (Panella, 2010). A precise date for the Ilovik-Paržine 1 amphoras is difficult to determine based on comparisons, as complete specimens are rarely found in well-dated contexts, but examination of their morphology, combined with radiocarbon dating of the hull (Beta-454977 Ilovik 1), places the sinking of the ship between 170 and 130/120 BC.

The macroscopic and microscopic analysis of the clay of the amphoras done by Claudio Capelli (Dipartimento di Scienze della terra, dell'ambiente e della vita-DISTAV, University of Genova)

corresponds to typical productions of the ancient *Picenum*, a region that matches the modern Marche and northern part of the Abruzzo regions of Italy (Carre *et al*., 2014).

The ship was also carrying a cargo of logs and boughs in the bow area. The trunks and boughs were mostly cut from evergreen oaks (*Quercus ilex* sp.), stone pines (*Pinus pinea* L.) and small trees and shrubs belonging to the genera *Phillyrea* or *Rhamnus*. A number of twigs were also found, mostly belonging to the same species as the larger timbers, likely resulting from the delimbing process. Wood analyses also attested to the presence of twigs from grape (*Vitis vinifera*) that probably served as dunnage protecting the cargo in the hold (Tchernia *et al.*, 1978: 20-21). At the time of writing, the results of analyses of the wood used in ship construction were not available.

A few fragments of black glazed and cooking ware, a small lamp with traces of soot, part of a *catillus* of a grinding stone, a marlin spike and part of a bow drill testify to life and others activities on board. A small female bronze statuette representing the tutelary goddess worshipped by the sailors has also been recovered. Finally, a flat-bottomed amphora or jug, currently without comparison and probably part of on-board equipment, may have originated in the southern Adriatic (study of ceramic of L. Cavassa, clay analysis C. Capelli).

As we have already said, the stern area was covered on a surface of approximately 8 m^2, by a layer of blocks and pebbles of various sizes corresponding to the ballast (**Fig. 2**). As the ship rested on its port side, the ballast moved on this side covering the ceiling at the level of the turn of the bilge (**Fig. 2E**). Here the ballast formed a very compact layer that helped in preserving the ship structures. Part of the stones were also found southward between the frames (**Fig. 2C and D**), in the bilge above the keel (**Fig. 2B**) and on the sandy bottom along the keel, on the southwest. The starboard side of the ship was completely destroyed after the sinking, causing the ballast to spread, forming piles along the starboard side of the keel (**Fig. 2A**).

1.2. Ballast

Ballast refers to any type of dead weight that is placed or stowed in the lower part of the ship's hold to provide stability during navigation. A ship is said to be "in ballast" when it has no cargo on board, but instead carries heavy materials such as stones, sand, rubbish or metals as ballast (Pâris and Bonnefoux, 1999: 408-409; Kemp, 1976; Lamb *et al.*, 1990; Casson, 1995: 176-177, note 43 and 330, note 8). Ballast is most often overlooked in nautical archaeology studies, yet assessing its provenance is crucial as it can provide insights not only into a sailing route but also into a possible home port for the ship (Keith and Simmons, 1985: 416-417, note 6; McGrail, 2001: 10). Ballast can also be classified into two groups: commercial or 'saleable' ballast, and non-commercial or 'unsaleable' ballast (McGrail 1989: 357). The ballast from Ilovik-Paržine 1 belongs to this second category, as do a number of other ancient wrecks from the Mediterranean, whose stones have been analysed, such as the Ma'agan Mikhael, Israel (about 400 BC), Marsala, Sicily (mid-3rd century BC, Mascle, 1981), Chrétienne H, Southern France (beginning of the 1st century AD, Santamaria, 1984: 48) and Yassi Ada I, Turkey (*c.* AD 625, Gifford, 1982). Unsurprisingly, the study of these stones has raised similar questions as those encountered in the study of ballast found on modern shipwrecks. Namely whether these stones were loaded at the ship's construction site or port of origin, or whether they provide information about the ports of call on the route followed by the ship.

It must be said that determining the provenance of a ballast stone is challenging given the mobility of ships and the different interpretations of the ballast itself (Keith and Simmons, 1985: 416-417, note 6; McGrail, 1989; Nantet, 2016: 201-202; Borrelli and Harris, 2016; Bar *et al*., 2019; Nantet and Martins, 2023): 1) permanent ballast used to balance the ship, providing insight into the place of building of the ship, or 2) temporary ballast loaded in the hold to compensate for the lack of cargo during the ship's return voyage, giving us information about one of the ports of call. The homogeneity or heterogeneity of the ballast composition are other

factors that complicate the reconstruction of the navigation route of the ship's last voyage before sinking, which must be based on other proxies such as the origin of the cargo and personal effects of the crew and passengers, or data resulting from the analysis of the ship's structure and the interpretation of its function.

Another challenge is connected to the extreme complexity of the geological history and resulting diversity of rocks cropping out in the Mediterranean region. Carbonate sedimentary rocks have proven to be relevant for provenance studies of archaeological materials (e.g. sculptural or building stones): their detailed analysis provides a set of elements (age, depositional environment, mineralogy, diagenetic evolution…) which, coupled with an in-depth review of the available regional geological knowledge, make it possible to assess with sometimes great precision the extraction localities of the stones (e.g. Flugel and Flugel, 1997; Antonelli *et al*., 2020; Fournier *et al*., 2023).

The aims of the present study are therefore to: 1) establish and test a methodology of ballast stone provenancing, based on a detailed, micropaleontologic, petrographic, sedimentologic, diagenetic and geochemical characterization of the ballast stones, together with the integration of the available geological knowledge of the Adriatic and neighboring coasts and of new geological data collected in the field; 2) assess the provenance of the Ilovik-Paržine 1 ballast based on such an integrated approach; and 3) discuss the implications of such provenance for the reconstruction of the last voyage of the ship and, possibly, the place where the ship was built.

2. Material and methods

The provenance assessment of ballast stones from the Ilovik-Paržine 1 wreck was based on the following workflow:

1. The first step involved a detailed petrographic, micropalaeontologic and isotopic (carbon, oxygen and strontium) characterization of the ballast stones and local carbonate rocks and sediments sampled in the Paržine Bay. A total of 854 ballast stones (diameter: 1 to 40 cm) were retrieved from the shipwreck during the 2021 survey. The stones were collected separately depending on their position from the different sectors of the site (**Fig. 2**): 236 stones in area A, 159 in area B, 135 in area C, 144 in area D and 180 in area E. A preliminary macroscopic characterization of their lithofacies and petrographic features was performed on-site during fieldwork. Thin-sections were then prepared from 20 ballast rocks representative of the different identified lithofacies. Additionally, four thin-sections were prepared from local limestones that crop out along the coast and two from local sand sampled within the Paržine Bay in the vicinity of the shipwreck. Thin-sections were observed under polarized-light microscopy for microfacies characterization of the limestones, including texture, grain composition, skeletal assemblages and diagenetic features. The thin-sections were additionally point-counted with the J-microvision® software, on the basis of 300 points, to quantify the composition of the sand-grained fraction of the ballast rocks. Thin-sections were also used to identify their benthic foraminiferal content. One poorly consolidated bulk sample (WC3) was additionally dried then soaked in a dilute solution of hydrogen peroxide for about 24 h and finally washed over a column of sieves (1, 0.5, 0.25, and 0.125 mm). The residues were oven-dried and the planktic foraminifera and some selected taxa of benthic foraminifera were picked and taxonomically identified. Benthic and planktonic foraminifer identification as well as strontium isotope measurements of their shells were used for constraining the age of the rocks forming the ballast. Stable carbon ($\delta^{13}C$) and oxygen ($\delta^{18}O$) isotope compositions of bulk carbonate powders were finally measured from 43 ballast stones (including the 20

thin-sectioned samples), as well as from local modern carbonate sand and Cretaceous limestones.

2. A comparison between facies, diagenetic features, stable isotope compositions and age of the ballast stones and local materials was then performed. In the case of a significant match, a local origin is privileged; otherwise, a more distant origin had to be considered. In the latter case, a detailed bibliographic investigation of geological studies published on the formations outcropping along the coasts of the Adriatic and Ionian Seas was carried out to identify potential sources of the ballast, based on an analogy in age and lithofacies. This study, coupled with the examination of published geological maps, made it possible to identify sampling sites for such potential analogous outcrops.
3. The implementation of steps 1 and 2 allowed us to identify and study 30 coastal outcrops located along the Italian coast of the Adriatic and Ionian Seas, with 28 of them located in Apulia (see location in **Fig. 4**). The macroscopic lithological, sedimentological and diagenetic characters were analysed in these outcrops and 82 rock samples were further collected in the field. For each of the 82 samples collected, powder was made and analysed for its stable carbon and oxygen isotope composition. In addition, 40 thin-sections were prepared, representing an adequate quantity to cover the entirety of the facies diversity of the collected rocks. Thin-sections from outcrops analogues were observed under polarized-light microscopy and point-counted for microfacies characterization of texture, grain composition, biotic assemblages and diagenetic features.
4. The degree of correspondence between ballast stones and outcrops was assessed, based on the comparison of macroscopic features (lithology, sedimentary structures, deformation features), quantified grain composition, foraminiferal assemblages, diagenetic features and $\delta^{13}C$ and $\delta^{18}O$ values, thus allowing us to identify a possible provenance site for the ballast of the Ilovik-Paržine 1 wreck.

Bulk stable carbon and oxygen stable isotope ratio measurements of carbonate powders were performed at the GeoZentrum Nordbayern department, Friedrich-Alexander-Universität Erlangen-Nürnberg (Germany) through reaction with phosphoric acid at 70°C using a Gasbench II connected to a Thermo Fisher Scientific DELTA V Plus mass spectrometer. All measured isotopic values are normalized against the international reference NBS-19 and are expressed in ‰ relative to V-PDB for $^{18}O/^{16}O$ and $^{13}C/^{12}C$. Mean external repeatabilities for $\delta^{13}C$ and $\delta^{18}O$ were better than 0.05‰ and 0.07‰ respectively.

Strontium isotope measurements on powdered planktonic and benthic foraminifera were performed by Isobar Science at the University of Miami Neptune Isotope Laboratory. Strontium was isolated from around 10 mg of powdered foraminifera (planktonics and *Elphidium spp.*) by extraction chromatography and analysed by MC-ICP-MS (Thermo Fisher Neptune Plus^{TM}) following the methods described by Pourmand *et al*. (2014) and Pourmand and Dauphas (2010). Strontium isotope ratio data are reported as $^{87}Sr/^{86}Sr$ ratios. The analytical accuracy and precision were assessed by multiple measurements of certified reference material (SRM 987) during the analysis. Uncertainties for each sample measurement is presented as the 95% confidence interval. Sr-derived ages were determined by using McArthur *et al*. (2001) look-up tables.

3. Petrographic, micropaleontologic and geochemical analyses of the ballast stones

3.1 Definition of lithofacies

The macroscopic analysis of 854 samples of ballast rocks led to the identification of six main classes of lithofacies.

3.1.1 Lithofacies LF1: tightly cemented quartzose grainstones and quartzarenites

Ballast stones of lithofacies LF1 consist of irregularly shaped pebbles to cobbles (1 to 20 cm in diameter) with well-rounded edges, made of tightly cemented, well-sorted, very fine to fine-grained (63 to 250 µm) quartzose grainstone or quartzarenite (**Fig. 5A, C, E** & **Fig. 6D**). Quartz grains are angular to sub-angular. The bioclastic fraction is dominated by benthic foraminifera, coralline algae, molluscs and serpulids. All LF1 ballast stones exhibit a dark, blackish patina which may affect the whole rock, but for various samples, the core of the pebbles has preserved a beige-orange color (**Fig. 5A**). Soft-deformation structures are commonly recognized in the largest ballast stones (**Fig. 5A**), as well as bioturbations (**Fig. 5E**), elongated, oriented structures related to calcite cementation (**Fig. 6C**), in some cases coalescent (**Fig. 5C**).

3.1.2 Lithofacies LF2: bioclastic quartzose grainstone with large molluscs and rhodoliths

Lithofacies LF2 consists of a tightly cemented fine to medium-grained (125 to 500 µm) quartzose grainstones encasing poorly sorted bioclasts mainly made of rhodoliths and mollusc shells. Ballast stones with LF2 lithofacies are darkened and may display angular or well-rounded shapes. Among the molluscan fragments, the bivalve *Aequipecten opercularis* has been recognized (**Fig. 6A**). Quartz grains are angular to sub-angular, as in LF1.

3.1.3 Lithofacies LF3: weakly indurated and bioturbated quartzose grainstone

Ballast stones of lithofacies LF3 consist of pebbles to boulders (1 to 40 cm in diameter) with irregular and angular edges, made of weakly cemented, well-sorted, very fine to fine-grained (63 to 250 µm) quartzose grainstone or quartzarenite (**Fig. 6C**). Quartz grains are angular to sub-angular. As for LF1, the bioclastic fraction is dominated by benthic foraminifera, coralline algae, molluscs and serpulids. Even though dominantly massive and structureless, bioturbations have been observed in a few samples.

3.1.4 Lithofacies LF4: quartzose wackestone

A reduced number (13) of small-sized (<5 cm) dark pebbles made of compact quartzose wackestone with scattered benthic foraminifers has been recovered from the ballast. No macrofossils or sedimentary structures were found in samples collected from lithofacies LF4.

3.1.5 Lithofacies LF5: conglomerates with quartzose grainstone matrix

Two ballast stones (5 and 20 cm in diameter) are made of conglomerates with tight, rounded quartzose grainstone pebbles (0.5 to 2 cm in diameter) of lithofacies LF1 encased within a poorly consolidated carbonate sand matrix (**Fig. 7 C**).

3.1.6 Lithofacies LF6: tight, fractured limestones

The lithofacies LF6 includes all the compact, fractured, white limestones, with an orange-to grayish patina (**Fig. 7 D**). LF6 ballast stones (from 5 to 20 cm in diameter) are very scarce (8 samples have been recovered) and were found scattered above the ballast. Two main depositional textures have been recognized: floatstone with rudist fragments (radiolitids) in a grainstone matrix (**LFA**) and bioclastic wackestone-packstone (**LF6B**).

3.2 Composition and spatial distribution of the ballast

The counting conducted on the 854 recovered stones (**Fig. 8**) indicates that the lithofacies LF1 is largely dominant (80% on average). Lithofacies LF2 and LF3 represent 5% and 11% of the sampled material, respectively. As a consequence, quartzose grainstones and quartzarenites (LF1, LF2 and LF3) represent 96% of the recovered ballast stones. The other lithofacies (LF4, LF5 and LF6) constitute very minor components (~1%). The counting results do not show any significant variation in the facies composition of the ballast within the wreck. However, the material dumped outside the wreckage (**Fig. 8A**) shows a slight enrichment in LF3 elements (19%). The quartzose wackestones LF4, although very rare, have only been recovered between frames in the northern area of the wreck.

3.3 Microfacies

3.3.1 Microfacies of quartzose grainstones and quartzarenites (LF1, LF2, LF3)

Four distinct microfacies (MF1, MF2, MF3 and MF4) have been identified on thin sections from quartzose grainstone and quartzarenite lithofacies LF1, LF2 and LF3. The correspondence between microfacies and lithofacies is given in **Table 1**. The quantitative composition of sand-sized grains is displayed in **Supplementary Material S1**.

3.3.2 Microfacies MF1: bioclastic quartzarenite

Microfacies MF1 has been evidenced only in lithofacies LF1. It consists of very fine to fine-grained (63 to 250 µm) quartzarenites with angular quartz grains and a significant amount (>40%) of carbonate bioclasts (**Fig. 9A, 9B**). The carbonate fraction is dominated by small (<2 mm) fragments of coralline algae (16%), benthic foraminifers (9%) and peloids (**Fig. 10**). The benthic foraminiferal association is dominated by *Elphidium macellum* and other small rotaliids. The intergranular pore space is entirely occluded by equant sparry to microsparry calcite cements. Some moldic pores are also present.

3.3.3 Microfacies MF2: bioclastic quartzose grainstone

MF2 is the dominant microfacies of lithofacies LF1 and also occurs in LF3. It consists of fine to medium-grained (125 to 500 µm) quartzose grainstones with angular to sub-angular quartz grains (12 to 42%) and bioclasts including coralline algae (26 to 39%), benthic foraminifers (14 to 25%), peloids (8 to 19%), mollusc fragments (2 to 11%), echinoids (2 to 8%), bryozoan (<2%) and occasional planktonic foraminifers and serpulids (**Fig. 9C, Fig. 10**). The benthic foraminiferal association is dominated by *Elphidium macellum*, *E. paraskevaidisi*, *Neoconorbina terquemi* and *Quinqueloculina sp.* In lithofacies LF1, the intergranular pore space is almost entirely occluded by equant sparry to microsparry calcite cements.

3.3.4 Microfacies MF3: rhodalgal-molluscan floatstone with quartz-rich bioclastic packstone-grainstone matrix

Microfacies MF3 characterizes the lithofacies LF3. It consists of large (cm-scale) mollusc and encrusting coralline algal fragments with rhodoliths encased within a quartz-rich (7 to 38%) bioclastic packstone to grainstone (**Fig. 9E, Fig. 10**). Quartz grains are very fine to fine-grained (63 to 250 µm) and angular to sub-angular in shape. The carbonate fraction is composed of rhodoliths and coralline algal fragments (33 to 48%), mollusc shells (3 to 21%), benthic foraminifera (10 to 20%), peloids (3 to 7%) echinoids (3 to 7%), bryozoan (<2%) and occasional planktonic foraminifers and serpulids. The foraminiferal assemblage is similar to that of MF2 and is dominated by *Elphidium macellum*, *Neoconorbina terquemi* and *Quinqueloculina* sp. The intergranular pore space is entirely occluded by equant sparry to microsparry calcite cements and moldic pores are common.

3.3.5 Microfacies MF4: bioclastic grainstone

MF4 is the dominant microfacies of lithofacies LF3 and also occurs in LF1. It consists of a well-sorted medium to coarse-grained (250 µm to 1 mm) bioclastic grainstone, dominated by coralline algae (>30%), benthic foraminifers (up to 30%) and mollusc fragments (up to 15%) together with echinoids, bryozoan, peloids as well as occasional planktic foraminifers and serpulids (**Fig. 9G, Fig. 10**). Quartz grains are scarce (<10%), fine-grained and angular to sub-angular. The benthic foraminiferal association is dominated by *Elphidium macellum*, together with textulariids and miliolids. In lithofacies LF3, the primary intergranular porosity is largely preserved and a fine-grained equant sparry calcite cement occludes the intergranular pore spaces only along selected laminae or around grain contacts as meniscus cements (**Fig. 9G)**.

3.3.6 Microfacies of wackestones LF4

Under polarized-light microscopy, quartzose wackestones LF4 exhibit a bioclastic wackestone texture whose matrix is composed of a mixture of carbonate mud and quartz silt (4 to 63 µm) (microfacies MF5: **Fig. 7A**). Carbonate grains mainly consist of benthic foraminifera, mollusc

fragments and peloids. The benthic foraminiferal assemblage is dominated by *Elphidium macellum*, *E. paraskevaidisi*, nonionids and other small hyaline foraminifers.

3.3.7 Microfacies of conglomerates LF5

Conglomerates LF5 are composed of rounded to sub-rounded pebbles of tightly cemented bioclastic quartzose grainstone, analogous to microfacies MF2, embedded within a poorly cemented bioclastic medium-grained (250 to 500 µm) grainstone with scarce quartz grains (**Fig. 7 B**). Carbonate grains in pebbles mainly consist of coralline algae, benthic foraminifera, molluscan fragments and peloids and the benthic foraminiferal assemblage is similar to that found in microfacies MF2 and MF3 with a dominance of *Elphidium* spp. The carbonate sand matrix is predominantly composed of rounded fragments of foraminifers (miliolids), coralline algae, echinoids and limestone lithoclasts.

3.3.8 Microfacies of tight, fractured limestones LF6

Among the tight and fractured limestone samples, only the lithofacies **LF6B** (wackestone-packstone) has been thin-sectioned and observed under polarized-light microscopy. It consists of a fractured wackestone-packstone with calcispheres (MF6 microfacies) and exhibits a neomorphosed matrix that is partly converted into microsparite (**Fig. 7 E**). Fractures are filled with equant sparry calcite cements.

3.4 Foraminiferal biostratigraphy

3.4.1 Benthic foraminifera

The list of identified benthic foraminifers in the analysed samples is given in **Supplementary Materials S2**. The thin sections analysed in quartzarenites and quartzose grainstones (LF1, LF2, LF3), quartzose wackestones (LF4) and conglomerates with quartzose grainstone matrix

(LF5) all exhibit the benthic foraminifer *Elphidium* (represented by *E. macellum* and *E. paraskevaidisi*) as the dominant taxon. *Neoconorbina terquemi* and *Quinqueloculina* sp. also constitute common taxa from the dominant lithofacies LF1 and LF2. *Elphidium macellum* commonly occurs in many temperate and sub-tropical shallow subtidal environments (Hayward *et al*., 1997). It is commonly found in modern as well as Miocene (e.g. Bossio *et al*., 1994) to Holocene sediments (e.g. Carboni *et al*., 2000) of the Mediterranean region. *Elphidium paraskevaidisi* is a scarce fossil species reported from Pliocene sediments (Christodoulou, 1960; Margerel, 1997). *Neoconorbina terquemi* is a rosalinid species that has been reported from various shallow to deep marine environments (Walker *et al*., 2011), from the Oligocene (Fenero *et al*., 2012) to the present (e.g. Jorissen, 1988). The benthic foraminiferal assemblage evidenced in lithofacies LF1 to LF5 therefore suggests a Miocene to Holocene age for these mixed carbonate-siliciclastic deposits.

3.4.2 Planktonic foraminifera

One poorly consolidated and washed bulk sample (WC3) of lithofacies LF3 yielded eleven morpho-species of planktic foraminifera: *Globigerinoides ruber*, *Globigerinoides elongatus*, *Globigerinoides conglobatus*, *Trilobatus quadrilobatus*, *Trilobatus sacculifer*, *Trilobatus trilobus*, *Orbulina universa*, *Globigerina bulloides*, *Globigerinella siphonifera*, *Globigerinatella uvula*, *Neogloboquadrina sp*. (dextral). This assemblage is consistent with a Late Miocene to Holocene age (Boudagher-Fadel, 2015). However, considering the absence of certain oligotrophic surface water taxa usually occurring in Mio-Pliocene shallow-water sediments of the Mediterranean (such as *Globigerinoides extremus*, *Globigerinoides obliquus*, *Globoturborotalita apertura* and/or *Globoturborotalita decoraperta*), the sample likely deposited during the Pleistocene or Holocene, after 1.28 Ma (last appearance datum of *G. obliquus;* Lirer *et al.*, 2019).

3.5 Strontium isotope stratigraphy

The adjusted $^{87}Sr/^{86}Sr$ ratio of planktonic foraminifers and *Elphidium* from WC3 sample are 0.709169±0.000009 and 0.709169±0.000007, respectively. According to McArthur *et al.* (2001) look-up tables, considering the analytical error bars, these measurements suggest an age younger than 550 ka (Middle Pleistocene to Holocene).

3.6 Stable carbon and oxygen isotopes

The stable carbon and oxygen isotope values of ballast stones, local sands and outcropping limestones from the Paržine Bay are displayed in **Figure 11A** and **Supplementary materials S3.**

In the dominant lithofacies LF1, $\delta^{13}C$ values range from -1.77 to –6.88 ‰ V-PDB and $\delta^{18}O$ values from -3.52 to -5.31 ‰ V-PDB. Such values significantly differ from those measured in modern carbonate sands of the Paržine Bay ($\delta^{13}C$=1.41‰ and $\delta^{18}O$=0.62‰). Such a combined depletion in both ^{13}C and ^{18}O in lithofacies LF1 likely results from a diagenetic overprint that should have occurred within the meteoric diagenetic environment (Allan and Matthews, 1982; Swart and Oehlert, 2018), which is consistent with the occurrence of equant sparry to microsparry calcite cements (**Fig. 9A, C**) occluding the intergranular pore spaces. In bioclastic quartzose grainstones LF2, $\delta^{13}C$ and $\delta^{18}O$ range from -2.07 to -7.58 ‰ V-PDB and from -3.02 to -5.15 ‰ V-PDB, respectively. As for LF1, such values indicate a meteoric overprint that is also consistent with our petrographic observations (equant sparry to microsparry calcite cement: **Fig. 9E**). In addition, the isotope values measured in calcite cements infilling an intraskeletal pore (KI-6-SP sample: $\delta^{13}C$=-3.36‰ and $\delta^{18}O$=-4.83 ‰ V-PDB) are within the range of those measured in

bulk rocks (**Fig. 11A**). Isotope signatures in poorly consolidated quartzose grainstones (LF3 lithofacies) are similar to those of LF1 and LF2 ($\delta^{13}C$ between -0.95‰ and -8.93 ‰ $_{V\text{-}PDB}$ and $\delta^{18}O$ between -3.94 and -5.07 ‰ $_{V\text{-}PDB}$) although most of the analysed samples display relatively low ^{13}C depletion, which probably results from the low amount of calcite cements. However, one sample (AC-8) exhibits a very negative $\delta^{13}C$ value. This value may result from a meteoric vadose diagenetic overprint as suggested by the occurrence of anisopacheous, meniscus cements (**Fig. 9G**). Carbon and oxygen isotope values in quartzose wackestone LF4 ($\delta^{13}C$ between -6.78‰ and -7.55 ‰ $_{V\text{-}PDB}$; $\delta^{18}O$ between-3.95 and -4.01 ‰ $_{V\text{-}PDB}$) fall within ranges of those of lithofacies LF1, LF2 and LF3.

The quartzose grainstone pebbles from LF5 conglomerates, in addition to being made up of the same microfacies as LF1, yield a similar isotopic signature (**Fig. 11A**). On the other hand, the sandy carbonate matrix exhibits an isotopic signature that is close to that of the local carbonate sand (**Fig. 11A**).

Finally, the positive $\delta^{13}C$ value (+0.37 ‰ $_{V\text{-}PDB}$) measured in a local Cretaceous limestone sampled in coastal outcrops in the Paržine Bay is clearly different to that of the ballast stones of lithofacies LF1 to LF5.

4. Provenance of ballast stones from the Ilovik-Paržine 1 wreck

4.1 Provenance assumptions

The multiple similarities observed among lithofacies LF1, LF2, LF3 and LF4, including bioclastic composition, benthic foraminiferal assemblages, morphology and size of quartz grains and stable carbon and oxygen isotope compositions, strongly suggest that these lithofacies formed in a similar depositional, paleogeographic, paleoclimatic and diagenetic setting. The high degree of similarity indicates that these rocks likely originated from the same

geographic area and geological formation. Furthermore, the roundness of most pebbles and cobbles from lithofacies LF1, LF2 and LF4 provides additional evidence that the ballast stones were collected from a shoreline subjected to significant wave action (Wentworth, 1922).

The conglomerate LF5, whose clasts belong to LF1 could have formed within the wreck itself, in the Paržine Bay. Indeed, grain composition of LF5 matrix (scarcity of quartz grains, dominance of coralline algae, echinoids and miliolids: **Fig. 7B, 7F** and **7G**) and stable isotopic composition closely matches that of the local sand (**Fig. 11**). Furthermore, the occurrence of rudist fragments and calcispheres within the scattered whitish limestone cobbles of lithofacies LF6 is consistent with a local provenance. This alignment is supported by the presence of Cenomanian calcisphere-rich limestones (Belej Formation) and Cenomanian to Coniacian rudist floatstones (Liski Formation) along the eastern and western coastline of the Paržine Bay, respectively (Fuček *et al*., 2018). Therefore, the composition of lithofacies LF6 provides further evidence supporting a local origin for these materials, suggesting they were sourced from nearby geological formations within the bay.

The blackening observed in all of the stones belonging to lithofacies LF1 to LF4 (**Fig. 5A**) is likely due to the impregnation of sediment by dissolved, colloidal, or finely particulate organic substances. This phenomenon occurs in anoxic and alkaline environment or microenvironment, which are commonly found invarious modern and ancient coastal settings (Strasser, 1984). The lack of blackening in local limestones LF6 is consistent with an early diagenetic transformation that likely occurred in the source site of the ballast stones, rather than in the Paržine Bay. This difference in blackening provides further evidence suggesting that the origin of the ballast stones is external to the bay and points to specific environmental conditions in their source area. Benthic and planktonic foraminiferal assemblages suggest a Quaternary age for the ballast stones while strontium isotope measurements help narrow down the chronostratigraphic interval, indicating a time frame between the Middle Pleistocene and the Holocene. Given the

absence of marine, consolidated Quaternary deposits along the coast of the Ilovik Island and the geological composition of the northern Adriatic coast, which primarily comprises Cretaceous carbonates overlain by Paleogene carbonates and siliciclastic sediments (e.g. Pamić *et al*., 1998; Vlahović *et al*., 2005), it is improbable that the main ballast components (LF1 to LF4 lithologies) originate from this region. Although there are some occurrences of Quaternary marine deposits in the vicinity, such as Upper Pleistocene shallow marine sediments reported onshore the Krk Island (Marjanac *et al*., 1993; Marjanac and Marjanac, 2000), their elevation at 30 m to 60 m above sea level (asl) make unlikely their use as ballast stones. In addition, some eolian deposits with reworked marine bioclasts have been reported from the island of Mjlet (Babić *et al*., 2012b). In the Central Adriatic, Pleistocene marine sediments were reported from the island of Brusnik at 9 m asl (Babić *et al*., 2012a), and palaeobeach deposits have been documented onshore Velika Palagruža Island (Korbar, 2009). However, the occurrence of a micritic matrix in lithofacies LF2 and LF4 excludes the hypothesis of a strictly aeolian or beach formation for the ballast stones. As a consequence, it appears very unlikely that the ballast stones of the Ilovik-Paržine 1 wreck originate from the Croatian coast of the Adriatic Sea.

In contrast, the Plio-Quaternary marine, mixed carbonate-siliciclastic deposits that extensively outcrop along the Italian coasts of the South Adriatic and Ionian Sea, particularly in Apulia and Calabria (Compagnoni *et al*., 2011) represent potential sources for the ballast stones of the Ilovik-Paržine 1 wreck.

Field investigations in South Apulia and Calabria have provided a comprehensive sedimentologic, petrographic and stable isotope database of these deposits which were compared with the characteristics of the ballast stones. In Apulia, the Plio-Quaternary marine succession begins with the carbonate-dominated "Calcarenite di Gravina" Formation (Upper Pliocene–Lower Pleistocene) onlapping three isolated structural domains (Gargano, Murge, and Salento) of the Apulian foreland (**Fig. 4**), composed of Cretaceous to Paleogene carbonates

(Azzaroli, 1968; Iannone and Pieri, 1979; Pomar and Tropeano, 2000). Although the bioclastic composition of Gravina calcarenites in Apulia resembles that of the ballast stones (**Fig. 12B**), it cannot be regarded as a potential source for the Ilovik-Paržine 1 ballast based on: 1) the absence of quartz grains in the samples from the investigated outcrops (**Fig. 12A-B** and **Supplementary Material S4**) confirming previous studies (Pomar and Tropeano, 2000; Tropeano and Sabato, 2002), 2) the oxygen isotopic composition of the Gravina calcarenites which is significantly ^{18}O-enriched compared to the analysed ballast stone carbonates (**Fig. 11B**), 3) its significantly older age (Late Pliocene–Early Pleistocene).

In the Salento Peninsula (Apulia), the carbonate-dominated Calcarenite di Gravina Formation is overlain by Lower Pleistocene clays (Subappeninic clays) and Middle to Upper Pleistocene mixed carbonate-siliciclastic marine units, including marine terrace deposits, cropping out both along the Adriatic coast (Ciaranfi *et al*., 1988; Margiotta *et al*., 2010; Mastronuzzi *et al*., 2011) and the Ionian coast in the Gulf of Taranto (Hearty and Dai Pra, 1992). The terrace deposits are locally capped by Holocene eolian deposits and paleosols (Mastronuzzi *et al*., 2011). Finally, Upper Pleistocene mixed carbonate-siliciclastic coastal outcrops including bioclastic quartzose grainstones and algal bioconstructions have been also reported from the Crotone Peninsula along the Ionian coast of Calabria (Zecchin *et al*., 2004; 2009; Bracchi *et al*., 2014, 2016; Caruso and Monaco, 2015).

Because of their age and mixed carbonate-siliciclastic nature, the Middle to Upper Pleistocene terrace deposits of Apulia and Calabria appear to be good candidates for the source of the Ilovik-Paržine 1 ballast stones.

4.2 Sedimentologic, petrographic and geochemical characterization of Middle to Upper Pleistocene terrace deposits of Apulia and Calabria

4.2.1 Brindisi Basin

Seven sections were logged and sampled along the coast of the Brindisi Basin (**Fig. 13**). North of the city of Brindisi (Posticeddu, Torre Resta, Torre Testa and Case Bianche sections), coastal cliffs exhibit the following typical succession, from base to top: 1) blue sandy clays (Sub-Apenninic clays) forming the base of the cliff (Posticeddu section: **Fig. 13**), 2) loose sand and/silty interbedded with centimeter to decimeter-thick lenses of tightly-cemented quartzarenite or quartzose grainstone (lithofacies LF1: **Fig. 14B-C-D**) and decimeter to meter-thick beds of rhodolitic and molluscan floatstones (lithofacies LF2), 3) massive, bioturbated, generally weakly cemented quartzose grainstones to grainstones (lithofacies LF3) and 4) Holocene reddish colluvium forming the top of the cliff.

The tightly-cemented quartzarenites and quartzose grainstones (LF1) form oriented, elongated structures (**Fig. 6E**, **14B-C**). Such oriented calcite concretions are interpreted as having grown from meteoric groundwater, with elongation axes parallel to the flow direction, reflecting the hydraulic gradient and conductivity anisotropy of the aquifer (Mc Bride *et al*., 1994; Pomar *et al*., 2004). Similar diagenetic features have been reported in Pleistocene terrace deposits of Basilicata, southern Italy (Mc Bride *et al*., 1994). These oriented calcite concretions are often coalescent (**Fig. 5D, 14D**). Bioturbations (**Fig. 5F**) and soft sediment deformation structures (**Fig. 5B**) are also common within lithofacies LF1. In Torre Testa, a 50 cm-thick cross-bedded lens of cemented quartzose grainstones occurs near the base of the section (**Fig. 14B**). Consequently, lithofacies LF1 has been subdivided into two sub-lithofacies. Tight quartzarenites and quartzose grainstones with isolated or coalescent oriented concretions, and bioturbations are assigned to sublithofacies LF1A while those with preserved cross-lamination are assigned to LF1B. In the Posticeddu section, a bioclastic floatstone (LF2) exhibit abundant and well-preserved shells of the bivalve *Aequipecten* (**Fig. 6B**). At the base of all the studied sections from the northern part of the Brindisi Basin, the beach is predominantly covered by rounded pebbles and cobbles of tightly-cemented quatzarenites and quatzose grainstones (LF1)

with bioturbations, oriented, elongated concretions and rhodolithic-molluscan floatstones (LF2), likely eroded from the lower part of the cliff. Additionally, angular blocks of massive, weakly indurated quartzose grainstones (LF3) are observed, having fallen from the top of the cliff (**Fig. 14A**).

In the suburbs of the city of Brindisi, the studied sections (Punta del Serrone and Centrale Termoelettrica, **Fig. 13**) exhibit a succession of weakly cemented, bioturbated grainstones (LF3) and quartzose grainstones and tightly-cemented cross-bedded quartzose grainstones (LF1B). A similar facies association has been reported in other sections of the marine terrace deposits around Punta Penne, situated in the northern neighborhood of Brindisi (Loiacono, 2010).

At Torre San Gennaro, in the southern part of the Brindisi Basin, large-scale soft-sediment deformation features affect cross-bedded quartzose grainstones LF1B (**Fig. 14E**). Deformed beds are unconformably overlain by LF3 quatzose grainstones and mollusc-rich floastones LF2 (**Fig. 13**). Soft-sediment deformation structures from Torre San Gennaro are interpreted to result from seismic-induced liquefaction and/or fluidization processes affecting eolian sediments (Moretti, 2000).

In the whole studied area, lithofacies LF1 is characterized by MF1 and MF2 microfacies with quartz content ranging from 40 to 66% (**Fig. 10**) and a carbonate grain composition dominated by coralline algae (10 to 29%), benthic foraminifers (4 to 14%), molluscs (2 to 15%) and peloids (5 to 19%). Quartz grains are fine to medium-grained (125 to 500 μm) and angular to sub-angular (**Fig. 9B** and **9D**). Microfacies of lithofacies LF2 consist of coralline algal and molluscan floatstones with a packstone to grainstone matrix. Quartz grains are fine-grained (125 to 250 μm) and angular to sub-angular (**Fig. 9F**) and their content ranges between 10 and 45% (**Fig. 10**). The composition of the carbonate sand-sized (63 μm to 2mm) grains from matrix is dominated by coralline algae (11 to 51%), benthic foraminifers (5 to 13%), molluscs (up to

49%) and peloids (6 to 11%). Lithofacies LF3 is characterized by microfacies MF2 (quartz content up to 39% in the Brindisi south section) or MF4 (quartz content down to 1% at Punta del Serrone). Similary to LF1 and LF2, the carbonate grain composition is dominated by coralline algae (up to 73%), benthic foraminifers (up to 20%), molluscs (up to 8%) and peloids (up to 13%). Equant sparry to microsparry calcite cements occlude almost entirely the intergranular pore spaces in MF1, MF2 and MF3 (**Fig. 9B, D**) while patchy, anisopacheous sparry calcite cements occur in MF4 (**Fig. 9H**). The various lithofacies yield a similar benthic foraminiferal association (**Supplementary Material S2**) dominated by *Elphidium* (*E. macellum* and *E. paraskevaidisi*) and *Neoconorbina terquemi*.

The Middle to Upper Pleistocene terrace deposits of the Brindisi Basin exhibit a wide range of negative $\delta^{13}C$ and $\delta^{18}O$ values ranging from -1.55 to –8.85 ‰ $_{V\text{-}PDB}$ and from -3.65 to -1.55 ‰ $_{V\text{-}PDB}$, respectively **(Fig. 11B** and **Supplementary Materials S5**). Such a combined depletion in both ^{13}C and ^{18}O is likely related to a diagenetic overprint within a meteoric diagenetic environment which is consistent with the occurrence of equant sparry calcite cements (**Fig. 9B, D**) occluding the intergranular pore space of quartzarenites and quartzose grainstones.

4.2.2 Gulf of Taranto

In the Middle to Upper Pleistocene terrace deposits of the studied Gallipoli-Borgo, Gallipoli North and Taranto South sections, the predominant lithofacies consist of weakly cemented, massive and made of bioturbated grainstones to quartzose grainstones (LF3) and bioclastic floatstones (LF2), featuring a diverse and abundant molluscan fauna with the *Strombus* gastropod commonly present.

In contrast to the Brindisi Basin, no oriented concretion or soft-sediment deformation features were observed. In the analysed samples (**Fig. 10** and **Supplementary Materials S4**), the quartz content is low (<13%), particularly in bioclastic floatstones MF3 (<4%). In the three identified

microfacies (MF1, MF2 and MF3), the carbonate grain composition is dominated by coralline algae (32 to 64%), benthic foraminifers (up to 26%) and molluscs (up to 17%). In contrast to lithofacies LF2 and LF3 of the Brindisi Basin which exhibit significant amounts of calcite cements that occupy the intergranular and intra-skeletal pore spaces, cements are extremely scarce in samples of the Gulf of Taranto (**Fig. 12C**). The scarcity of meteoric calcite cements explains the ^{18}O and ^{13}O-enriched isotope signatures of the samples collected in the Gulf of Taranto compared to the terrace deposits of the Brindisi area (**Fig. 11B** and **Supplementary Materials S5**).

4.2.3 Crotone Peninsula

In the Crotone Peninsula (Ionian Calabria), Upper Pleistocene marine terraces are made of carbonate and siliciclastic sediments (up to 10 m thick) unconformably overlying the Plio-Pleistocene Cutro Clay (Zecchin *et al*., 2009) (**Fig. 4B**). These deposits show abundant coralline algal buildups interfingered within mixed carbonate-siliclastic shoreface sands (Zecchin *et al*., 2009; Bracchi *et al*., 2014, 2016). Foreshore deposits may exhibit significant bioturbation (Caruso and Monaco, 2015). Upper shoreface sands are characterized by trough cross-bedding and occasional bioturbation, while hummocky-cross stratifications are indicative of the lower shoreface to shelf transition settings (Zecchin *et al*., 2009). In contrast to the Brindisi Basin, no oriented calcite concretion or soft-sediment deformation features have been evidenced by previous authors (see above-mentioned references) and our new field observations. Massive, bioturbated quartzose grainstones (lithofacies LF3) have been sampled near Cape Colonna for microfacies characterization (**Fig. 9** and **Supplementary Materials S4**) and stable isotope measurements (**Fig. 11B** and **Supplementary Materials S5**). These samples exhibit a MF2 microfacies with quartz grain content ranging from 43 to 49%. Quartz grains are fine to medium-grained (125 to 500 µm) and very angular (**Fig. 12D**). Carbonate grain composition (**Fig. 10**) is dominated by coralline algae (19 to 27%), benthic foraminifers (7 to 14%), molluscs

(7 to 12%) and peloids (10 to 11%) and the intergranular pore spaces are partly filled by equant sparry calcite cements (**Fig. 12D**). The stable isotope composition of the collected samples is significantly ^{13}C and ^{18}O-depleted with $\delta^{13}C$ and $\delta^{18}O$ values ranging from -4.73 to -6.97‰ V-PDB and from -3.82 to -4.26‰ V-PDB, respectively (**Fig. 11B**) which is consistent with a meteoric diagenetic overprint.

4.3 The Brindisi Basin (Apulia, Italy) as a provenance area for the Ilovik-Paržine 1 ballast

Many lines of evidence indicate that the ballast stones of the Ilovik-Paržine 1 wreck have been collected from the Middle to Upper Pleistocene marine terraces of the Brindisi Basin, Apulia (**Table 2**):

1) Biostratigraphic (benthic and planktonic foraminifera) and strontium ages suggest an age for the ballast rocks (< 500 ka) which is consistent with that of the marine terrace deposits of the Brindisi region.

2) The three major lithofacies (LF1, LF2 and LF3) composing 96% of the ballast of Illovik-Paržine correlate with the lithofacies association found in the coastal outcrops of the Brindisi area, and most remarkably with those located north of the city of Brindisi (**Fig 13**).

3) Similar sedimentary and diagenetic structures, such as oriented calcite concretions and soft-sediment deformation features, were identified in both datasets (**Fig. 5** and **Fig. 6**).

4) The four dominant microfacies (MF1 to MF4) of the ballast are identical to those identified in the dominant lithofacies LF1, LF2 and LF3 of the Brindisi Basin (**Fig. 9** and **Fig. 10**). The ranges of grain composition (quartz grains and biota) and the depositional textures are similar.

5) The size and morphology of quartz grains (typically angular to sub-angular) are identical (**Fig. 9**).

6) The benthic foraminiferal assemblages are dominated by *Elphidium* (*E. macellum* and *E. paradaiskivi*) and *Neoconorbina terquemi* in both datasets (**Supplementary Material S2**).

7) The nature of the cements occluding the intergranular and intraskeletal pore space is similar: mosaic infill of equant sparry to microsparry calcite in microfacies MF1, MF2 and MF3 and patchy, anisopachous cements in microfacies MF4 (**Fig. 9**).

8) A remarkable similarity exists between the carbon and oxygen isotope signatures of the dominant ballast lithofacies and those of the Middle-Upper Pleistocene deposits of Brindisi (**Fig. 11B**).

9) The blackening of the ballast stones, which probably developed prior to the sinking of the ship, has been evidenced in the rolled pebbles of lithofacies LF1 and LF2 from the beaches located at the foot of the coastal cliffs in the Brindisi Basin (**Fig. 5A-B**).

10) The field observations made north of Brindisi have shown that at the foot of the coastal cliffs, there is an assemblage of rounded pebbles and cobbles dominantly made of lithofacies LF1 and LF2, resulting from the marine erosion of the base of the cliffs, and massive angular blocks (LF3) fallen from the uppermost part of the cliff (**Fig. 14A**). The lithology combined with the morphology of the Ilovik-Paržine 1 material are consistent with a picking up and loading of ballast stones from the site of the northern coast of the Brindisi Basin (Torre-Testa, Torre-Resta and Case Bianche sections).

Although Plio-Quaternary mixed carbonate-siliciclastic marine terrace deposits are quite widespread in the Mediterranean region (e.g. in Sicilia: Zimbardo *et al*., 2011; in Crete: Ott *et al*., 2019; Peloponnese islands: Karymbalis *et al*., 2022; Corinth Isthmus: Pallikarakis *et al*., 2018; Rhodes: Titschack *et al*., 2005; Mediterranean Spanish coast: Zazo *et al*., 2003), the existence and co-occurrence of certain mineralogical and diagenetic features are not systematic. The quartz contents seem to vary on a regional scale even within a formation of similar age: the Upper Pleistocene terrace deposits of the Ionian coast of Apulia have proven to be depleted in

quartz grains in the studied outcrops, in contrast to most of the studied sections from the Brindisi coast. The isolated or coalescent oriented calcite concretions as well as the soft-sediment deformation features, which are very common in the Middle-Upper Pleistocene terrace deposits of Brindisi, are absent on the Ionian coast. The weak cementation of grainstones and quartzose grainstones in the studied outcrops also strongly differ from what was observed at Brindisi and from the ballast stones. We therefore conclude that the Pleistocene marine terrace deposits from the Ionian Sea coast of Apulia do not constitute a likely source for the ballast stones.

The quartzose grainstones of the Crotone Peninsula were found to be very similar to those of the ballast stones with respect to microfacies (quartz content, biological assemblage, cements) and isotope signatures. Our observations and previous published data do not mention any oriented calcite concretions or soft-sediment deformation features for coastal outcrops south of Crotone. However, oriented calcite concretions have been reported in Plio-Quaternary inland outcrops north of Crotone (Balsamo *et al*., 2012). On the contrary, coastal outcrops of the Crotone peninsula exhibit mixed carbonate-siliciclastic arenitic facies interbedded within well-developed reef-algal buildups (Zecchin *et al*., 2009; Bracchi *et al*. Basso, 2014, 2016). However, bioconstructed algal facies were not identified in the ballast material of Ilovik-Paržine, making an Ionian Calabria origin highly unlikely. While oriented calcite concretions similar to those of the ballast and the Brindisi Basin have been described in marine Pleistocene terrace deposits of Basilicata (west of Metaponto), such formations are only found inland above 50 meters asl.

5. Implications for the identification of the building place and sailing route of the Ilovik-Paržine 1 ship

The city of Brindisi (Latin *Brundisium*) was a Messapian harbour. After being conquered by Rome in 266 BC, it supplanted Taranto (Latin *Tarentum*) as the main port for ships sailing between Greece and Italy (Čašule, 2013). The mapping of the Late Hellenistic and Roman shipwrecks found in the Adriatic Sea shows significant concentrations around Brindisi (Auriemma, 2004, 2006), confirming the major port activity of *Brundisium* during the Antiquity. Our geological survey of the various coastal outcrops shows that the ballast rocks bear the closest hallmarks of the sections cropping out along the northern coast of Brindisi, between Punta Penne and Torre Guaceto. The current littoral urbanization of the port of Brindisi has not made it possible to carry out a detailed study of its geology, and to determine whether the ballast has been loaded in one of the horns of the port or in a port of lesser importance, most likely located north of the city. Ancient harbors active from the Archaic period have been discovered along the northern coast of the Brindisi Basin, in particular *mansio ad speluncas* (Torre San Sabina), which has yielded an exceptional repertory of artefacts that testifies to significant activity from the Late Republic time (2^{nd}-1^{st} centuries BC) onwards (Auriemma *et al*., 2005).

For the Ilovik-Paržine 1 ship, the analyses raise more questions than they provide answers, because data from the underwater excavations are, as mentioned above, extremely incomplete due to the state of preservation of the shipwreck. Only working hypotheses can be proposed at this stage of knowledge.

The presence of an extremely homogeneous ballast is intriguing because it implies either 1) that there has never been temporary ballast, thus suggesting that the ballast of Ilovik-Paržine 1 is permanent, or 2) that the ballast has always been sourced from the same area during successive journeys.

The first hypothesis gives presumptions in favor of a wrecking of the Ilovik-Paržine 1 ship quite quickly after its first loading, before the use of a temporary ballast was required. Indeed, even

if temporary ballast is partly adjusted for each trip, it is generally never completely replaced, thus resulting in a mixture of rocks from various sources. According to this hypothesis of permanent ballast, the provenance of the stones can give indications about the place of construction of the ship, a shipyard near *Brundisium*: the loading of the ballast would thus be contemporary with the launch of the ship.

The second hypothesis would imply that the home port of Ilovik-Paržine 1 was *Brundisium* or a neighboring harbor and that all successive cargoes were loaded in this area. Nothing is known regarding the various maritime routes taken by the Ilovik-Paržine 1 ship, but such a medium-sized cargo ship of around 120 tons may have potentially sailed, in addition to the Adriatic, in the Ionian Sea and the Aegean Sea. The commercial links between Apulia and the Greek world are indeed well attested by archaeological findings (Auriemma and Silvestrelli, 2013). On the other hand, for its last journey, a departure from one of the ports of the mid-Adriatic coast such as *Ostia Aterni* (Pescara) or *Truentum* (S. Benedetto del Tronto, Nuovo, 2019), where the amphoras would have been loaded, is the more likely. These river mouth ports are located close to the amphora workshops which were already active in the 2nd century BC (Carre *et al*., 2014). The place of loading of logs is more difficult to establish regarding the relative ubiquity of the corresponding tree species that are common in the Mediterranean basin (Quézel and Médail 2003), but it may have occurred in any harbor between *Brundisium* and the *Picenum*.

In our opinion, the location of the Ilovik-Paržine 1 wreck suggests that the ship sank while heading north, possibly aiming to to reach one of the recently founded cities north of the Adriatic, such as the colony of Aquileia, established in 181 BC. Strabo (5, 1, 8) noted that Aquileia served as a significant market for communities along the eastern Adriatic coast, attracting traders who sought wine and oil. Our assumption does not imply that a regular sailing route between *Brundisium*, the *Picenum* and northern Adriatic cities existed, as it would suggest

a type of commerce based on regular exchanges, which are not attested in the Adriatic in the second century BC.

6. Conclusions

The identification of the origin of the ballast of Ilovik-Paržine 1 ship relied on several factors: 1) systematic sampling of most of the ballast remains found on the shipwreck; 2) a high degree of geological knowledge of coastal outcrops at the scale of the Adriatic Sea and adjacent areas, resulting from a large body of published data; and 3) acquisition of new data in the field, including isotopic compositions and quantitative facies analyses, which are typically absent in the literature.

The results of the present integrated multi-proxy study, based on prevailing regional geological knowledge, field sampling and including planktic and benthic foraminiferal biostratigraphy, strontium isotope stratigraphy, carbonate micro- and macrofacies analyses, diagenetic features characterization and stable isotope geochemistry, confirm the homogeneous composition of the ballast stones. Given the close resemblance between these ballast stones and the Middle to Upper Pleistocene terrace deposits that are exposed along the coast of the Brindisi region, it is likely that this formation served as the source material for the ballast. However, the possibility of a more distant source cannot be entirely dismissed. This hypothesis is further supported by the location of the Brindisi Basin on the Adriatic coast, which offers the closest geographical proximity to all the sources identified for the Ilovik-Paržine 1 ballast.

Given the homogeneity of the ballast and its provenance from a well-defined zone in Apulia region, we propose the hypothesis that the stone ballast of Ilovik-Paržine 1 is a permanent ballast loaded after the launch of the ship, most likely indicating that the ship was constructed in *Brundisium* or another smaller shipyard from the region of Brindisi. The identification of the timbers used in the construction of the ship, which is still in progress at the time of writing,

along with the final reconstruction of the shape and structure of the ship, hydrostatic calculations and the estimation of the total weight of the ballast stones, will provide further important data to either confirm or dismiss this hypothesis.

ACKNOWLEDGEMENT

The excavation on the site of the wreck Ilovik-Paržine 1 received support from the Ministry of Culture of the Republic of Croatia, the Croatian Conservation Institute and the Lošinj Museum. The research project is part of the program "Adriboats-Ships and navigation in the north-eastern Adriatic in ancient times" supported by the French Ministry of Foreign Affairs and the Centre Camille Jullian UMR 7299. The study of the ballast stones received support from the French government under the France 2030 investment plan, as part of the Initiative d'Excellence d'Aix-Marseille Université - A*MIDEX - Institute for Mediterranean Archaeology ARKAIA (AMX-19-IET-003). Thanks to an agreement between the Croatian Conservation Institute and the Croatian Ministry of the Interior, the Special Forces of the Police in the bay of Kovčanje on the island of Lošinj offered a fundamental logistic support to the project. Carine Cenzon-Salvayre is acknowledged for the identifications of wooden species of the logs, as well as Loïc Damelet and Vincent Dumas for photographic and photogrammetric acquisition and processing. Special thanks go to the two anonymous reviewers, for their valuable comments and suggestions.

REFERENCES

Allan, J.R., Matthews, R.K., 1982. Isotope signatures associated with early meteoric diagenesis. Sedimentology 29 (6), 797–817. https://doi.org/10.1111/j.1365-3091.1982.tb00085.x

Antonelli, F., Bloise, A., Bruni, F., De Luca, R., Allegretta, I., Taliano Grasso, A., Terzano, R., Miriello, D., 2020. Archaeometric approach to identifying the provenance of white marble from the shipwreck of Cala Cicala (Crotone, Camabria, Italy). Journal of Archaeological Science: Reports 30, 102204. https://doi.org/10.1016/j.jasrep.2020.102204

Auriemma, R., 2004. Salentum a salo. Porti, approdi, merci e scambi lungo la costa adriatica del Salento, 2 vol. Congedo, Galatina (Lecce).

Auriemma, R., 2006. Relitti lungo la costa occidentale dell'Adriatico. In: Čače, S., Kurilić, A., Tassaux F. (Eds.), Les Routes de l'Adriatique antique, géographie et économie, actes de la Table ronde du 18 au 22 septembre 2001 (Zadar) = Putovi antičkog Jadrana : geografija i gospodarstvo : radovi s Okruglog stola održanog u Zadru od 18. do 22. rujna 2001. Ausonius éditions-University of Zadar, Bordeaux-Zadar, Memoires 17, pp. 167–77.

Auriemma, R., Silvestrelli, F., 2013. Rotte e commerci marittimi tra Ellenismo e prima età imperiale. In: Olcese, G. (Ed.), *Immensa Aequora*. Ricerche archeologiche, archeometriche e informatiche per la ricostruzione dell'economia e dei commerci nel bacino occidentale del Mediterraneo: metà IV sec. a.C. - I sec. d.C. Quasar, Roma, pp. 439–454.

Auriemma, R., Mastronuzzi, G., Sansò, P., Zongolo, F., 2005. The harbour of the *mansio ad speluncas* (Brindisi, Italy): a key to the lecture of sea level changes in the past 3500 years? In: R. Marcet i Barbe, C.A. Brebbia, J. Olivella (Eds.), Maritime Heritage and Modern Ports, WIT Transactions on The Built Environment 79, pp. 5–14.

Azzaroli, A., 1968, Studi illustrativi della Carta Geologica d'Italia – Formazioni Geologiche: Servizio Geologico d'Italia 1, 183–185.

Babić, Lj., Zupanič, J., Vidović, J., Razum, I., Crnjaković, M., 2012a. Succession of Pleistocene non-marine sediments containing marine fossils, Mljet Island, eastern Adriatic (Croatia). Natura Croatica 21 (2), 269–299.

Babić, Lj., Crnjaković, M., Asmerom, Y., 2012b. Uplifted Pleistocene marine sediments of the Central Adriatic Island of Brusnik. Geologica Croatica 65 (2), 223–232. https://doi.org/10.4154/GC.2012.13

Balsamo, F., Storti, F., Gröcke, D.R., 2002. Fault-related fluid flow history in shallow marine sediments from carbonate concretions, Crotone basin, south Italy. Journal of the Geological Society 169, 613 –626. https://doi.org/10.1144/0016-76492011-109

Bar, A., Olivarius, M., Boldreel, L.-O., Sheldon, E., Mart, Y., Cvikel, D., 2019. Analyses of ballast stones from Akko Tower Wreck, Israel: A clue to the sailing route of the ship. Journal of Archaeological science: Reports 26,101311. https://doi.org/10.1016/j.jasrep.2019.101911

Boetto, G., Miholjek, I., Dugonijć, P., Divić, A., Dumas, V., Poveda, P., Vidulić, I. (forthcoming). The Romano-Republican wreck Ilovik-Paržine 1, island of Ilovik (Croatia): a preliminary report. In: Radić Rossi, I., Batur, K., Fabijanić, T., Romanović, D. (Eds.), Sailing through History. Reading the Past – Imagining the Future, Proceedings of the Sixteenth Symposium on Boat and Ship Archaeology (ISBSA 16), Zadar, 2021. University of Zadar, Zadar.

Bonnefoux de, P.-M.-J., Pâris, F.-E., 1999. Dictionnaire de la Marine à voile. Editions du Layeur, Marseille (1st edition 1847).

Borrelli, J., Harris, L.B., 2016. Bricks as Ballast: An Archaeological Investigation of a Shipwreck Site in Cahuita National Park, Costa Rica. In: Johnston, P.F. (Ed.), Underwater Archaeology Proceedings, Society for Historical Archaeology Proceedings. PAST Foundation, 8–16.

BouDagher-Fadel, M.K., 2015. Biostratigraphic and Geological Significance of Planktonic Foraminifera. (Updated Second ed.). UCL Press, London.

Bossio, A., Costantini, A., Foresi, L.M., Gandin, A., Mazzanti, R., Mazzei, R., Salvatorini, G., 1994. Su alcuni affioramenti miocenici della Val di Cornia (Province di Grosseto e Pisa). Atti Soc. Tosc. Nat. Mem. Serie A, 100, 167–185.

Bracchi, V.A., Nalin, R., Basso, D., 2014. Paleoecology and dynamics of coralline-dominated facies during a Pleistocene transgressive–regressive cycle (Capo Colonna marine terrace, Southern Italy). Palaeogeography, Palaeoclimatology, Palaeoecology 414, 296–309. https://doi.org/10.1016/j.palaeo.2014.09.016

Bracchi, V.A., Nalin, R., Basso, D., 2016. Morpho-structural heterogeneity of shallow-water coralligenous in a Pleistocene marine terrace (Le Castella, Italy). Palaeogeography, Palaeoclimatology, Palaeoecology 454, 101–112. https://doi.org/10.1016/j.palaeo.2016.04.014

Bully, S., Čaušević-Bully, M. 2012. Saint-Pierre d'Ilovik. Une station maritime majeure du nord de l'Adriatique, de l'Antiquité au Moyen-Âge. Histria Antiqua 21, 413–426.

Carboni, M.G., Bellotti, P., Bergamin, L., Di Bella, L., Matteucci, R., 2000. Benthic foraminiferal assemblages from the Ombrone and Tiber deltas (Central Tyrrhenian Sea): a preliminary comparison. Géologie Méditerranéenne 27 (1-2), 3–13. https://doi.org/10.3406/geolm.2000.1662

Carre, M. B., 2022. Les amphores. In: Boetto, G. (Ed.), ADRIBOATS - Navires et navigation en Adriatique orientale dans l'Antiquité. Rapport des opérations 2022. Centre Camille Jullian, Aix-en-Provence, pp. 9–12 (unpublished report).

Carre, M. -B., Monsieur, P., Pesavento Mattioli, S., 2014. The transport amphoras Lamboglia 2 and Dressel 6A: some clarifications. Journal of Roman Archaeology 27, 417–428. https://doi.org./10.1017/S1047759414001329

Caruso, C, Monaco, P., 2015. *Bichordites monastiriensis* ichnofabric from the Pleistocene shallow-marine sandstones at Le Castella (Crotone), Ionian Calabria, Southern Italy. Rivista Italiana di Paleontologia e Stratigrafia 121 (3), 381–397. https://doi.org/10.13130/2039-4942/6524

Casson, L., 1995, Ship and Seamanship in the Ancient World. Johns Hopkins University Press, Baltimore and London, 2nd edition.

Čašule, N., 2013. *Brundisium*. In: Bagnall, R.S., Brodersen, K., Champion, C. B., Erskine, A., Huebner, S. R. (Eds.), The Encyclopedia of Ancient History, First Edition, pp. 1195–1196.

Christodoulou, G., 1960. Geologische und mikropaläontologische Untersuchungen auf der Insel Karpatos (Dodekanes). Palaeontographica Abt. A 115., Schweizerbart, Stuttgart.

Ciaranfi, N., Pieri, P., Ricchetti, G., 1988. Note alla carta geologica delle Murge e del Salento (Puglia centromeridionale). Memorie Società Geologica Italiana 41, 449–460.

Compagnoni, B., Galluzzo, F., Bonomo, R., Capotorti, F., D'Ambrogi, C., Di Stefano, R. Graziano, R., Martarelli, L., Pampaloni, M.L., Pantaloni, M., Ricci, V., Tacchia, D., Masella, G., Pannuti, V., Ventura, R., Vitale, V., 2011. Carta geologica d'Italia, scala 1:1.000.000. Servizio Geologico d'Italia – ISPRA.

Coppa, G., De Castro, P., Marino, M., Rosso, A., Sanfilippo, R, 2001. The Pleistocene with Aequipecten opercularis (Linneo) of "Campo di Mare" (Brindisi, Italy). Bollettino della Società Paleontologica Italiana, 40, 405-429.

Cotecchia, V., 2014. Carta geologico-strutturale, scala 1: 500.000. In: Cotecchia V. (Ed.), Le acque sotterranee e l'intrusione marina in Puglia: dalla ricerca all'emergenza nella salvaguardia della risorsa, Memorie descrittive della Carta Geologica d'Italia 92, plate 1.

Dunham R.J. 1962. Classification of Carbonate Rocks According to Depositional Texture. In: Ham, W.E. (Ed.), Classification of Carbonate Rocks. AAPG, Tulsa, pp. 108–121.

Fenero, R., Thomas, E., Alegret, L., Molina, E., 2012. Oligocene benthic foraminifera from the Fuente Caldera section (Spain, Western Tethys): taxonomy and paleoenvironmental inferences. Journal of Foraminiferal Research 42, (4), 286–304. https://doi.org/10.2113/gsjfr.42.4.286

Flügel, E., Flügel, C., 1997. Applied microfacies analysis: provenance studies of Roman mosaic stones. Facies 37, 1–48. https://doi.org/10.1007/BF02537369

Fournier, F., Ouass, A., Rochette, P., Bromblet, P., Léonide, P., Conesa, G., Marié, L., Boularand, S., D'Ovidio, A.-M., Vigie, B., Del Furia, L., Lemke, A.L., Niaissa, T., Tendil, A., Fleury, J., 2023. Provenance of sculptural limestones in protohistoric Provence (SE France): insights from carbonate rock petrography and stable isotope geochemistry. Journal of Archaeological Science: Reports 48, 103922. https://doi.org/10.1016/j.jasrep.2023.103922

Fuček, L., Korbar, T., Palenik, D., Matiček, D., 2018. Basic Geological Map of the Republic of Croatia, scale 1:50 000: sheet Silba 1, (468/1). Croatian Geological Survey (Department of Geology), 1 sheet, Zagreb.

Gifford, J.A., 1982. Description of the Ballast Stones. In: Bass, G., van Doornick, F., Yassi Ada, vol. I, Texas A&M University Press, College Station, p. 321.

Hayward, B.W., Hollis, C.J., Grenfell, H.R., 1997. Recent *Elphidiidae* (Foraminiferida) of the South-West Pacific and Fossil *Elphidiidae* of New Zealand. Institute of Geological and Nuclear Sciences Monograph 16. Lower Hutt, Institute of Geological and Nuclear Sciences Limited.

Hearty, P.-J., Dai Pra, G., 1992. The Age and Stratigraphy of Middle Pleistocene and Younger

Deposits along the Gulf of Taranto (Southeast Italy). Journal of Coastal Research 8 (4), 882–905.

Iannone, A., Pieri, P., 1979. Considerazioni critiche sui “Tufi calcarei” delle Murge. Nuovi dati litostratigrafici e paleoambientali. Geografia Fisica e Dinamica Quaternaria 2, 173–186.

Jorissen, F.J., 1988. Benthic foraminifera from the Adriatic Sea; principles of phenotypic variations. Utrecht Micropaeontological Bulletins 37., C.W. Drooger, Utrecht.

Jurišić, M., 2000. Ancient Shipwrecks of the Adriatic: Maritime transport during the first and second centuries AD. BAR 828. Oxford.

Karymbalis, E., Tsanakas, K., Tsodoulos, I., Gaki-Papanastassiou, K., Papanastassiou, D., Batzakis, D.V., Stamoulis, K., 2022. Late Quaternary Marine Terraces and Tectonic Uplift Rates of the Broader Neapolis Area (SE Peloponnese, Greece). Journal of Marine Science and Engineering 10, 99. https://doi.org/10.3390/jmse10010099

Keith, D.H., Simmons, J.J., 1985. Analysis of the Hull Remains, Ballast, and Artifact Distribution of a 16th-Century Shipwreck, Molasses Reef, British West indies. Journal of Field Archaeology 22 (4) 411–424. https://doi.org/10.1179/009346985791169805

Kemp, P., 1976. Oxford Companion to Ships and the Sea. Oxford University Press, London/New York/Melbourne.

Korbar, T., 2009. Orogenic evolution of the External Dinarides in the NE Adriatic region: a model constrained by tectonostratigraphy of Upper Cretaceous to Palaeogene carbonates. Earth-Science Reviews 96 (4), 296–312. https://doi.org/10.1016/j.earscirev.2009.07.004

Kozličić, M., 2012. Adriatic Sea routes from the Antiquity to the early Modern Age. Histria Antiqua 21, 13–20.

Kurilić, A., Serventi, Z. 2013/2014. The inscription of Gaius Cornelius from Ilovik. Opuscula Archaeologica 37-38, 219–247.

Lamb, W.R., Keith, D.H., Judy, S.A., 1990. Analysis of the ballast of the Molasses Reef Wreck. National Geographic Research 6 (3), 291–305

Loiacono, F., 2010. Growth process of a long-lived Late Pleistocene spit along the Adriatic coast (Brindisi, southern Italy). Il Quaternario. Italian Journal of Quaternary Sciences 23 (2), 217–228.

McArthur, J.M., Howarth, R.J., Bailey, T.R., 2001. Strontium isotope stratigraphy: LOWESS version 3: best fit to the marine Sr-isotope curve for 0-509 Ma and accompanying look-up table

for deriving numerical age. The Journal of Geology 109 (2), 155–170. https://doi.org/10.1086/319243

McBride, E.F., Picard, M.D., Folk, R.L., 1994. Oriented concretions, Ionian coast, Italy: Evidence of groundwater flow direction. Journal of Sedimentary Research 64, 535–540.

Margerel, J.-P., 1997. La faune de foraminifères du Néogène de la France nord-occidentale : un exemple de colonisation de milieux littoraux. In: Bodergat, A.M., Marmonier, P. (Eds.), Contraintes et instabilité de l'environnement : stratégies adaptatives des organismes récents et fossiles. Geobios, MS 21, pp. 81–89.

Margiotta, S., Mazzone, F., Negri, S., 2010. Stratigraphic revision of Brindisi-Taranto plain: hydrogeological implications. Memorie Descrittive della Carta geologica d'Italia 90, 165–180.

Marjanac, T., Marjanac, Lj, 2000. Glacioisostatic rebound of External Dinarides. PANCARDI – Geological Meeting on Dynamics of Ongoing Orogeny, Dubrovnik, 1–3 October 2000 (Abstracts 77–78).

Marjanac, Lj, Poje, M., Marjanac, T., 1993. Pleistocene marine and terrestrial sediments with Striata fauna on the Island of Krk. Rad HAZU 26 (463), 49–62.

Mascle, G.H., 1981. Identification d'échantillons de lest. In: Frost, H. (Ed.), Lilybaeum (Marsala). – The Punic Ship: Final Excavation Report. Accademia dei Lincei, Roma, Notizie e Scavi di Antichità XXX, pp. 103–116.

Mastronuzzi, G., Caputo R., Di Bucci, D., Fracassi, U., Milella, M., Pignatelli, C., Sanso, P., Selleri, G., 2011. Middle-Late Pleistocene Evolution of the Adriatic Coastline of Southern Apulia (Italy) in Response to Relative Sea-level Changes. Geografia Fisica e Dinamica Quaternaria 34 (2), 207–222.

McGrail, S., 1989. The shipment of traded goods and of ballast in antiquity. Oxford Journal of Archaeology 8 (3), 353–358.

McGrail, S., 2001. Boats of the World: From Stone Age to Medieval Times. Oxford University Press, Oxford.

Milli, S., Girasoli, D.E., Tentori, D., Tortora, P., 2017. Sedimentology and coastal dynamics of carbonate pocket beaches: the Ionian-Sea Apulia coast between Torre Colimena and Porto Cesareo (Southern Italy). Journal of Mediterranean Earth Sciences 9, 29–66. https://doi.org/10.3304/JMES.2017.003

Moretti, M., 2000. Soft-sediment deformation structures interpreted as seismites in middle-late Pleistocene aeolian deposits (Apulian foreland, southern Italy). Sedimentary Geology 135, 167–179. https://doi.org/10.1016/S0037-0738(00)00070-1

Nantet, E., 2016. *Phortia*. Le tonnage des navires de commerce en Méditerranée. PUR, Rennes.

Nantet, E., Martins, G., 2023. From Old Cannon to Iron Pigs: The introduction of Kentledge ballast in the early modern French navy. The Mariner's Mirror 109 (4), 401–428. https://doi.org/10.1080/00253359.2023.2260249

Nuovo, M.M.S, 2019. Porti e approdi del medio e basso Adriatico occidentale in età romana. Alcuni casi studio. In: Fioriello, C.S., Tassaux, F. (Eds.), I paesaggi costieri dell'Adriatico tra Antichità e Altomedioevo. Ausonius éditions, Bordeaux, 277–300.

Orlić, M. 1986. Antički brod kod otoka Ilovika, Mala biblioteka Godišnjaka zaštite spomenika kulture, prilog uz broj 0/11 (1984-1985), Zagreb.

Ott, R.F., Gallen, S.F., Wegmann, K.W., Biswas, R.H., Herman, F., Willet, S.D., 2019. Pleistocene terrace formation, Quaternary rock uplift rates and geodynamics of the Hellenic Subduction Zone revealed from dating of palaeoshorelines on Crete, Greece. Earth and Planetary Science Letters 525, 115757. https://doi.org/10.1016/j.epsl.2019.115757

Pallikarakis, A., Triantaphyllou, M.V., Papanikolaou, I., Dimiza, M.D., Reicherter, K., Migiros, G., 2018. Age constraints and paleoenvironmental interpretation of a borehole sedimentary sequence along the eastern part of the Corinth Isthmus, Greece. Journal of Coastal Research, 34 (3), 602–617. https://doi.org/10.2112/JCOASTRES-D-16-00191.1

Pamić, J., Gušić, I., Jelaska, V., 1998. Geodynamic evolution of the Central Dinarides. Tectonophysics 297 (4), 251–268. https://doi.org/10.1016/S0040-1951(98)00171-1

Panella, C. 2010. Roma, il suburbio e l'Italia in età medio- e tardo- repubblicana: cultura materiale, territori, economie. Facta. A Journal of Roman Material Studies 4, 11–123.

Pastore, N., Cherubini, C., Giasi, C.I., 2023. Integrated hydrogeological modelling for sustainable management of the Brindisi Plain aquifer (Southern Italy). Water 15, 2943. https://doi.org/10.3390/w15162943

Pomar, L., Tropeano, M., 2000. The Calcarenite di Gravina Formation in Matera (southern Italy): New insights for coarse-grained, large-scale, cross-bedded bodies encased in offshore deposits. AAPG Bulletin 85 (4), 661–689. https://doi.org/10.1306/8626C979-173B-11D7-8645000102C1865D

Pomar, L., Westphal, H., Obrador, A., 2004. Oriented calcite concretions in Upper Miocene carbonate rocks of Menorca, Spain: evidence for fluid flow through a heterogeneous porous system. Geologica Acta 2 (4), 271–284.

Pourmand, A. Dauphas, N., 2010. Distribution coefficients of 60 elements on TODGA resin: application to Ca, Lu, Hf, U and Th isotope geochemistry. Talanta 81, 741–753. https://doi.org/10.1016/j.talanta.2010.01.008

Pourmand, A., Prospero, J.-M., Sharifi, A., 2014. Geochemical fingerprinting of trans-Atlantic African dust based on radiogenic Sr-Nd-Hf isotopes and rare earth element anomalies. Geology 42, 675–678. https://doi.org/10.1130/G35624.1

Quézel, P. Médail, F., 2003. Écologie et biogéographie des forêts du bassin méditerranéen, Elsevier, Paris.

Santamaria, C., 1984. L'épave « H » de la Chrétienne à Saint-Raphaël (Var). Archaeonautica 4, 9–52.

Serventi, Z. 2012. Važnost otoka Ilovika i Sv. Petra za plovidbenu rutu duž istočne obale Jadrana u svjetlu novijih istraživanja. Histria Antiqua 21, 401–412.

Shimron A.E., Avigad D., 2003. The rock assemblage. In: Linder, E., Kahanov, Y., The Ma'agan Mikhael Ship. The Recovery of a 2400-Year-Old Merchantman, IES and University of Haifa, Jerusalem, pp.153–182.

Starac, R. 2011. Ilovik - Sićadrija (crkva sv. Andrije). Hrvatski arheološki godišnjak 6, 432–434.

Strasser, A., 1984. Black-pebble occurrence and genesis in Holocene carbonate sediments (Florida Keys, Bahamas, and Tunisia). Journal of Sedimentary Research 54 (4), 1097–1109. https://doi.org/10.1306/212F856C-2B24-11D7-8648000102C1865D

Swart, P.K., Oehlert, A.M., 2018. Revised interpretations of stable C and O patterns in carbonate rocks resulting from meteoric diagenesis. Sedimentary Geology 364, 14–23. https://doi.org/10.1016/j.sedgeo.2017.12.005

Tchernia, A., Pomey, P. Hesnard, A., 1978. L'épave romaine de la Madrague de Giens (Var). Editions du CNRS, Paris, XXXIV^{e} Suppl. à Gallia.

Titschack, J., Bromley, R.G., Freiwald, A. 2005. Plio-Pleistocene cliff-bound, wedge-shaped, warm-temperate carbonate deposits from Rhodes (Greece): Sedimentology and facies. Sedimentary Geology 180, 29–56. https://doi.org/10.1016/j.sedgeo.2005.06.009

Tropeano, M., Sabato, L., 2002. Response of Plio-Pleistocene mixed bioclastic-lithoclastic temperate-water carbonate systems to forced regressions: the Calcarenite di Gravina Formation, Puglia, SE Italy. In: Hunt, D., Gawthorpe, R.L. (Eds.), Sedimentary Responses to Forced Regressions. Geological Society, London, Special Publications 172, pp. 217–243.

Vlahović, I., Tišljar, J., Velić, I., Matičec, D., 2005. Evolution of the Adriatic Carbonate Platform: Palaeogeography, main events and depositional dynamics. Palaeogeography, Palaeoclimatology, Palaeoecology 220, 333–360. https://doi.org/10.1016/j.palaeo.2005.01.011

Walker, S.E., Parsons-Hubbard, K., Richardson-White, S., Brett, C., Powell, E., 2011. Alpha and beta diversity of encrusting foraminifera that recruit to long-term experiments along a carbonate platform-to-slope gradient: Paleoecological and paleo-environmental implications. Palaeogeography, Palaeoclimatology, Palaeoecology 312, 325–349. https://doi.org/10.1016/j.palaeo.2011.04.028

Wentworth, C.K., 1922. The shape of beach pebbles. US Geological Survey Professional Paper 131, 75-83.

Zazo, C., Goy, J.-L., Dabrio, C.J., Bardaji, T., Hillaire-Marcel, C., Ghaleb, B., González-Delgado, J.-A., Soler, V., 2003. Pleistocene raised marine terraces of the Spanish Mediterranean

and Atlantic coasts: records of coastal uplift, sea-level highstands and climate changes. Marine Geology 194 (1-2), 103–133. https://doi.org/10.1016/S0025-3227(02)00701-6

Zecchin, M., Nalin, R., Roda, C., 2004. Raised Pleistocene marine terraces of the Crotone peninsula (Calabria, southern Italy): facies analysis and organization of their deposits. Sedimentary Geology 172, 165–185. https://doi.org/10.1016/j.sedgeo.2004.08.003

Zecchin, M., Caffau, M., Civile, D., Roda, C., 2009. Facies and cycle architecture of a Pleistocene marine terrace (Crotone, southern Italy): A sedimentary response to late Quaternary, high-frequency glacio-eustatic changes. Sedimentary Geology 216, 138–157. https://doi.org/10.1016/j.sedgeo.2009.03.004

Zimbardo, M., Nocilla, N., Evangelista, A., Ramondini, M., Scotto di Santolo, A., 2011. Destructuration of typical Sicilian calcarenites. Bulletin of Engineering Geology and the Environment 70, 507–515. https://doi.org/10.1007/s10064-010-0341-8

Figure captions

Figure 1: A: Location map of Ilovik island (drawing: V. Dumas CNRS/CCJ)**; B:** Aerial view of the Bay of Paržine; the white arrow indicates the location of the shipwreck (photograph: L. Damelet CNRS/CCJ); **C:** Geological map of Ilovik island (modified from Fuček *et al*. (2018) and location of the Bay of Paržine; **D**: Location map of the stern and prow of the Ilovik-Paržine 1 shipwreck (drawing: V. Dumas CNRS/CCJ).

Figure 2: A: Plan of the stern area of the ship with the position of the ballast (drawing: V. Dumas CNRS/CCJ); **B:** View of the ballast spilled out around the sternpost area; **C:** view of the ballast in place between the frames of the port side (photographs: L. Damelet, CCJ-CNRS).

Figure 3: Ilovik-Paržine 1 shipwreck. Greco-Italic amphoras (drawings: L. Cavassa, V. Dumas CNRS/CCJ).

Figure 4: **A:** Simplified geological map of southern Italy (modified from Milli *et al*., 2017) and location of studied outcrops; **B:** Geological map of the southern Crotone Peninsula (modified from Bracchi *et al*., 2014) showing the distinct Pleistocene marine terraces; the yellow star indicates the location of the rock samples analysed in the present work.

Figure 5: Comparison of depositional, diagenetic and deformation features evidenced in tightly cemented quartzose grainstones (lithofacies LF1) from the Ilovik-Paržine 1 ballast stones and

Middle-Upper Pleistocene deposits from the Brindisi basin. **A** and **B**: Soft sediment deformation structures from a ballast stone (**A**) and from Torre San Gennaro (**B**); **C** and **D**: Coalescent oriented concretions (fluid circulation-related cementation features) from the ballast (**C**) and from Torre Testa section (**D**); **E** and **F**: bioturbations from the ballast (**E**) and from Case Bianche (**F**). The location of sampled localities is given in **Fig. 2A**.

Figure 6: Comparison of rock samples from the Ilovik-Paržine 1 ballast stones and Middle-Upper Pleistocene deposits from the Brindisi basin. **A** and **B**: samples of bioclastic floatstones (lithofacies LF2) showing valves of *Aequipecten* from the ballast (**A**) and Case Bianche section (**B**); **C:** ballast stone of massive, weakly cemented quartzose grainstone (lithofacies LF3); **D:** ballast stone of tightly cemented quartzose grainstone (LF1) showing elongated, oriented calcite cementation features; **E:** view of the Torre Testa section showing in the lower part quartzose grainstone (LF1) with elongated, oriented calcite cementation features (white arrow) and in the upper part massive, quartzose grainstones and grainstones (LF3). The location of sampled localities is given in **Fig. 2A**.

Figure 7: **A:** Thin-section micro-photograph of a quartzose foraminiferal wackestone-packstone (microfacies MF5) from a ballast stone of lithofacies LF4; **B:** Thin-section micro-photograph of the conglomerate LF5 showing a tightly cemented clast of quarztose grainstone (***Cl.***) encased in a porous, weakly indurated coralline algal and foraminiferal sand matrix (***Mat.***); **C:** Ballast stone of a conglomerate showing LF1 dark pebbles set in weakly indurated sand matrix (lithofacies LF5); **D:** Piece of white limestone samples among the ballast, of probable local origin (lithofacies LF6); note the beige-orange patina (top side of sample) contrasting with the blackish patina of dominant elements of the ballast.; **E:** Thin-section micro-photograph of

a LF6 limestone showing a fractured calcispheres-rich (white arrow) wackestone-packstone (MF6 microfacies); **F** and **G**: Thin-section micro-photograph under polarized-light (**F**) and polarized-analysed light (**G**) of a local sand sampled underwater at the vicinity of the wreckship; the sediment is characterized by abundant miliolids (white arrows) and by the scarcity of quartz grains (***Qz.***).

Figure 8: Lithofacies composition of the ballast as a function of the area of sampling (**A-E**) and lithofacies composition of all sampled ballast stones (**F**). The different areas of sampling are indicated in **Fig 2A**.

Figure 9: Thin-section micro-photographs of microfacies from LF1, LF2 and LF3 lithofacies of the ballast stones and of the Middle to Upper Pleistocene terrace deposits from the Brindisi basin. Blue areas represent macropores (methylene blue staining of the resin). **A** and **B**: bioclastic quartzarenite (microfacies MF1) with a dominance of angular quartz grains (***Qz***) together with fragments of bioclasts including coralline algae (white arrow); the intergranular space is occupied by a fine mosaic of equant sparry to microsparry calcite cements; **A**: sample KI_4 from the ballast; **B**: sample TR_TST_6 from Torre Testa section. **C** and **D**: bioclastic quartzose grainstone (microfacies MF2) with angular to subangular quartz grains (Qz), benthic foraminifers including miliolids (Mil) and Elphidium (*Elph.*), coralline algae (Cor.); the intergranular space is occupied by a fine mosaic of equant sparry to microsparry calcite cements. **C**: sample 2020C from the ballast; **D**: sample POD_2 from Posticeddu section. **E** and **F**: Rhodolithic-molluscan floatstone with quartz-rich bioclastic packstone-grainstone matrix (microfacies MF3); ***Cor.***: coralline algae. **E**: sample AC_6 from the ballast; **F**: sample POD_1 from Posticeddu section. **G** and **H**: bioclastic grainstone (microfacies MF4) with coralline algae

(Cor.), benthic foraminifers including *Elphidium* (Elph.). A fine mosaic of sparry calcite cements occludes the intergranular pore space along selected laminae (black arrow) or around grain contacts (meniscus cements: white arrow). **G**: sample KI_14 from the ballast; **H**: sample BR_N_1 from Brindisi North (Punta del Serrone) section.

Figure 10: Composition of sand-sized (63 µm – 2 mm) grains in lithofacies LF1, LF2 and LF3 from the Ilovik-Paržine 1 ballast and from Middle to Upper terrace deposits from various outcrops of Adriatic and Ionian Apulia and Ionian Calabria.

Figure 11: Carbon and oxygen isotope signatures of carbonates the Ilovik-Paržine 1 ballast stones and from various Plio-Quaternary carbonate rocks of Adriatic and Ionian Apulia and Ionian Calabria. **A**: $\delta^{13}C$ vs $\delta^{18}O$ crossplot for the Ilovik-Paržine 1 ballast stones with measurements of local carbonate sand and Cretaceous limestone. . **B**: $\delta^{13}C$ vs $\delta^{18}O$ crossplot for Plio-Quaternary calcarenitic deposits of the Italian coast of the Adriatic and Ionian seas, superimposed with values from the Ilovik-Paržine 1 ballast.

Figure 12: **A**: Thin-section micro-photographs of an Upper Pliocene to Lower Pleistocene grainstone (*Calcarenite di Gravina* formation) from the Adriatic Apulian coast (Torre Incine section); **B**: Sand-sized grain average composition of the samples from the *Calcarenite di Gravina* formation formation analysed in the present work (9 samples). **C**: Thin-section micro-photographs of a coralline algal-molluscan floatstone-rudstone from Middle to Upper Pleistocene terrace deposits of Ionian Apulia (Gallipoli-North section). **D**: tightly cemented quartzose grainstone with coralline algal fragments and benthic foraminifers (microfacies MF2) from Middle to Upper Pleistocene terrace deposits of the Crotone Peninsula, Cape Colonna.

Figure 13: The Brindisi Basin: **A:** lithologic and sedimentologic log sections for selected coastal outcrops; **B:** simplified geological map of the Brindisi basin (modified after Cotecchia, 2014; and Pastore *et al*., 2023).

Figure 14: Photographs of coastal outcrops from the Brindisi Basin (see location on **Fig.4A**). **A:** Torre Testa section showing the vertical succession of lithofacies LF1 (quartzose grainstones and quartzarenites with oriented calcite concretions) and LF3 (massive, weakly cemented quartzose grainstones and grainstones). A mixture of boulders with angular edges (lithofacies LF3) fallen from the top the cliff and rolled pebbles/cobbles (LF1 and LF2 lithofacies dominantly) resulting from the marine erosion of the cliff, lie on the beach and at the foot of the cliff. **B:** closer view of Torre Testa section showing in the lower part of the cliff the oriented calcite concretions within LF1A lithofacies. **C:** Torre Resta cliff showing in its lower part lenses of tightly cemented quartzose grainstones (LF1 lithofacies) embedded within very-fine grained loose sand. **D:** Torre Resta: detail of a cemented quartzose grainstone lens showing elongated, oriented structures (oriented calcite concretions). **E:** Torre San Gennaro: macro-scale soft-sediment deformation structures affecting partly cemented quartzose grainstones (LF1B).

Table 1: Depositional and diagenetic features of lithofacies LF1, LF2 and LF3

Table 2: Comparison of the geological and geochemical characteristics of the Ilovik-Paržine 1 ballast stones with the Pleistocene terraced deposits of the Brindisi Basin.

Figure 1

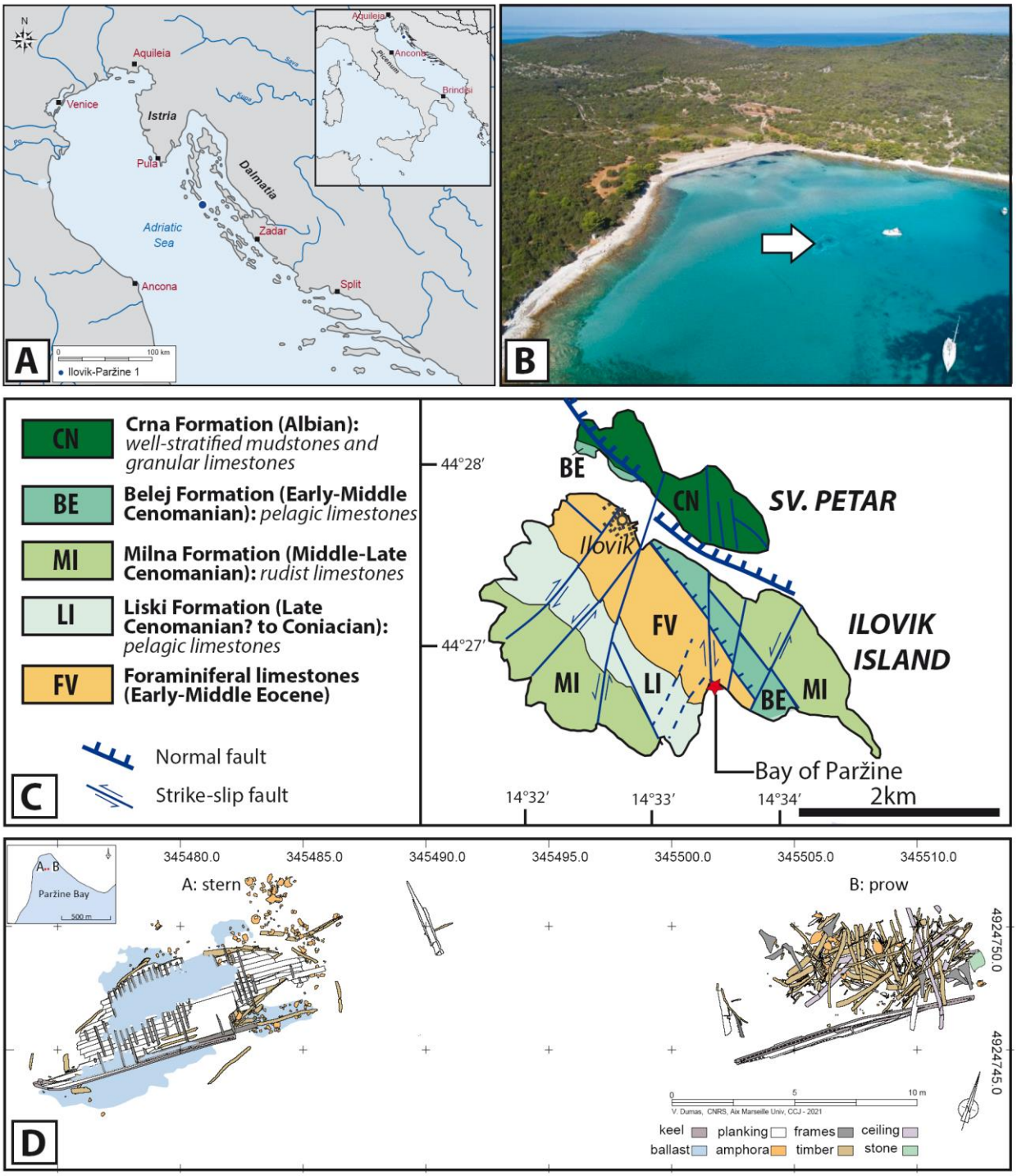

Figure 1: A: Location map of the Ilovik island (drawing: V. Dumas CNRS/CCJ)**; B:** Aerial view of the Bay of Paržine; the white arrow indicates the location of the shipwreck (photograph: L. Damelet CNRS/CCJ); **C:** Geological map of the Ilovik island (modified from Fuček *et al*. (2018) and location of the Bay of Paržine; **D**: Location map of the stern and prow of the Ilovik-Paržine 1 wreck (drawing: V. Dumas CNRS/CCJ).

Figure 2

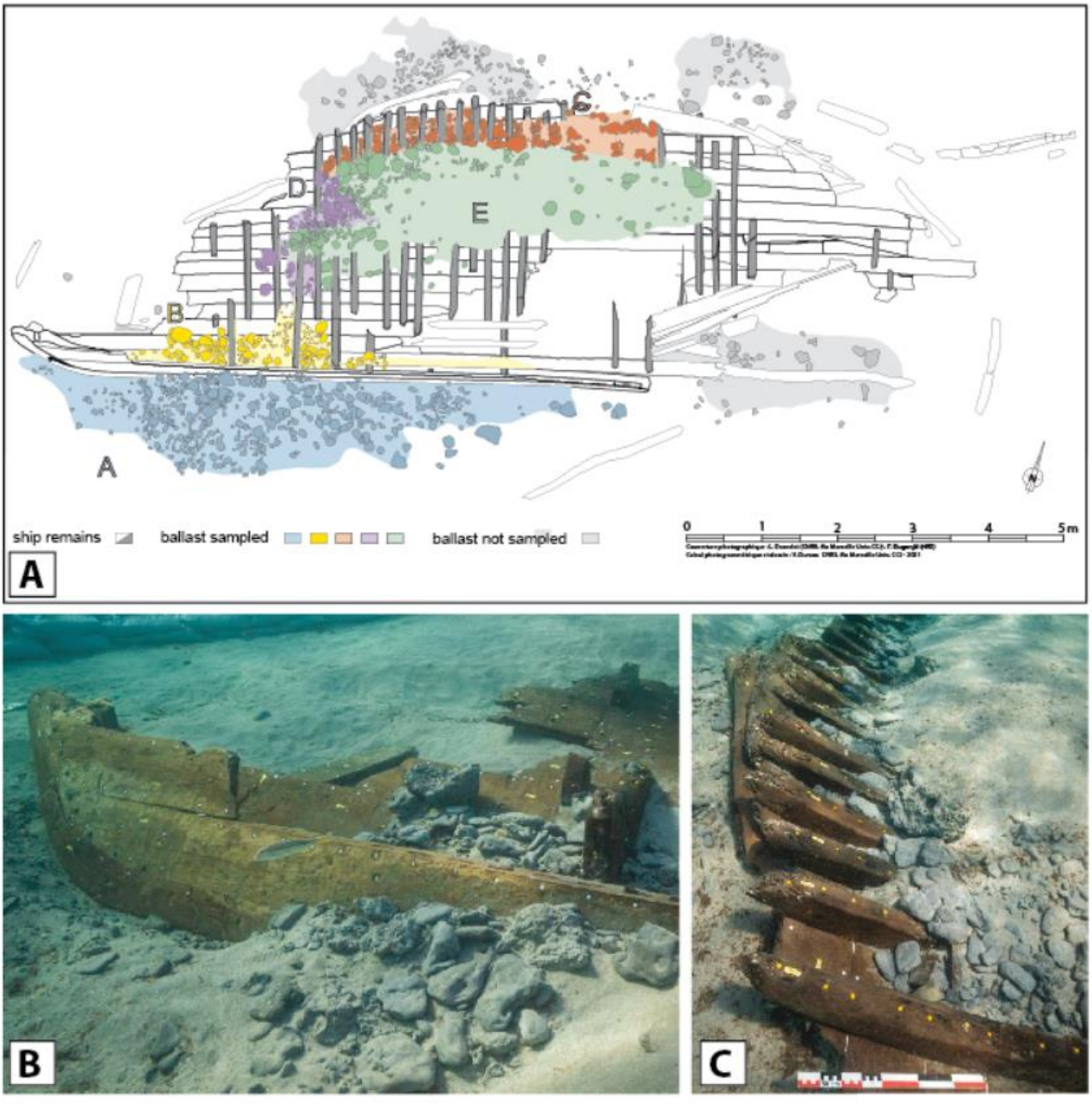

Figure 2: A: Plan of the stern area of the ship with the position of the ballast (drawing: V. Dumas CNRS/CCJ); **B:** View of the ballast spilled out around the sternpost area; **C:** view of the ballast in place between the frames of the port side (photographs: L. Damelet, CCJ-CNRS).

Figure 3

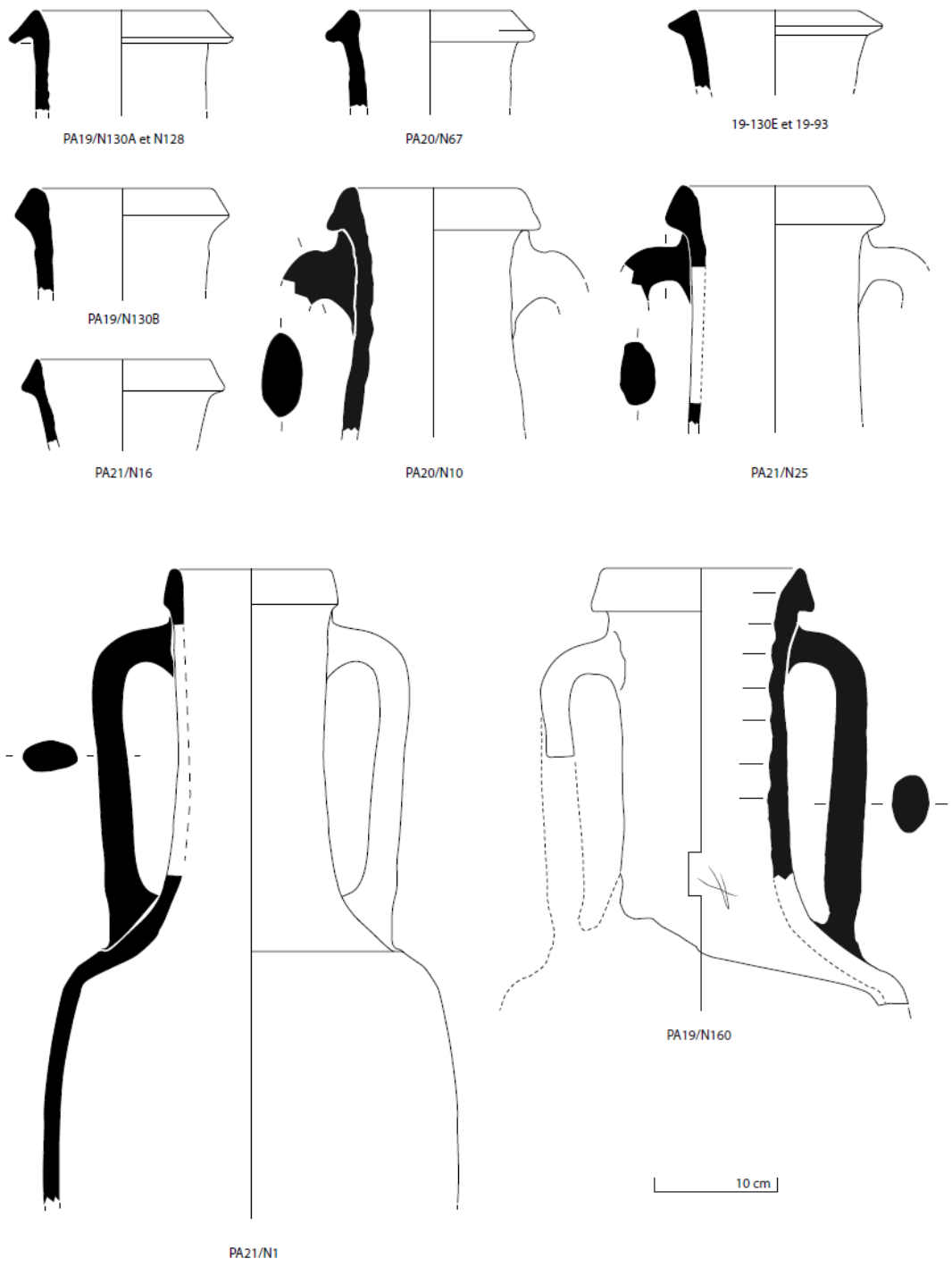

Figure 3: Ilovik-Paržine 1 shipwreck. Greco-Italic amphoras (drawings: L. Cavassa, V. Dumas CNRS/CCJ).

Figure 4

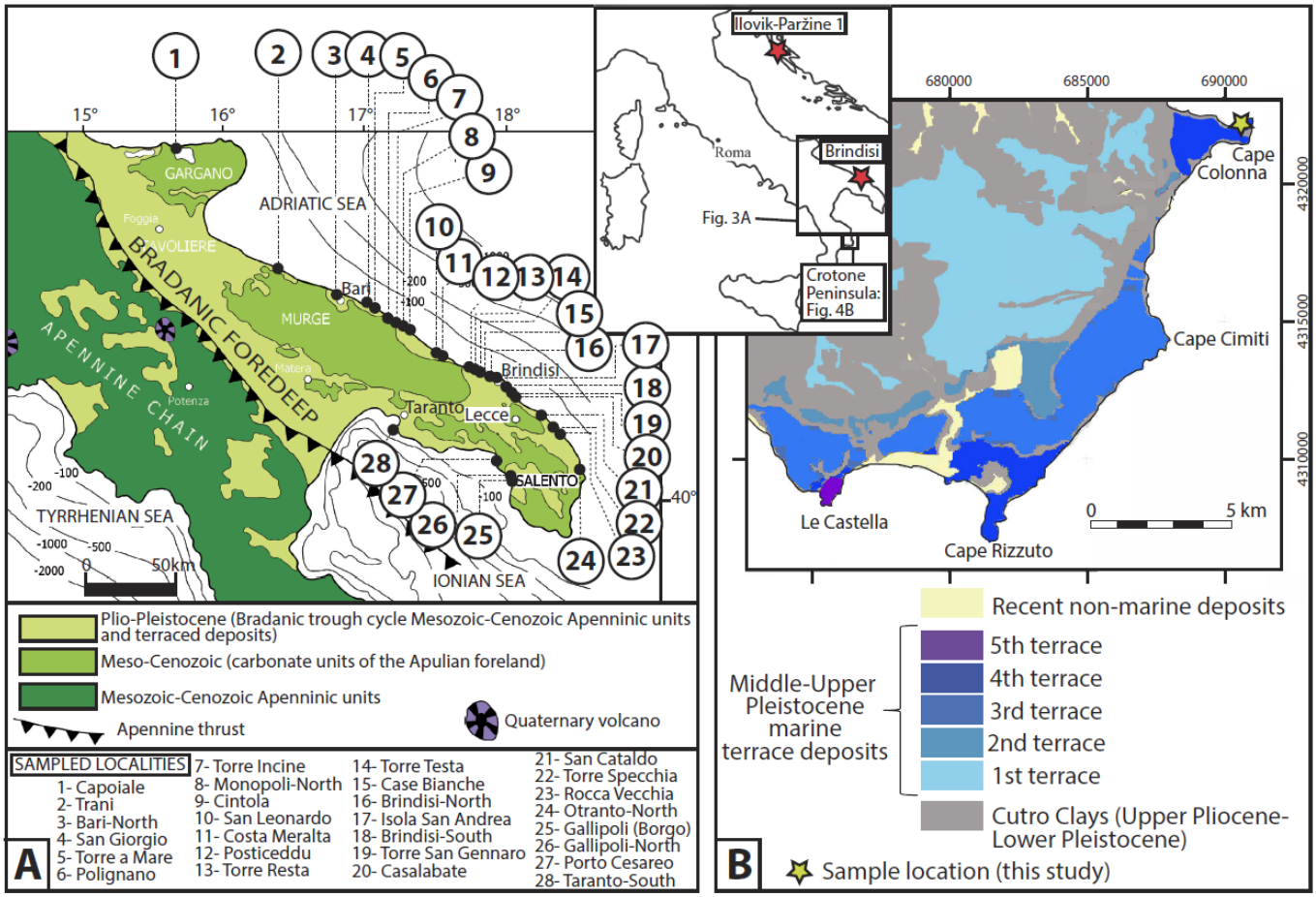

Figure 4: **A:** Simplified geological map of southern Italy (modified from Milli *et al*., 2017) and location of studied outcrops; **B:** Geological map of the southern Crotone Peninsula (modified from Bracchi *et al*., 2014) showing the distinct Pleistocene marine terraces; the yellow star indicates the location of the rock samples analysed in the present work.

Figure 5

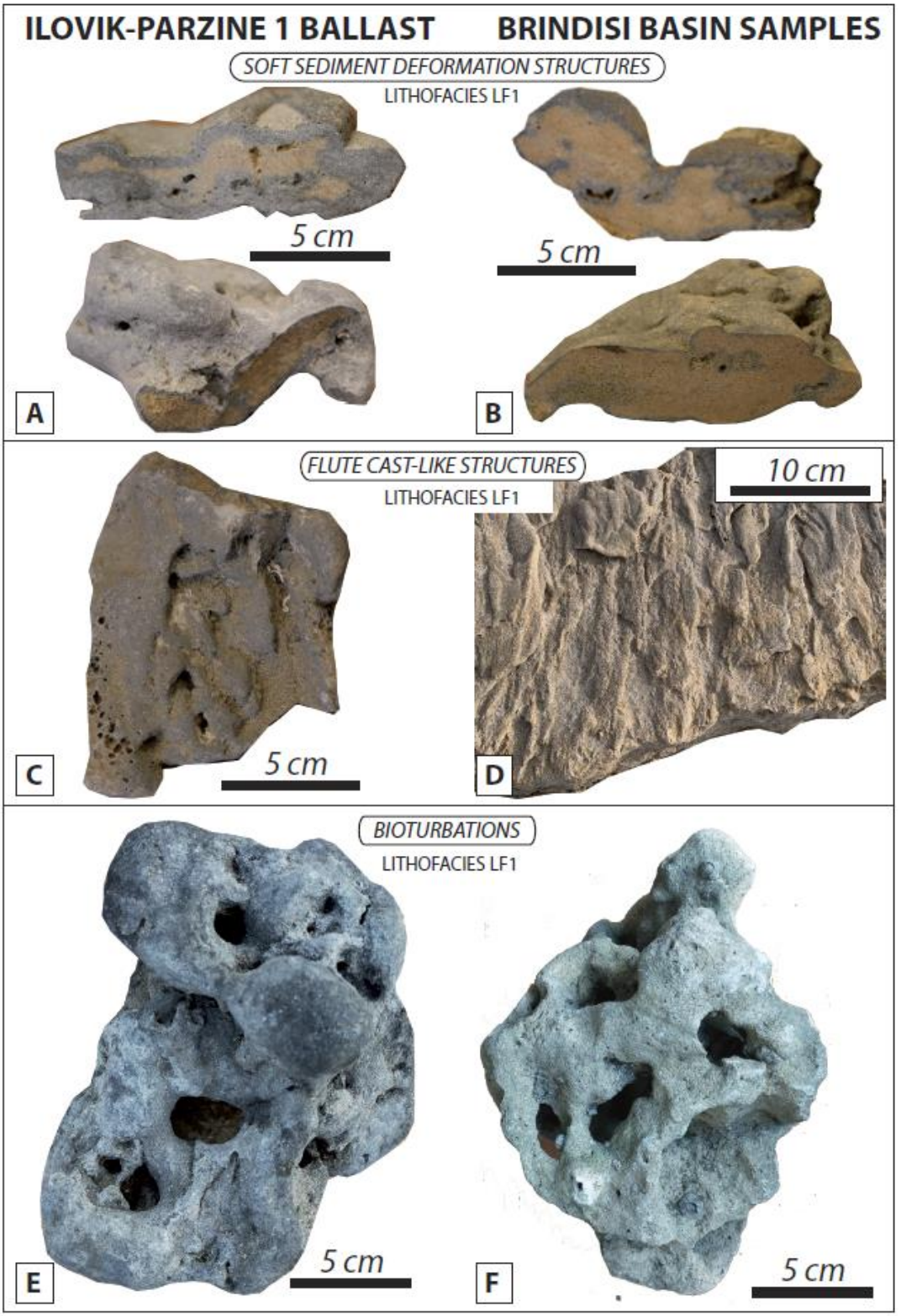

Figure 5: Comparison of depositional, diagenetic and deformation features evidenced in tightly cemented quartzose grainstones (lithofacies LF1) from the Ilovik-Paržine 1 ballast stones and Middle-Upper Pleistocene deposits from the Brindisi basin. **A** and **B**: Soft sediment deformation structures from a ballast stone (**A**) and from Torre San Gennaro (**B**); **C** and **D**: Coalescent oriented concretions (fluid circulation-related cementation features) from the ballast (**C**) and from Torre Testa section (**D**); **E** and **F**: bioturbations from the ballast (**E**) and from Case Bianche (**F**). The location of sampled localities is given in **Fig. 2A**.

Figure 6

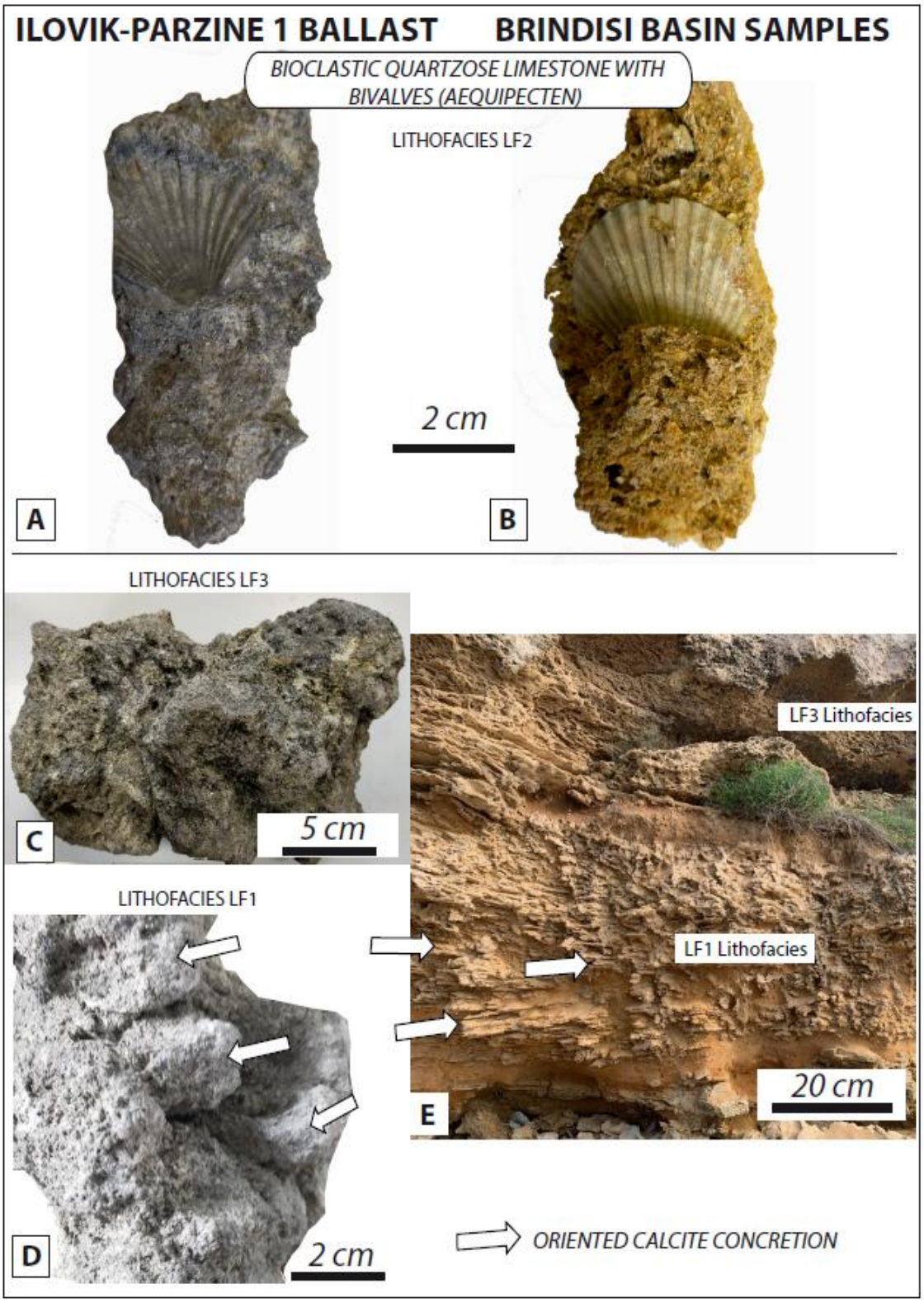

Figure 6: Comparison of rock samples from the Ilovik-Paržine 1 ballast stones and Middle-Upper Pleistocene deposits from the Brindisi basin. **A** and **B**: samples of bioclastic floatstones (lithofacies LF2) showing valves of Aequipecten from the ballast (**A**) and Case Bianche section (**B**); **C**: ballast stone of massive, weakly cemented quartzose grainstone (lithofacies LF3); **D**: ballast stone of tightly cemented quartzose grainstone (LF1) showing elongated, oriented calcite cementation features; **E**: view of the Torre Testa section showing in the lower part quartzose grainstone (LF1) with elongated, oriented calcite cementation features (white arrow) and in the upper part massive, quartzose grainstones and grainstones (LF3). The location of sampled localities is given in **Fig. 2A.**

Figure 7

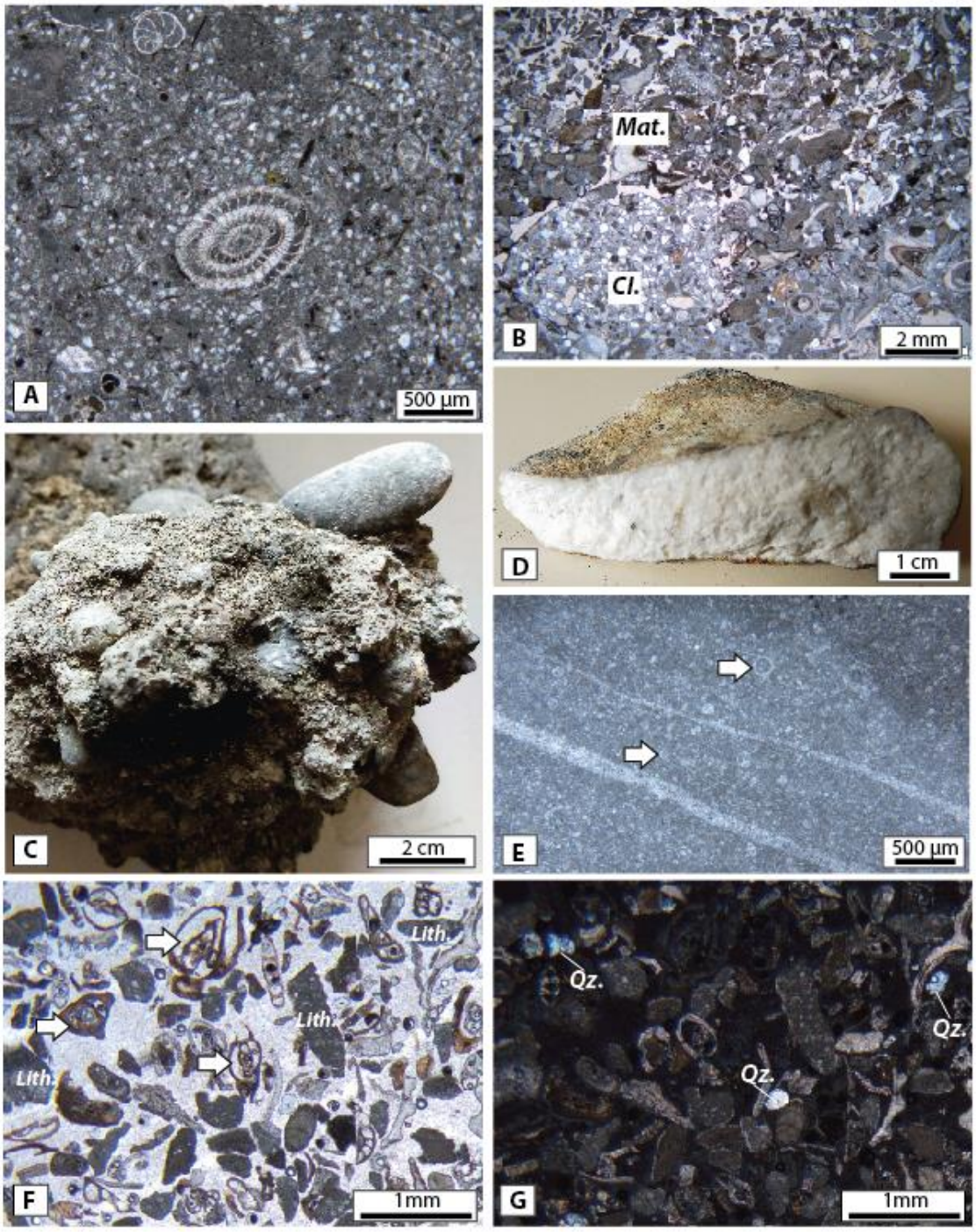

Figure 7: A: Thin-section micro-photograph of a quartzose foraminiferal wackestone-packstone (microfacies MF5) from a ballast stone of lithofacies LF4; **B**: Thin-section micro-photograph of the conglomerate LF5 showing a tightly cemented clast of quarztose grainstone (*Cl.*) encased in a porous, weakly indurated coralline algal and foraminiferal sand matrix (*Mat*.); **C:** Ballast stone of a conglomerate showing LF1 dark pebbles set in weakly indurated sand matrix (lithofacies LF5); **D**: Piece of white limestone samples among the ballast, of probable local origin (lithofacies LF6); note the beige-orange patina (top side of sample) contrasting with the blackish patina of dominant elements of the ballast.; **E**: Thin-section micro-photograph of a LF6 limestone showing a fractured calcispheres-rich (white arrow) wackestone-packstone (MF6 microfacies); **F** and **G**: Thin-section micro-photograph under polarized-light (**F**) and polarized-analysed light (**G**) of a local sand sampled underwater at the vicinity of the wreckship; the sediment is characterized by abundant miliolids (white arrows) and by the scarcity of quartz grains (*Qz*.).

Figure 8

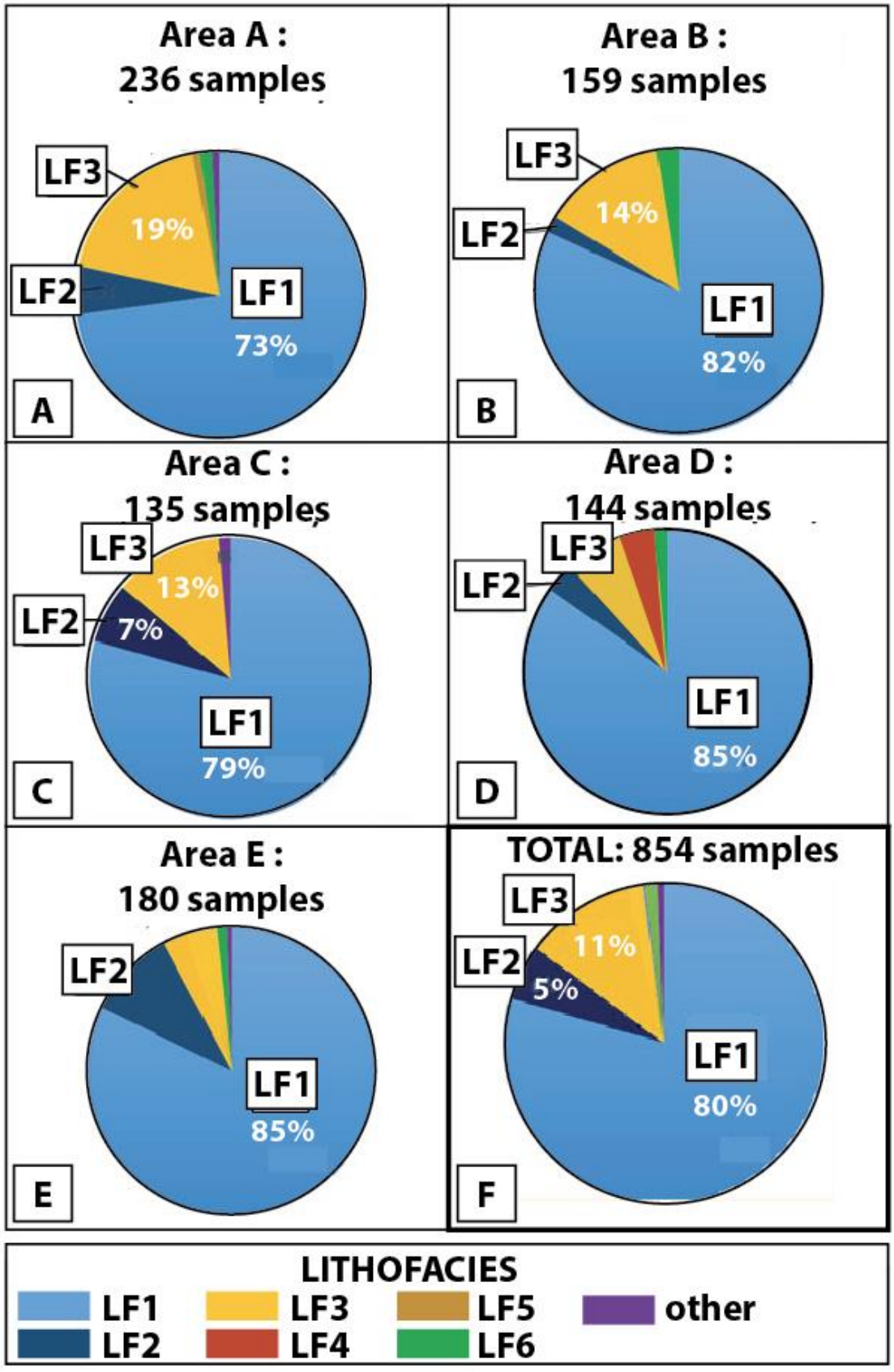

Figure 8: Lithofacies composition of the ballast as a function of the area of sampling (**A-E**) and lithofacies composition of all sampled ballast stones (**F**). The different areas of sampling are indicated in **Fig 2A**.

Figure 9

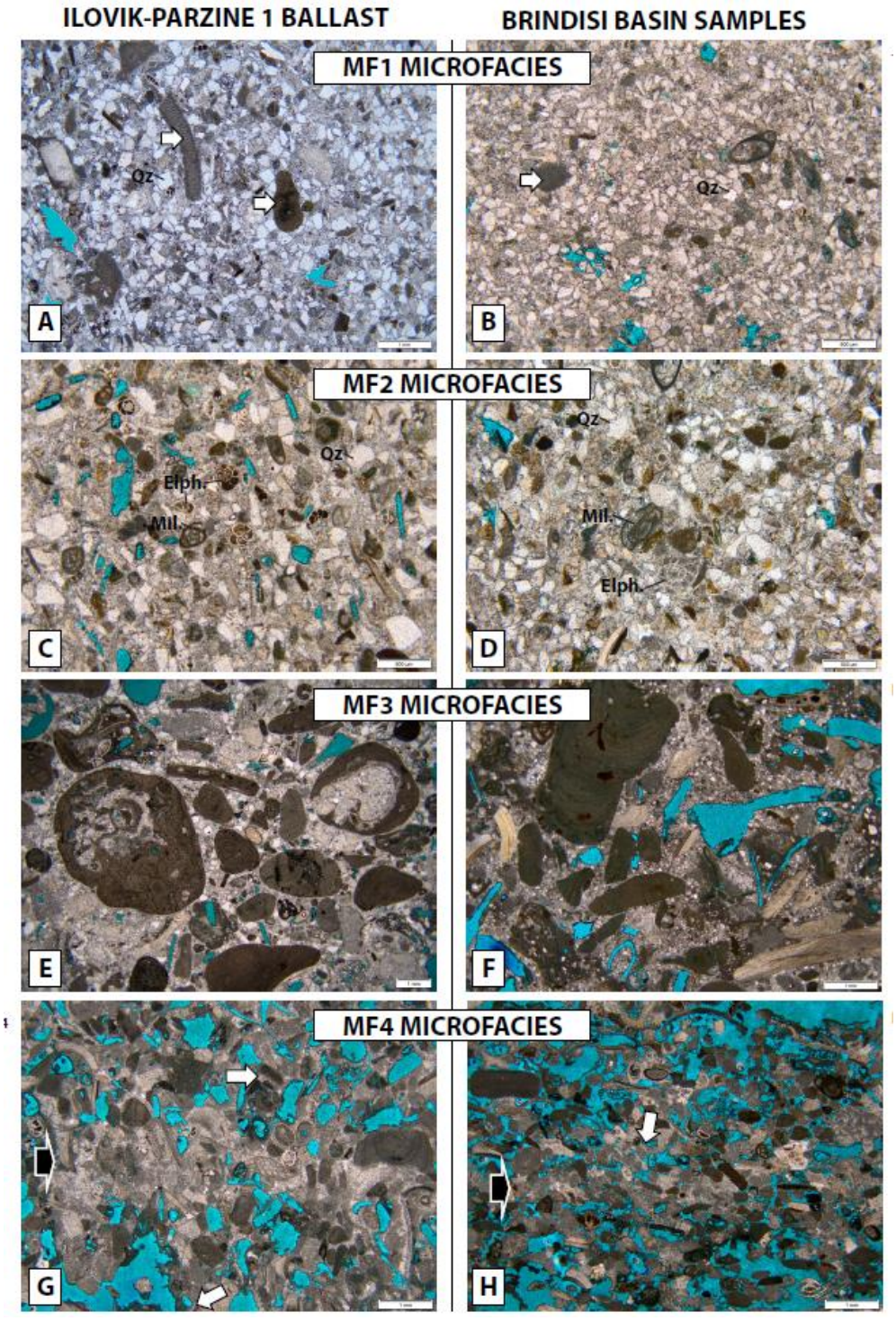

Figure 9: Thin-section micro-photographs of microfacies from LF1, LF2 and LF3 lithofacies of the ballast stones and of the Middle to Upper Pleistocene terrace deposits from the Brindisi basin. Blue areas represent macropores (methylene blue staining of the resin). **A** and **B**: bioclastic quartzarenite (microfacies MF1) with a dominance of angular quartz grains (*Qz*) together with fragments of bioclasts including coralline algae (white arrow); the intergranular space is occupied by a fine mosaic of equant sparry to microsparry calcite cements; **A**: sample KI_4 from the ballast; **B**: sample TR_TST_6 from Torre Testa section. C and D: bioclastic quartzose grainstone (microfacies MF2) with angular to subangular quartz grains (*Qz*), benthic foraminifers including miliolids (*Mil*) and Elphidium (*Elph*.), coralline algae (*Cor*.); the intergranular space is occupied by a fine mosaic of equant sparry to microsparry calcite cements. C: sample 2020C from the ballast; **D**: sample POD_2 from Posticeddu section. **E** and **F**: Rhodolithic-molluscan floatstone with quartz-rich bioclastic packstone-grainstone matrix (microfacies MF3); Cor.: coralline algae. **E**: sample AC_6 from the ballast; **F**: sample POD_1 from Posticeddu section. **G** and **H**: bioclastic grainstone (microfacies MF4) with coralline algae (*Cor*.), benthic foraminifers including Elphidium (*Elph*.). A fine mosaic of sparry calcite cements occludes the intergranular pore space along selected laminae (black arrow) or around grain contacts (meniscus cements: white arrow). **G**: sample KI_14 from the ballast; **H**: sample BR_N_1 from Brindisi North (Punta del Serrone) section.

Figure 10

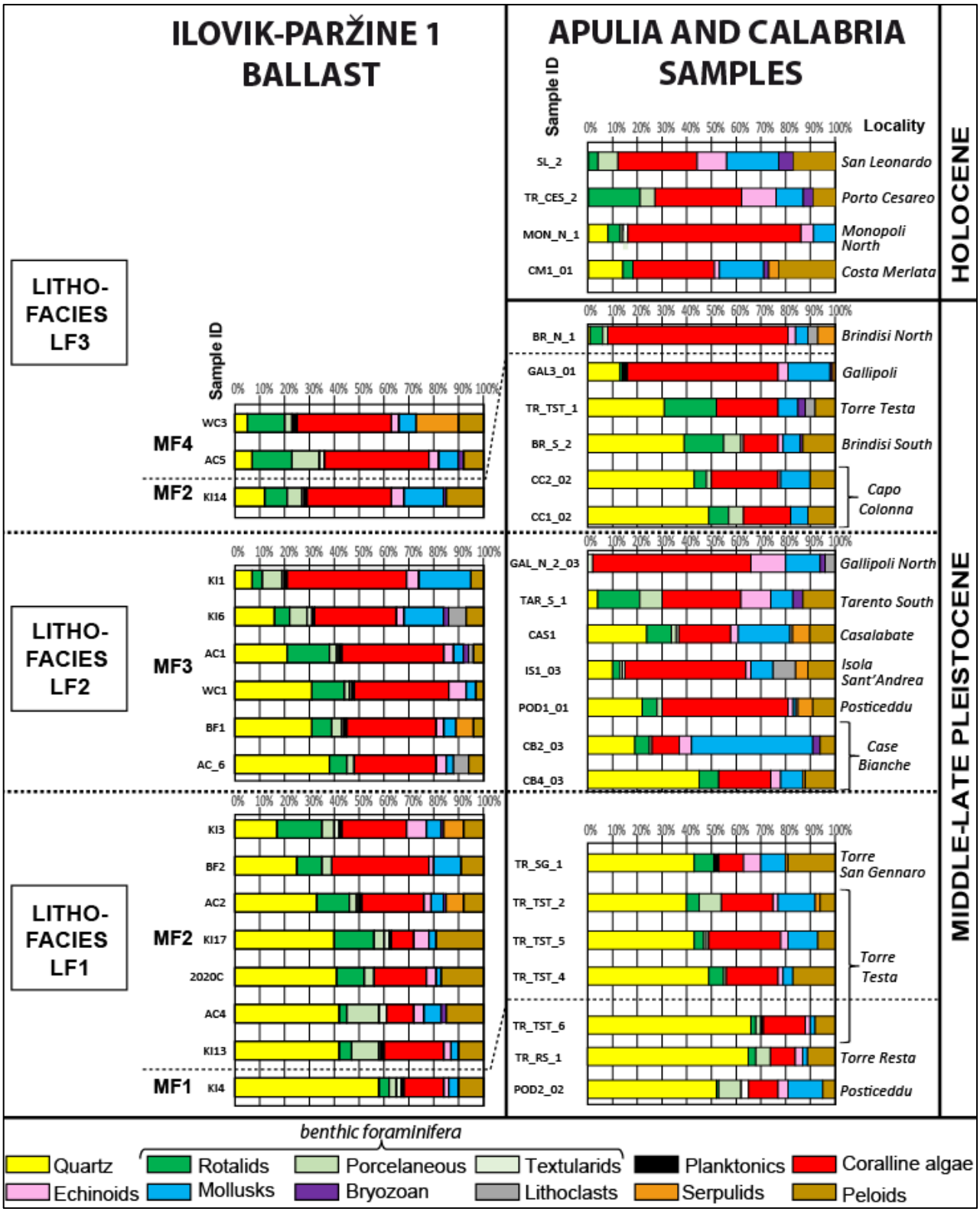

Figure 10: Composition of sand-sized (63 µm – 2 mm) grains in lithofacies LF1, LF2 and LF3 from the Ilovik-Paržine 1 ballast and from Middle to Upper terrace deposits from various outcrops of Adriatic and Ionian Apulia and Ionian Calabria.

Figure 11

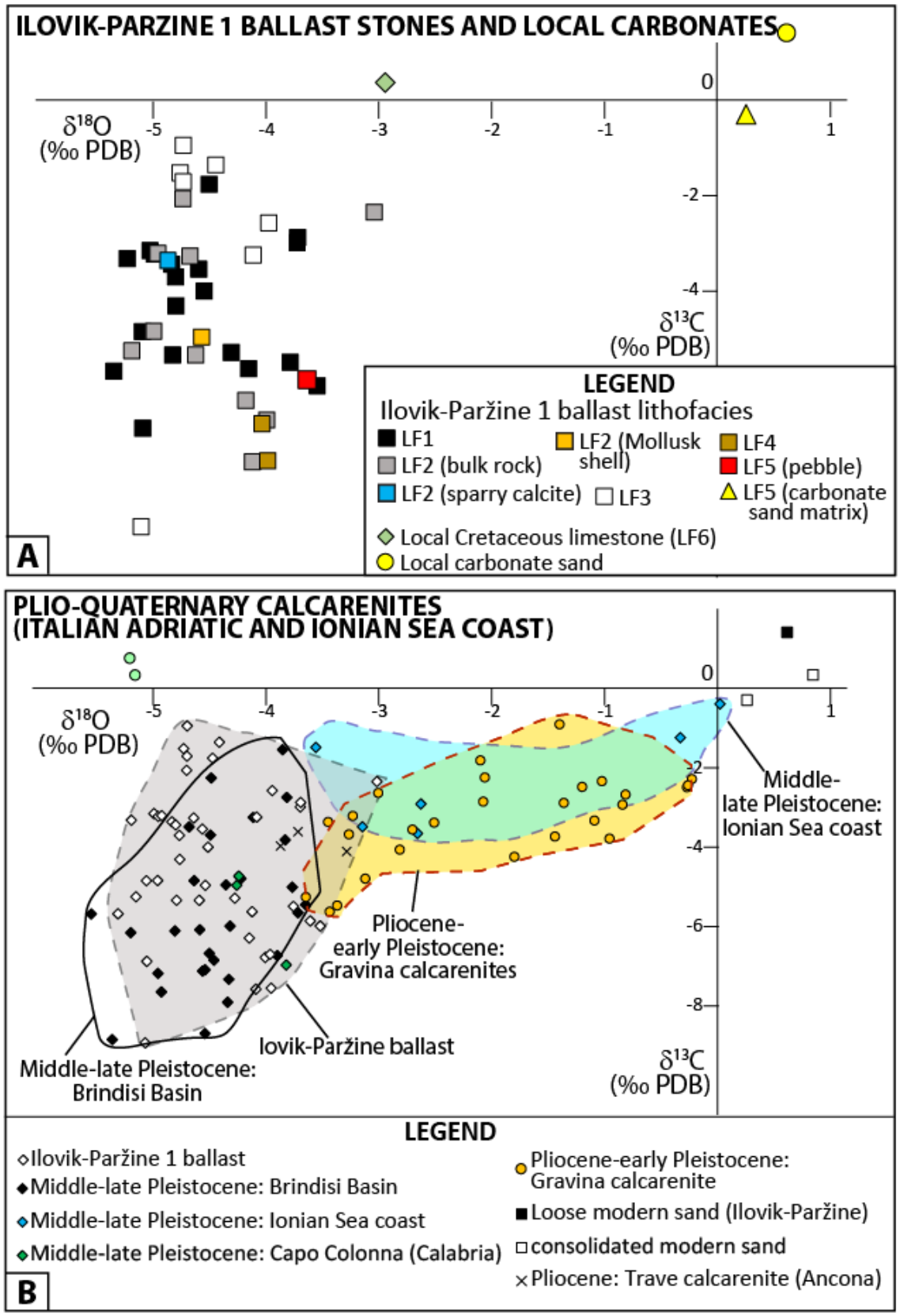

Figure 11: Carbon and oxygen isotope signatures of carbonates the Ilovik-Paržine 1 ballast stones and from various Plio-Quaternary carbonate rocks from Adriatic and Ionian Apulia and Ionian Calabria. **A**: $d^{13}C$ vs $d^{18}O$ crossplot for the Ilovik-Paržine 1 ballast stones with measurements of local carbonate sand and Cretaceous limestone. . **B**: $d^{13}C$ vs $d^{18}O$ crossplot for Plio-Quaternary calcarenitic deposits from the Italian coast of the Adriatic and Ionian seas, superimposed with values from the Ilovik-Paržine 1 ballast.

Figure 12

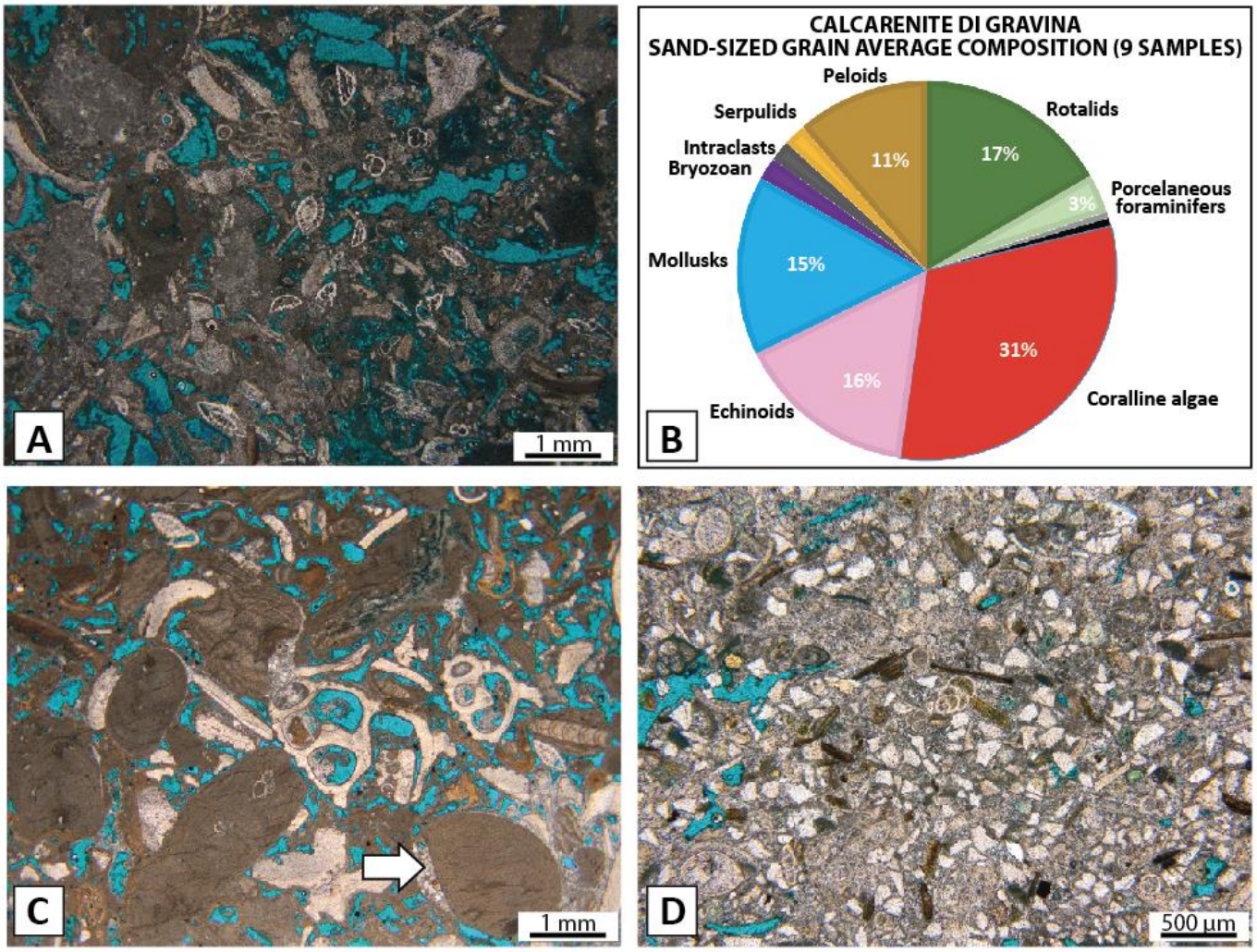

Figure 12: A: Thin-section micro-photographs of an Upper Pliocene to Lower Pleistocene grainstone (Calcarenite di Gravina formation) from the Adriatic Apulian coast (Torre Incine section); **B:** Sand-sized grain average composition of the samples from the Calcarenite di Gravina formation formation analysed in the present work (9 samples). **C:** Thin-section micro-photographs of a coralline algal-molluscan floatstone-rudstone from Middle to Upper Pleistocene terrace deposits of Ionian Apulia (Gallipoli-North section). **D:** tightly cemented quartzose grainstone with coralline algal fragments and benthic foraminifers (microfacies MF2) from Middle to Upper Pleistocene terrace deposits of the Crotone Peninsula, Cape Colonna.

Figure 13

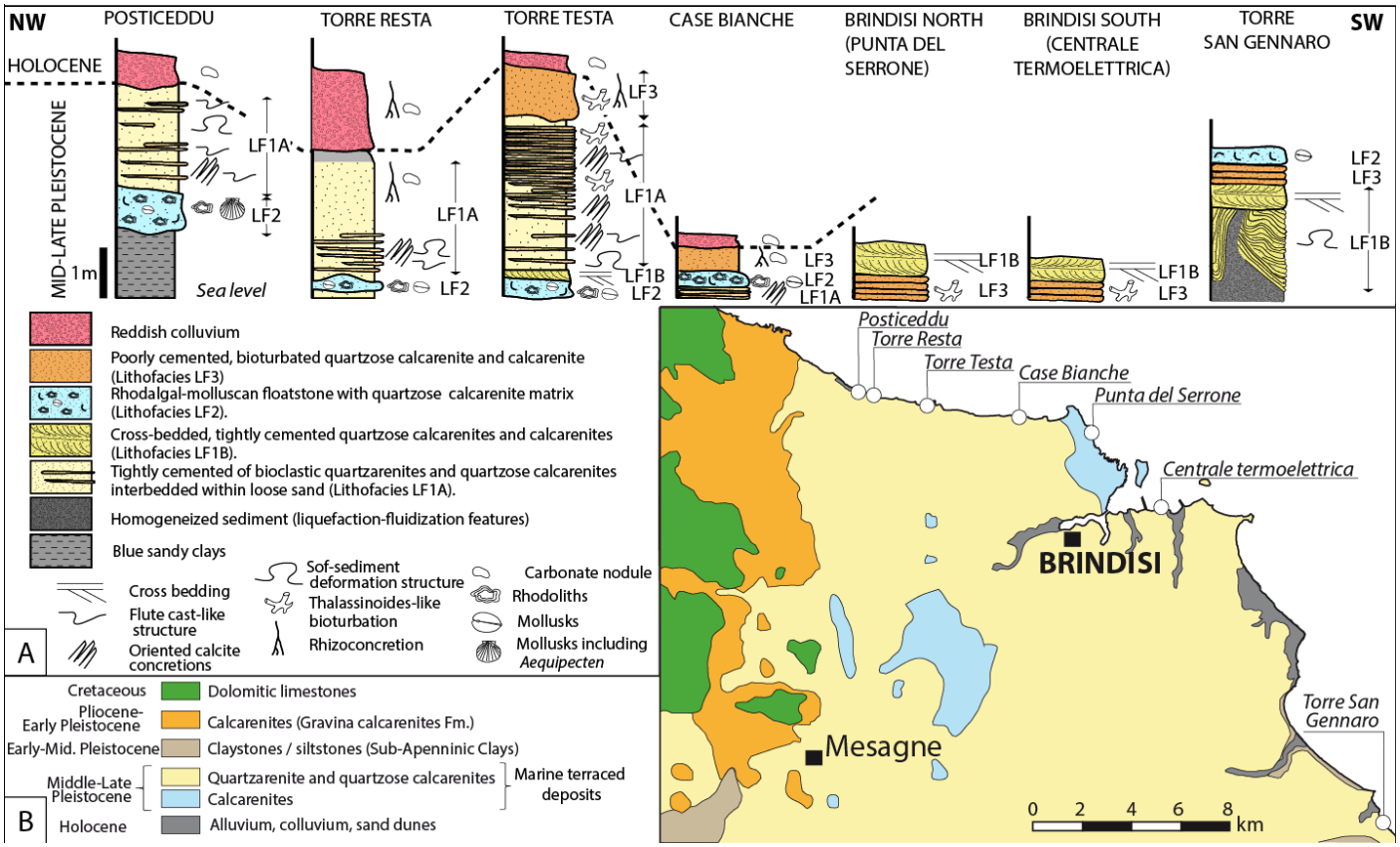

Figure 13: The Brindisi basin: **A:** lithologic and sedimentologic log sections for selected coastal outcrops; **B:** Simplified geological map of the Brindisi basin (modified after Cotecchia, 2014; and Pastore *et al*., 2023).

Figure 14

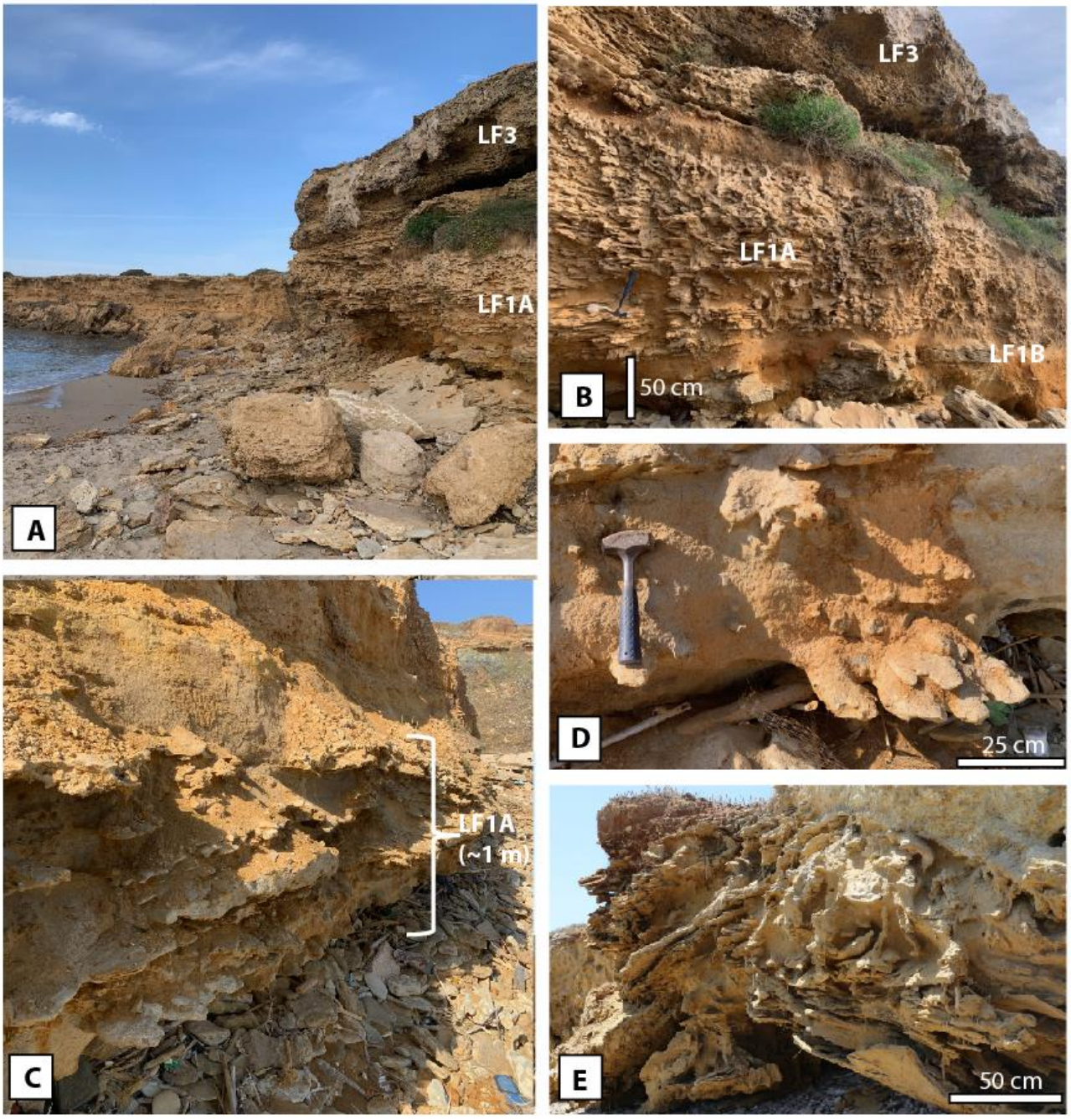

Figure 14: Photographs of coastal outcrops from the Brindisi Basin (see location on Fig.4A). **A:** Torre Testa section showing the vertical succession of lithofacies LF1 (quartzose grainstones and quartzarenites with oriented calcite concretions) and LF3 (massive, weakly cemented quartzose grainstones and grainstones). A mixture of boulders with angular edges (lithofacies LF3) fallen from the top the cliff and rolled pebbles/cobbles (LF1 and LF2 lithofacies dominantly) resulting from the marine erosion of the cliff, lie on the beach and at the foot of the cliff. **B:** closer view of Torre Testa section showing in the lower part of the cliff the oriented calcite concretions within LF1A lithofacies. **C:** Torre Resta cliff showing in its lower part lenses of tightly cemented quartzose grainstones (LF1 lithofacies) embedded within very-fine grained loose sand. **D:** Torre Resta: detail of a cemented quartzose grainstone lens showing elongated, oriented structures (oriented calcite concretions). **E:** Torre San Gennaro: macro-scale soft-sediment deformation structures affecting partly cemented quartzose grainstones (LF1B).

LITHOFACIES	Microfacies				Macro-scale features						
	MF1	MF2	MF3	MF4	flute-cast-like structures	Oriented calcite concretions	soft-sediment deformation features	mollusk accumulations	rhodoliths	bioturbations	cross-bedding
LF1A: Tightly cemented bioclastic quartzarenite and quartzose calcarenite with oriented calcite concretions	X	X			X	X	X			X	
LF1B: Cross-bedded, tightly cemented quartzose calcarenite and calcarenite		X		X			X				X
LF2: Rhodalgal-molluscan floatstone with quartzose calcarenite matrix			X					X	X		
LF3: Poorly cemented, bioturbated quartzose calcarenite and calcarenite		X		X						X	

Table 1: Depositional and diagenetic features of lithofacies LF1, LF2 and LF3

	Ilovik-Parzine ballast stones	Terraced deposits of the Brindisi Basin
Age	Planktic foraminiferal biostratigraphy: Pleistocene (after 1,28 Ma) to Holocene" Sr isotope stratigraphy: younger than 500 ka (Middle Pleistocene to Holocene)	Middle to Late Pleistocene (Ciaranfi et al., 1988; Margiotta et al., 2010; Mastronuzzi et al., 2011)
Lithofacies association	LF1A: Tightly cemented bioclastic quartzarenite and quartzose calcarenite with oriented calcite concretions (80% of the studied ballast) LF2: Rhodalgal-molluscan floatstone with quartzose calcarenite matrix (5% of the studied ballast) LF3: Poorly cemented, bioturbated quartzose calcarenite and calcarenite (11% of the studied ballast) LF4: quartzose calcisistite (<1% of the studied ballast). LF5: conglomerates with quartzose calcarenite matrix (likely to be formed locally) (~1% of the studied ballast). LF6: tight, fractured limestones (Local limestones) (~1% of the studied ballast).	LF1A: Tightly cemented bioclastic quartzarenite and quartzose calcarenite with oriented calcite concretions (Middle to Upper Pleistocene) LF1B: Cross-bedded, tightly cemented quartzose calcarenite and calcarenite (Middle to Upper Pleistocene) LF2: Rhodalgal-molluscan floatstone with quartzose calcarenite matrix (Middle to Upper Pleistocene) LF3: Poorly cemented, bioturbated quartzose calcarenite and calcarenite (Middle to Upper Pleistocene and Holocene)
Sedimentary / diagenetic structures	Bioturbations, elongated-oriented calcite concretions	Bioturbations, cross bedding, elongated-oriented calcite concretions
Macrofauna	Occurrence of *Aequipecten*	Occurrence of *Aequipecten* in Posticeddu section (this study) and San Gennaro (Coppa et al., 2001)
Microfacies (in LF1, LF2 and LF3 lithofacies)	MF1: bioclastic quartzarenite; MF2: bioclastic quartzose grainstone; Microfacies MF3: rhodalgal-molluscan floatstone with quartz-rich bioclastic packstone-grainstone matrix; Microfacies MF4: bioclastic grainstone	MF1: bioclastic quartzarenite; MF2: bioclastic quartzose grainstone; Microfacies MF3: rhodalgal-molluscan floatstone with quartz-rich bioclastic packstone-grainstone matrix; Microfacies MF4: bioclastic grainstone
Morphology of quartz sand	angular to sub-angular	angular to sub-angular
Quartz grain size	very fine to fine-grained (63 to 250 µm) in MF1 and MF3; fine to medium-grained (125 to 500 µm) in MF2; medium to coarse-grained (250 µm to 1 mm) in MF4	Fine to medium-grained (125 to 500 µm) in MF1 and MF2; fine grained (125 to 250 µm) in MF3; medium to coarse-grained (250 µm to 1 mm) in MF4.
Benthic foraminiferal association	Dominated by *Elphidium* (*E. macellum* and *E. paraskevaidisi*) and *Neoconorbina terquemi*.	Dominated by *Elphidium* (*E. macellum* and *E. paraskevaidisi*) and *Neoconorbina terquemi*.
Nature of cement	Equant sparry to microsparry calcite	Equant sparry to microsparry calcite
Carbon and oxygen isotope composition	$\delta^{18}O$: from -5.51 to -3.02‰ $\delta^{13}C$: from -8.93 to -0.95‰	$\delta^{18}O$: from -5.55 to -3.65‰ $\delta^{13}C$: from -8.85 to -1.55‰

Table 2: Comparison of the geological and geochemical characteristics of the Ilovik-Paržine 1 ballast stones with the Pleistocene terraced deposits of the Brindisi Basin.

Figure 1

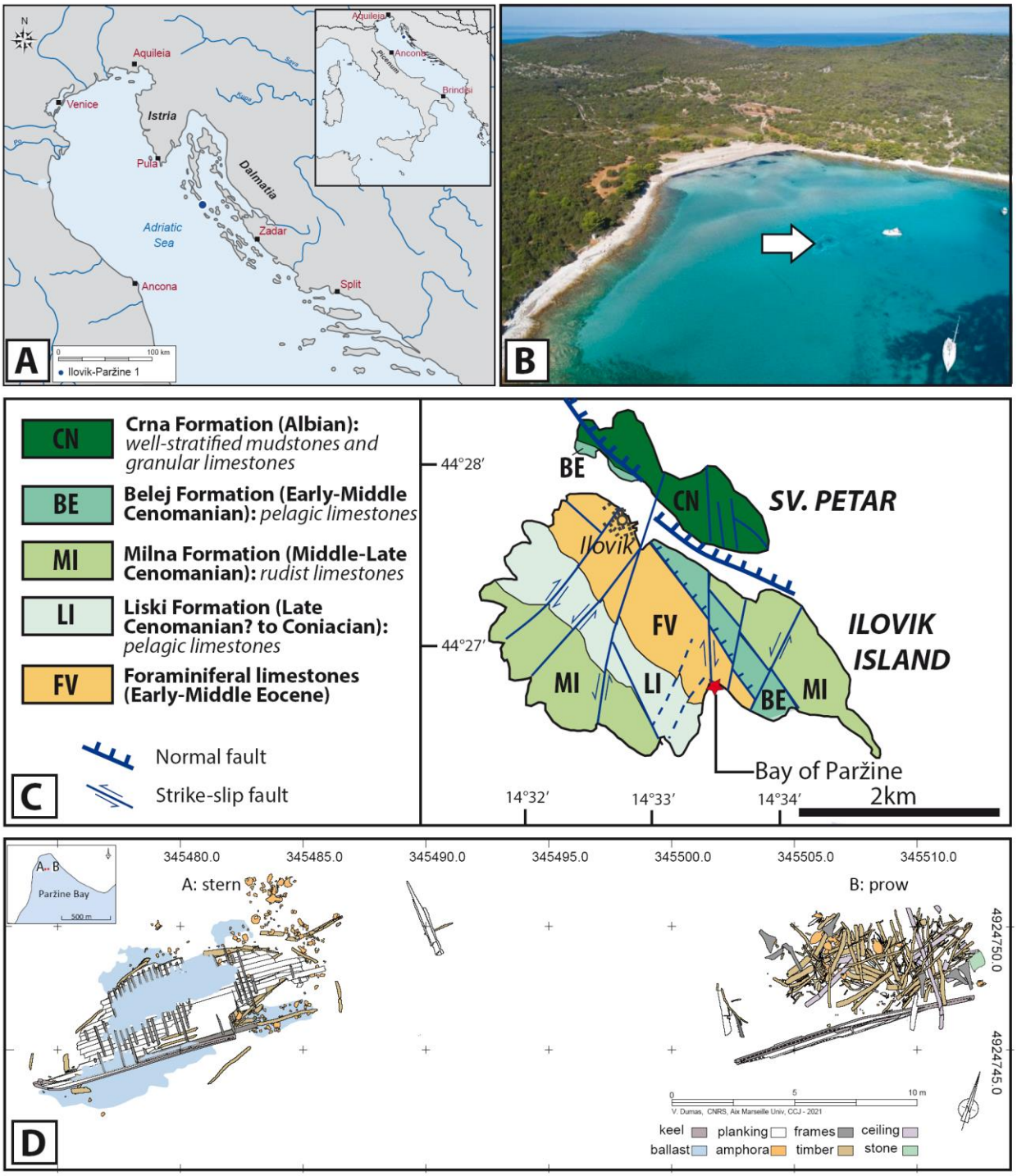

Figure 1: A: Location map of the Ilovik island (drawing: V. Dumas CNRS/CCJ)**; B:** Aerial view of the Bay of Paržine; the white arrow indicates the location of the shipwreck (photograph: L. Damelet CNRS/CCJ); **C:** Geological map of the Ilovik island (modified from Fuček *et al*. (2018) and location of the Bay of Paržine; **D**: Location map of the stern and prow of the Ilovik-Paržine 1 wreck (drawing: V. Dumas CNRS/CCJ).

Figure 2

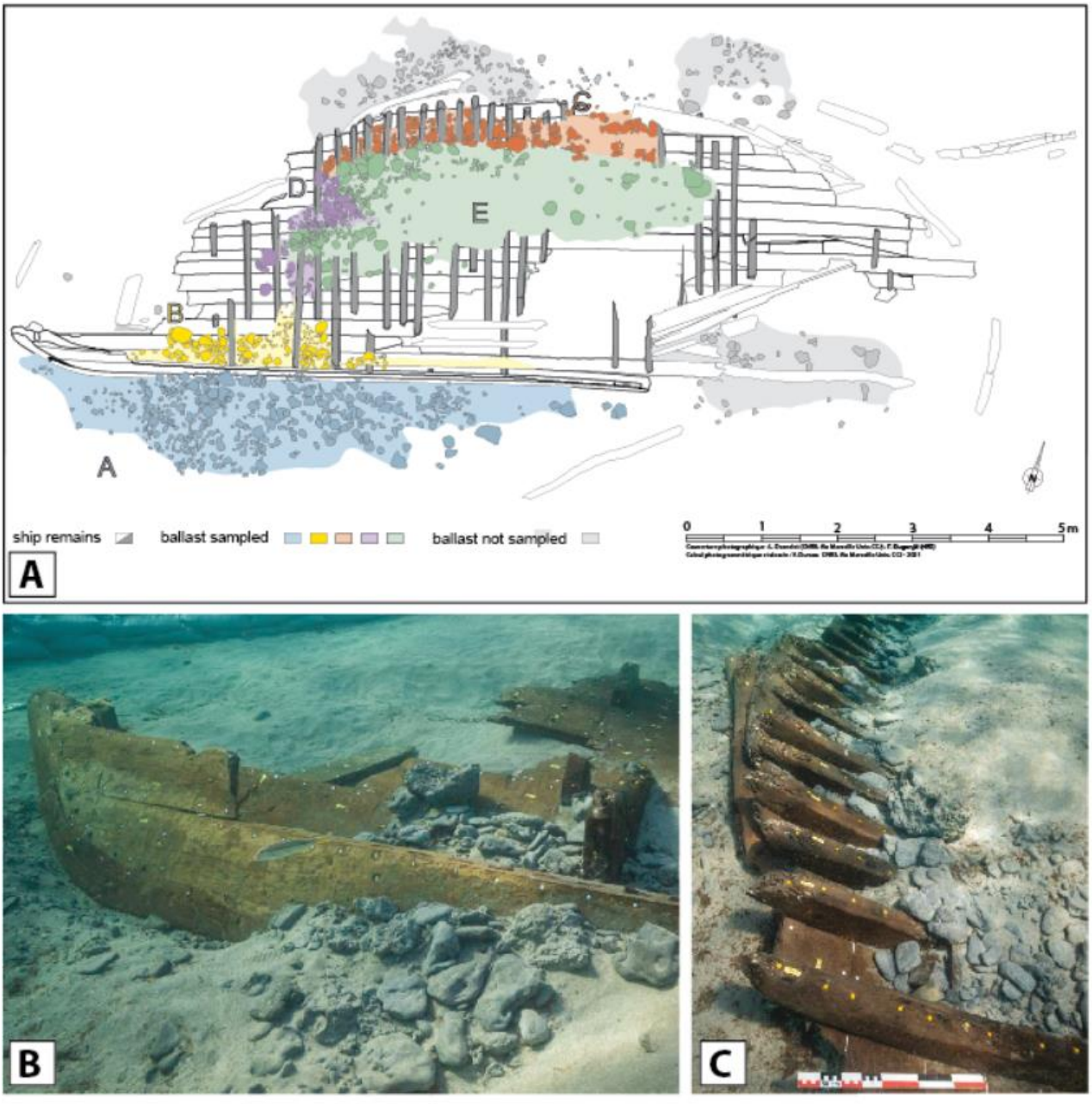

Figure 2: A: Plan of the stern area of the ship with the position of the ballast (drawing: V. Dumas CNRS/CCJ); **B:** View of the ballast spilled out around the sternpost area; **C:** view of the ballast in place between the frames of the port side (photographs: L. Damelet, CCJ-CNRS).

Figure 3

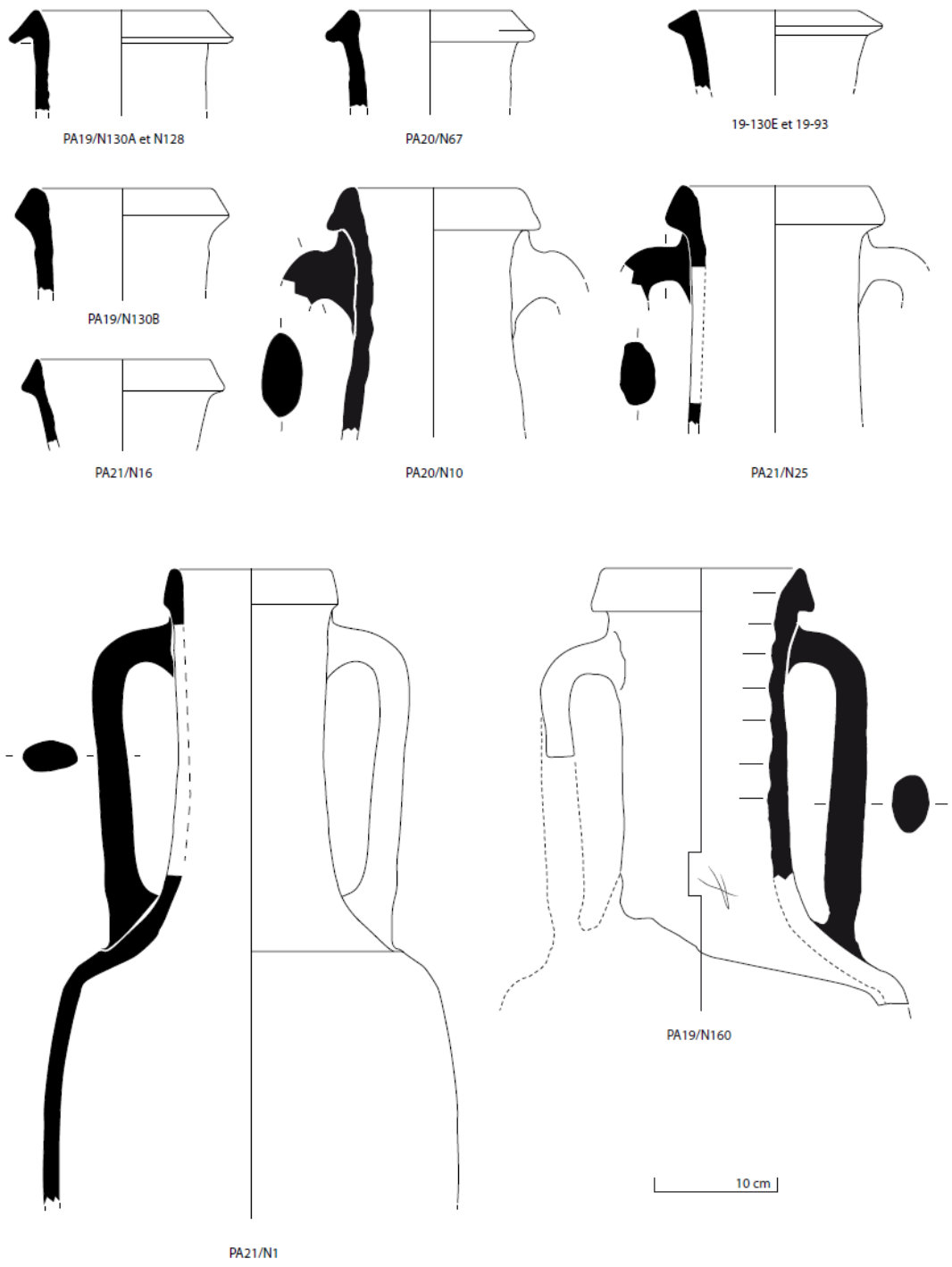

Figure 3: Ilovik-Paržine 1 shipwreck. Greco-Italic amphoras (drawings: L. Cavassa, V. Dumas CNRS/CCJ).

Figure 4

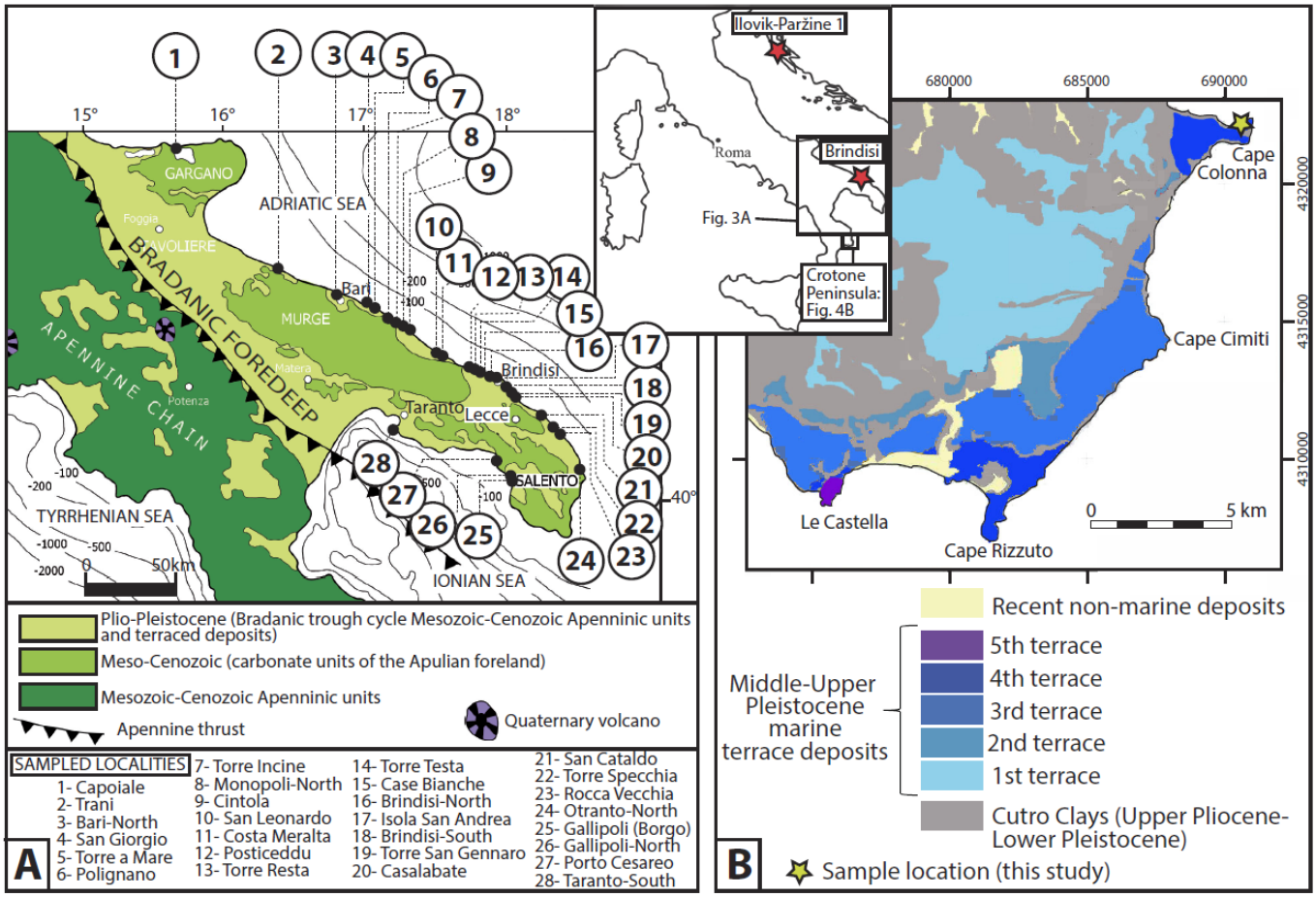

Figure 4: **A:** Simplified geological map of southern Italy (modified from Milli *et al*., 2017) and location of studied outcrops; **B:** Geological map of the southern Crotone Peninsula (modified from Bracchi *et al*., 2014) showing the distinct Pleistocene marine terraces; the yellow star indicates the location of the rock samples analysed in the present work.

Figure 5

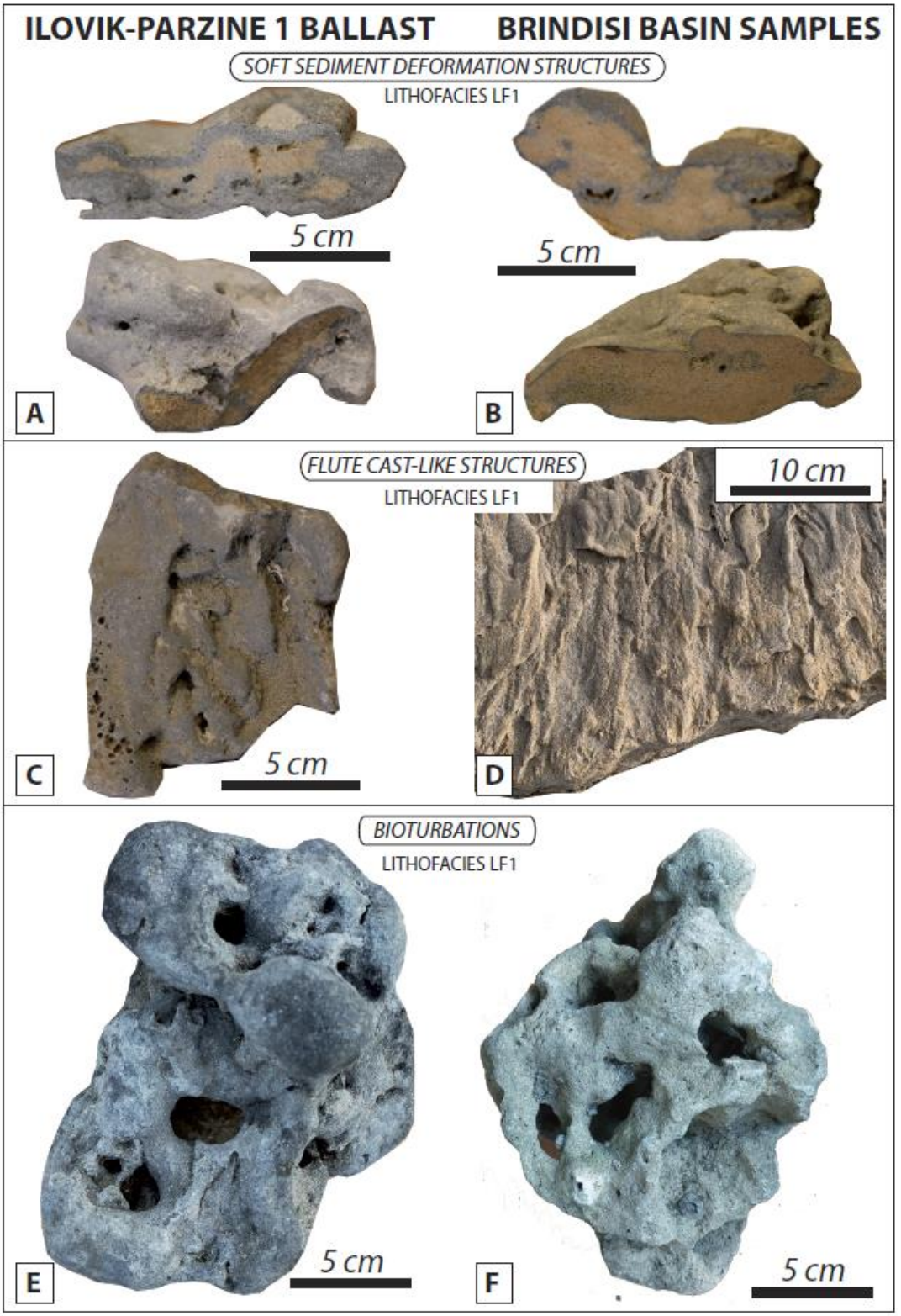

Figure 5: Comparison of depositional, diagenetic and deformation features evidenced in tightly cemented quartzose grainstones (lithofacies LF1) from the Ilovik-Paržine 1 ballast stones and Middle-Upper Pleistocene deposits from the Brindisi basin. **A** and **B**: Soft sediment deformation structures from a ballast stone (**A**) and from Torre San Gennaro (**B**); **C** and **D**: Coalescent oriented concretions (fluid circulation-related cementation features) from the ballast (**C**) and from Torre Testa section (**D**); **E** and **F**: bioturbations from the ballast (**E**) and from Case Bianche (**F**). The location of sampled localities is given in **Fig. 2A**.

Figure 6

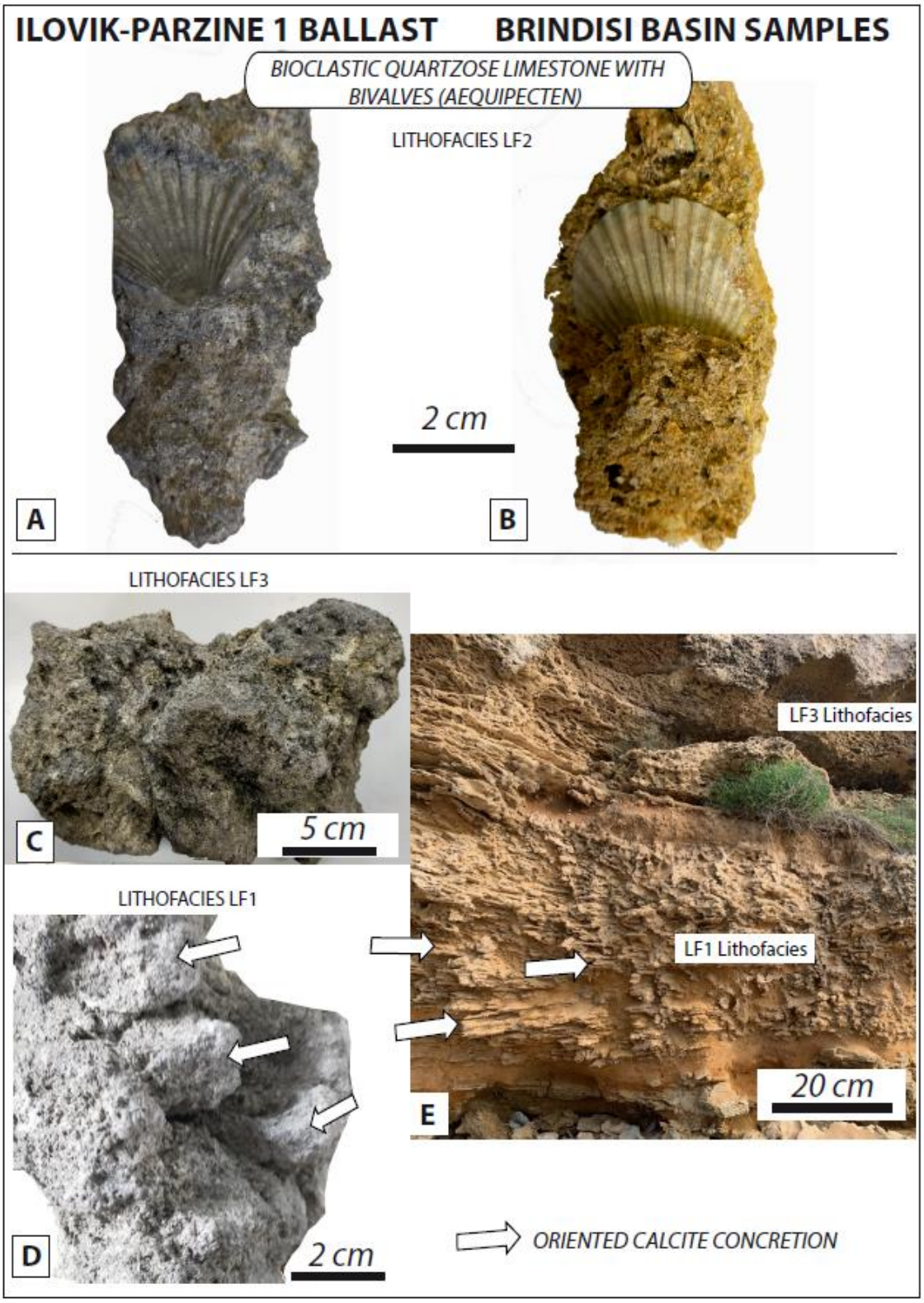

Figure 6: Comparison of rock samples from the Ilovik-Paržine 1 ballast stones and Middle-Upper Pleistocene deposits from the Brindisi basin. **A** and **B**: samples of bioclastic floatstones (lithofacies LF2) showing valves of Aequipecten from the ballast (**A**) and Case Bianche section (**B**); **C**: ballast stone of massive, weakly cemented quartzose grainstone (lithofacies LF3); **D**: ballast stone of tightly cemented quartzose grainstone (LF1) showing elongated, oriented calcite cementation features; **E**: view of the Torre Testa section showing in the lower part quartzose grainstone (LF1) with elongated, oriented calcite cementation features (white arrow) and in the upper part massive, quartzose grainstones and grainstones (LF3). The location of sampled localities is given in **Fig. 2A.**

Figure 7

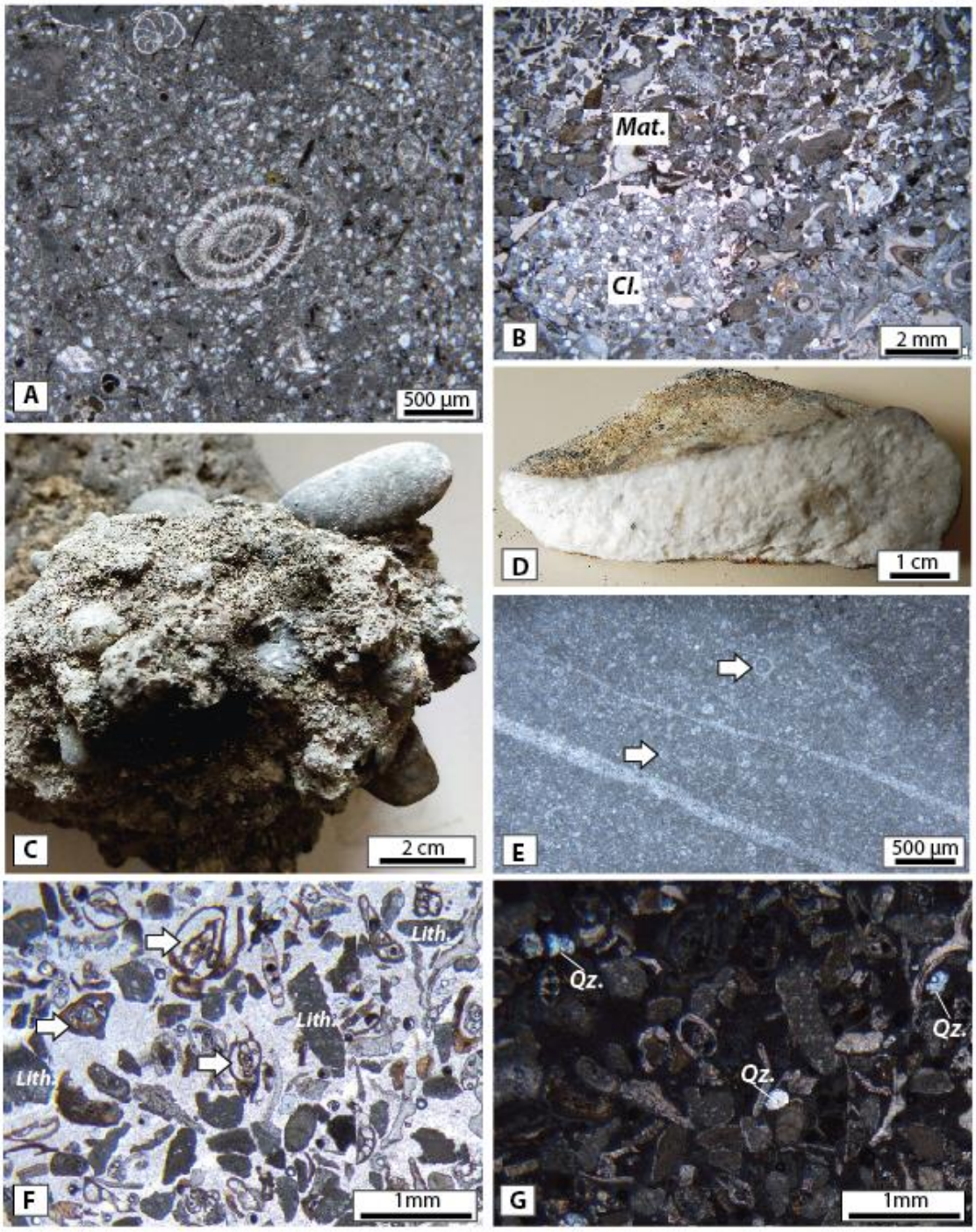

Figure 7: A: Thin-section micro-photograph of a quartzose foraminiferal wackestone-packstone (microfacies MF5) from a ballast stone of lithofacies LF4; **B**: Thin-section micro-photograph of the conglomerate LF5 showing a tightly cemented clast of quarztose grainstone (*Cl.*) encased in a porous, weakly indurated coralline algal and foraminiferal sand matrix (*Mat*.); **C:** Ballast stone of a conglomerate showing LF1 dark pebbles set in weakly indurated sand matrix (lithofacies LF5); **D**: Piece of white limestone samples among the ballast, of probable local origin (lithofacies LF6); note the beige-orange patina (top side of sample) contrasting with the blackish patina of dominant elements of the ballast.; **E**: Thin-section micro-photograph of a LF6 limestone showing a fractured calcispheres-rich (white arrow) wackestone-packstone (MF6 microfacies); **F** and **G**: Thin-section micro-photograph under polarized-light (**F**) and polarized-analysed light (**G**) of a local sand sampled underwater at the vicinity of the wreckship; the sediment is characterized by abundant miliolids (white arrows) and by the scarcity of quartz grains (*Qz*.).

Figure 8

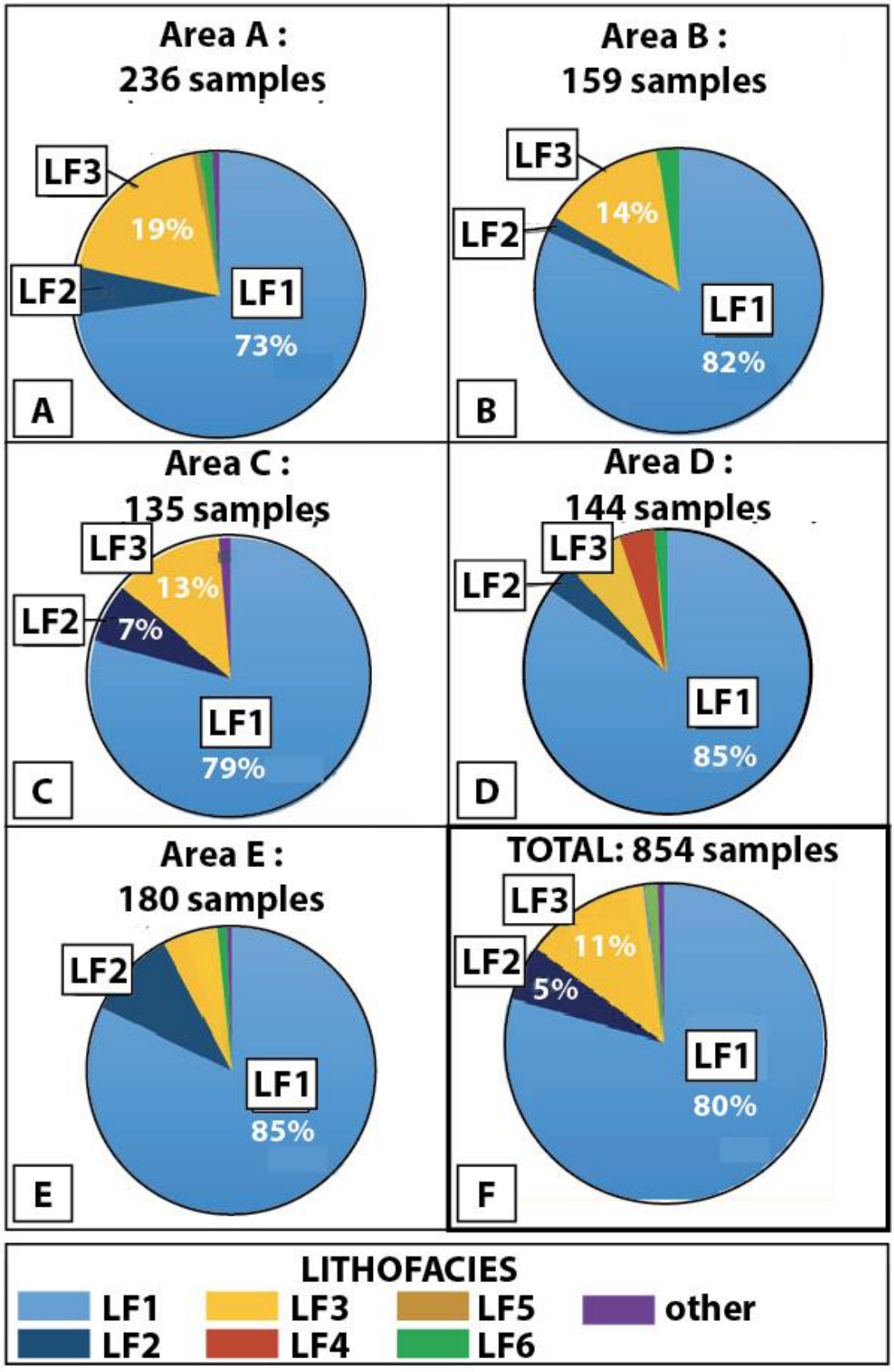

Figure 8: Lithofacies composition of the ballast as a function of the area of sampling (**A-E**) and lithofacies composition of all sampled ballast stones (**F**). The different areas of sampling are indicated in **Fig 2A**.

Figure 9

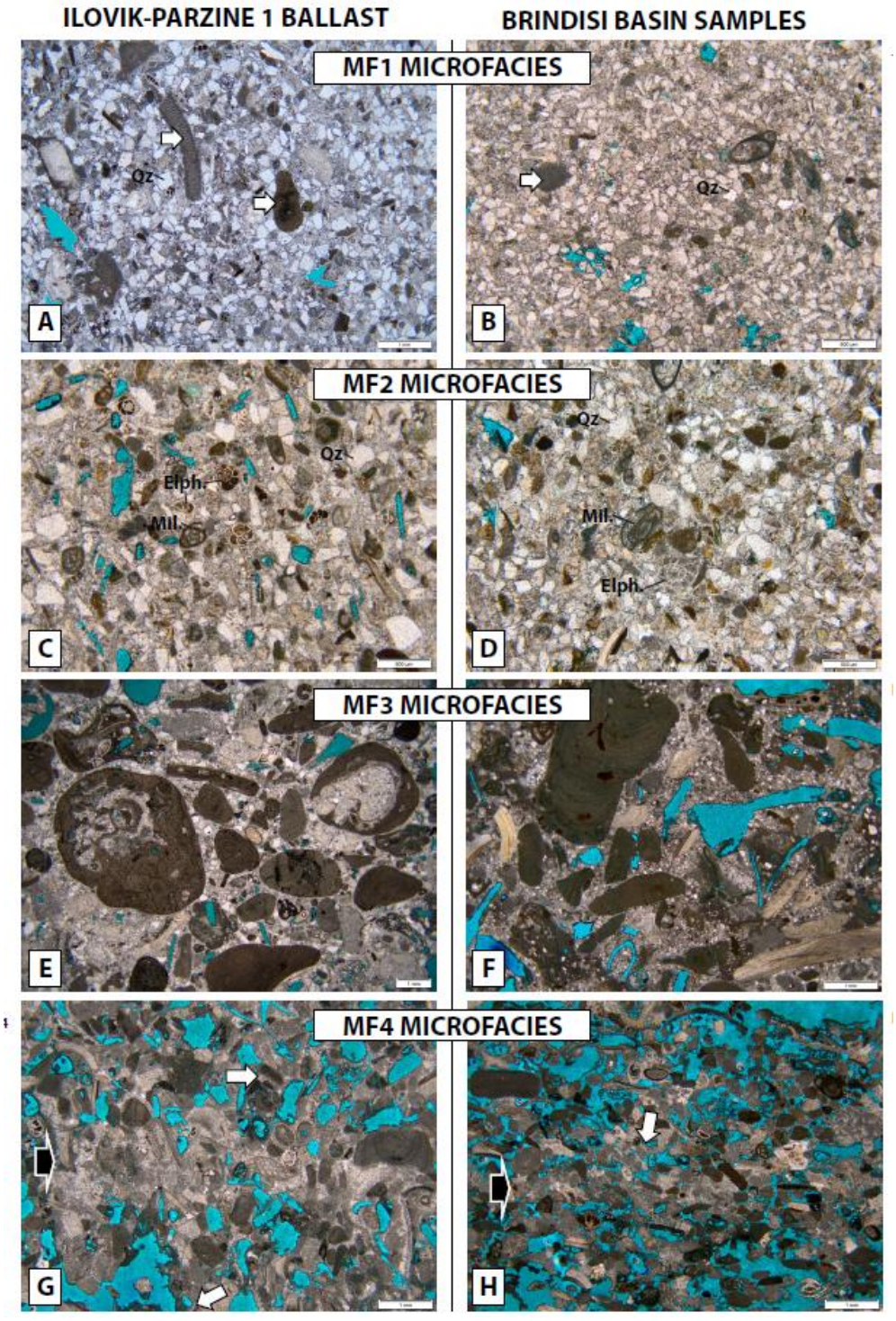

Figure 9: Thin-section micro-photographs of microfacies from LF1, LF2 and LF3 lithofacies of the ballast stones and of the Middle to Upper Pleistocene terrace deposits from the Brindisi basin. Blue areas represent macropores (methylene blue staining of the resin). **A** and **B**: bioclastic quartzarenite (microfacies MF1) with a dominance of angular quartz grains (*Qz*) together with fragments of bioclasts including coralline algae (white arrow); the intergranular space is occupied by a fine mosaic of equant sparry to microsparry calcite cements; **A**: sample KI_4 from the ballast; **B**: sample TR_TST_6 from Torre Testa section. C and D: bioclastic quartzose grainstone (microfacies MF2) with angular to subangular quartz grains (*Qz*), benthic foraminifers including miliolids (*Mil*) and Elphidium (*Elph*.), coralline algae (*Cor*.); the intergranular space is occupied by a fine mosaic of equant sparry to microsparry calcite cements. C: sample 2020C from the ballast; **D**: sample POD_2 from Posticeddu section. **E** and **F**: Rhodolithic-molluscan floatstone with quartz-rich bioclastic packstone-grainstone matrix (microfacies MF3); Cor.: coralline algae. **E**: sample AC_6 from the ballast; **F**: sample POD_1 from Posticeddu section. **G** and **H**: bioclastic grainstone (microfacies MF4) with coralline algae (*Cor*.), benthic foraminifers including Elphidium (*Elph*.). A fine mosaic of sparry calcite cements occludes the intergranular pore space along selected laminae (black arrow) or around grain contacts (meniscus cements: white arrow). **G**: sample KI_14 from the ballast; **H**: sample BR_N_1 from Brindisi North (Punta del Serrone) section.

Figure 10

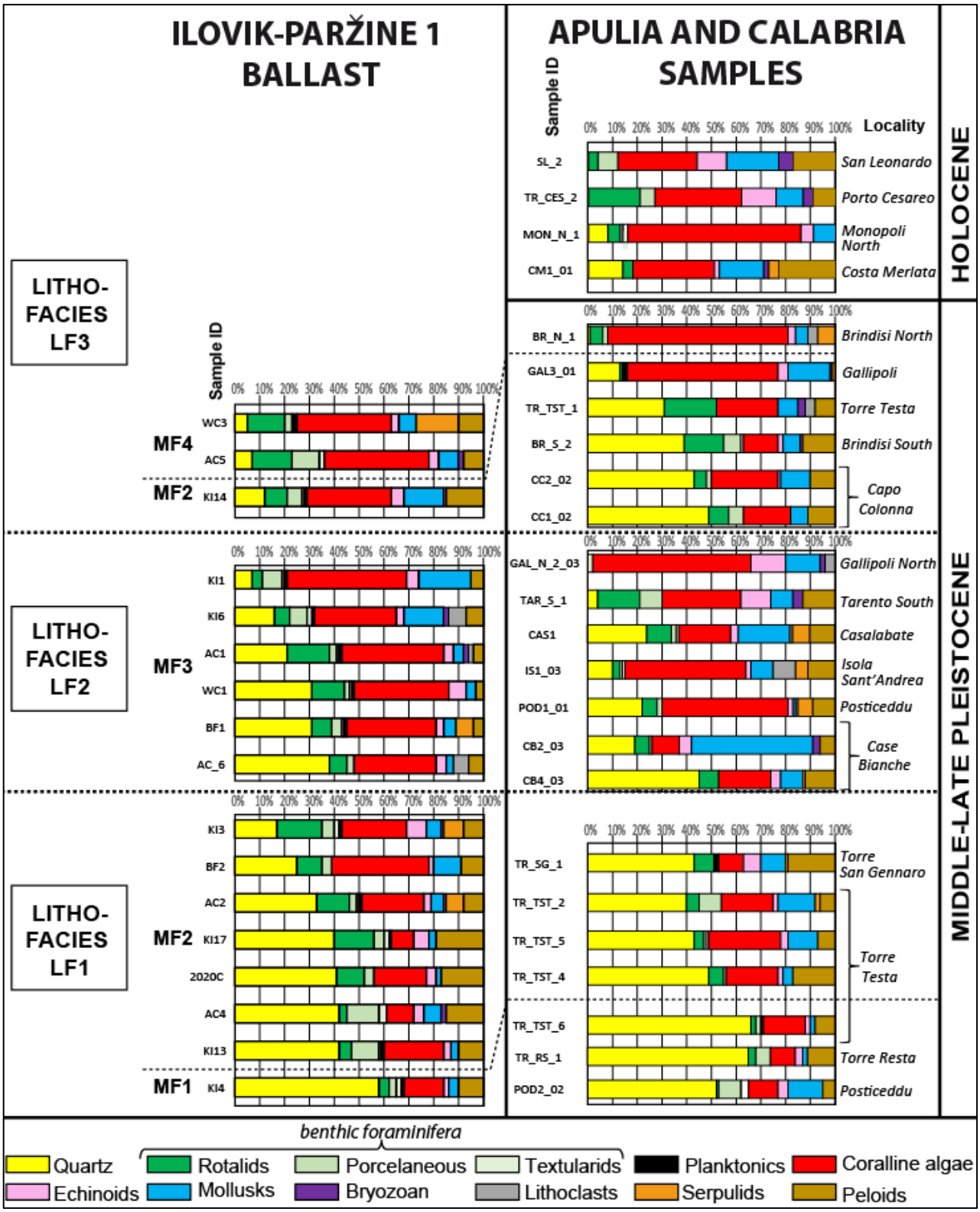

Figure 10: Composition of sand-sized (63 µm – 2 mm) grains in lithofacies LF1, LF2 and LF3 from the Ilovik-Paržine 1 ballast and from Middle to Upper terrace deposits from various outcrops of Adriatic and Ionian Apulia and Ionian Calabria.

Figure 11

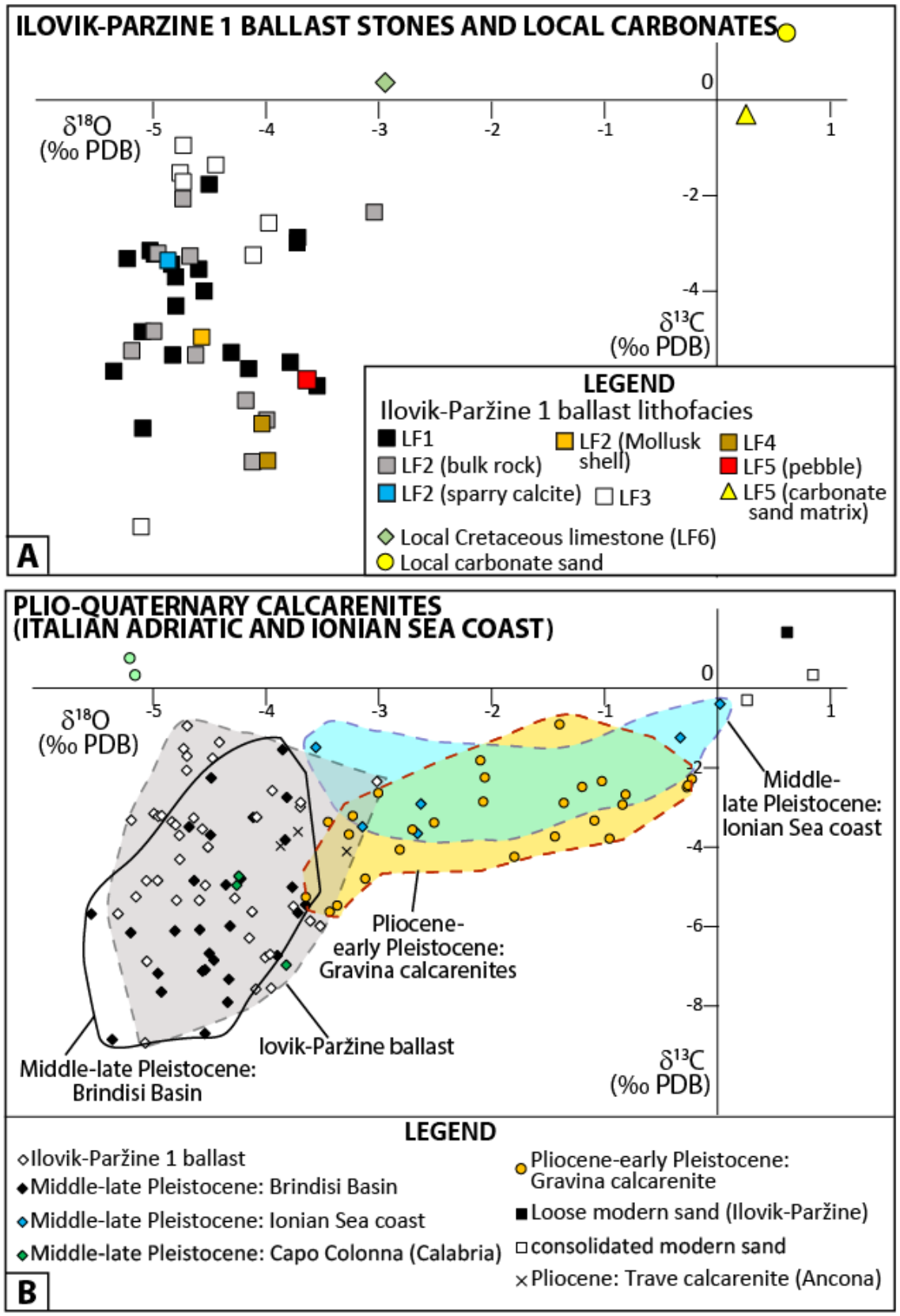

Figure 11: Carbon and oxygen isotope signatures of carbonates the Ilovik-Paržine 1 ballast stones and from various Plio-Quaternary carbonate rocks from Adriatic and Ionian Apulia and Ionian Calabria. **A**: $d^{13}C$ vs $d^{18}O$ crossplot for the Ilovik-Paržine 1 ballast stones with measurements of local carbonate sand and Cretaceous limestone. . **B**: $d^{13}C$ vs $d^{18}O$ crossplot for Plio-Quaternary calcarenitic deposits from the Italian coast of the Adriatic and Ionian seas, superimposed with values from the Ilovik-Paržine 1 ballast.

Figure 12

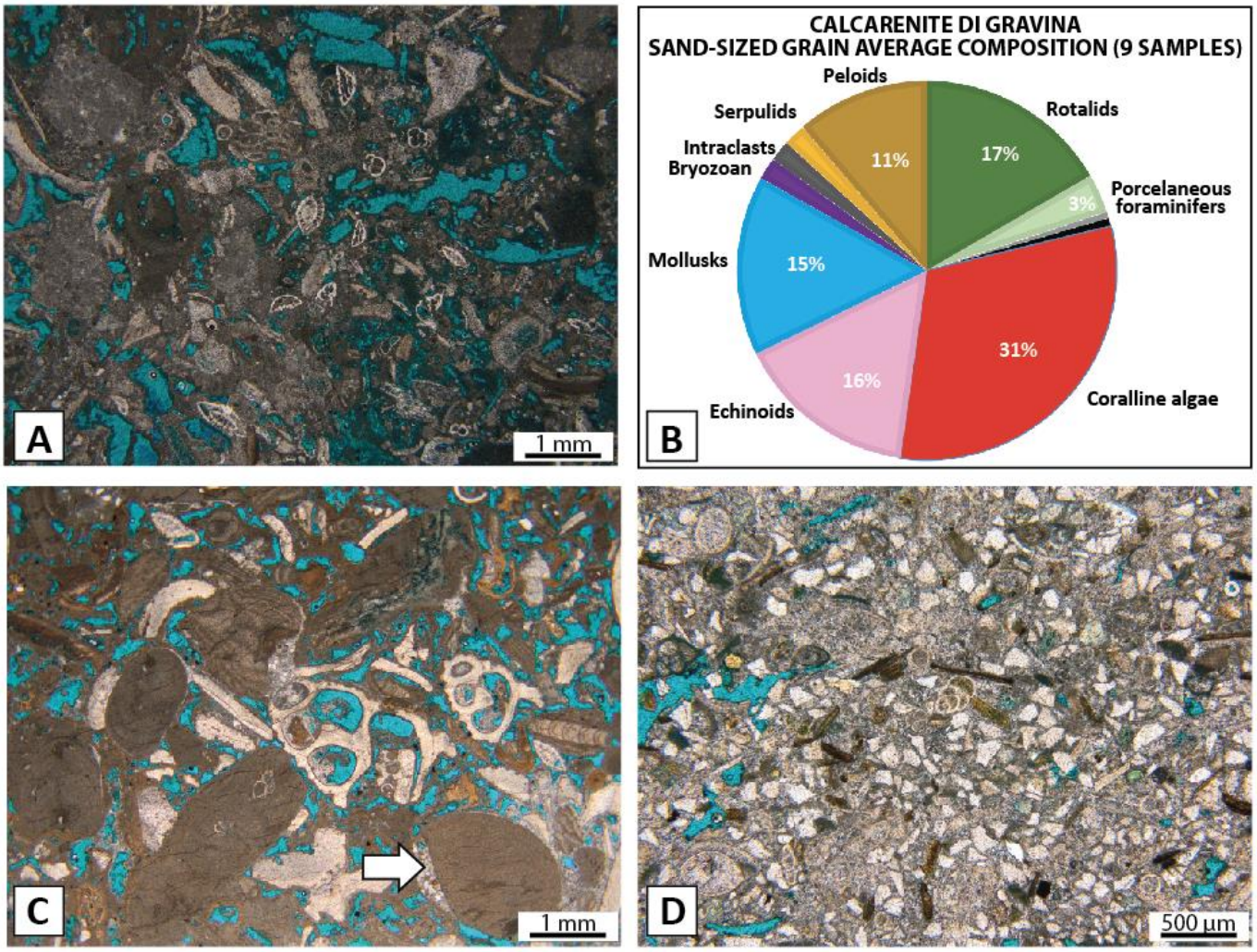

Figure 12: A: Thin-section micro-photographs of an Upper Pliocene to Lower Pleistocene grainstone (Calcarenite di Gravina formation) from the Adriatic Apulian coast (Torre Incine section); **B:** Sand-sized grain average composition of the samples from the Calcarenite di Gravina formation formation analysed in the present work (9 samples). **C:** Thin-section micro-photographs of a coralline algal-molluscan floatstone-rudstone from Middle to Upper Pleistocene terrace deposits of Ionian Apulia (Gallipoli-North section). **D:** tightly cemented quartzose grainstone with coralline algal fragments and benthic foraminifers (microfacies MF2) from Middle to Upper Pleistocene terrace deposits of the Crotone Peninsula, Cape Colonna.

Figure 13

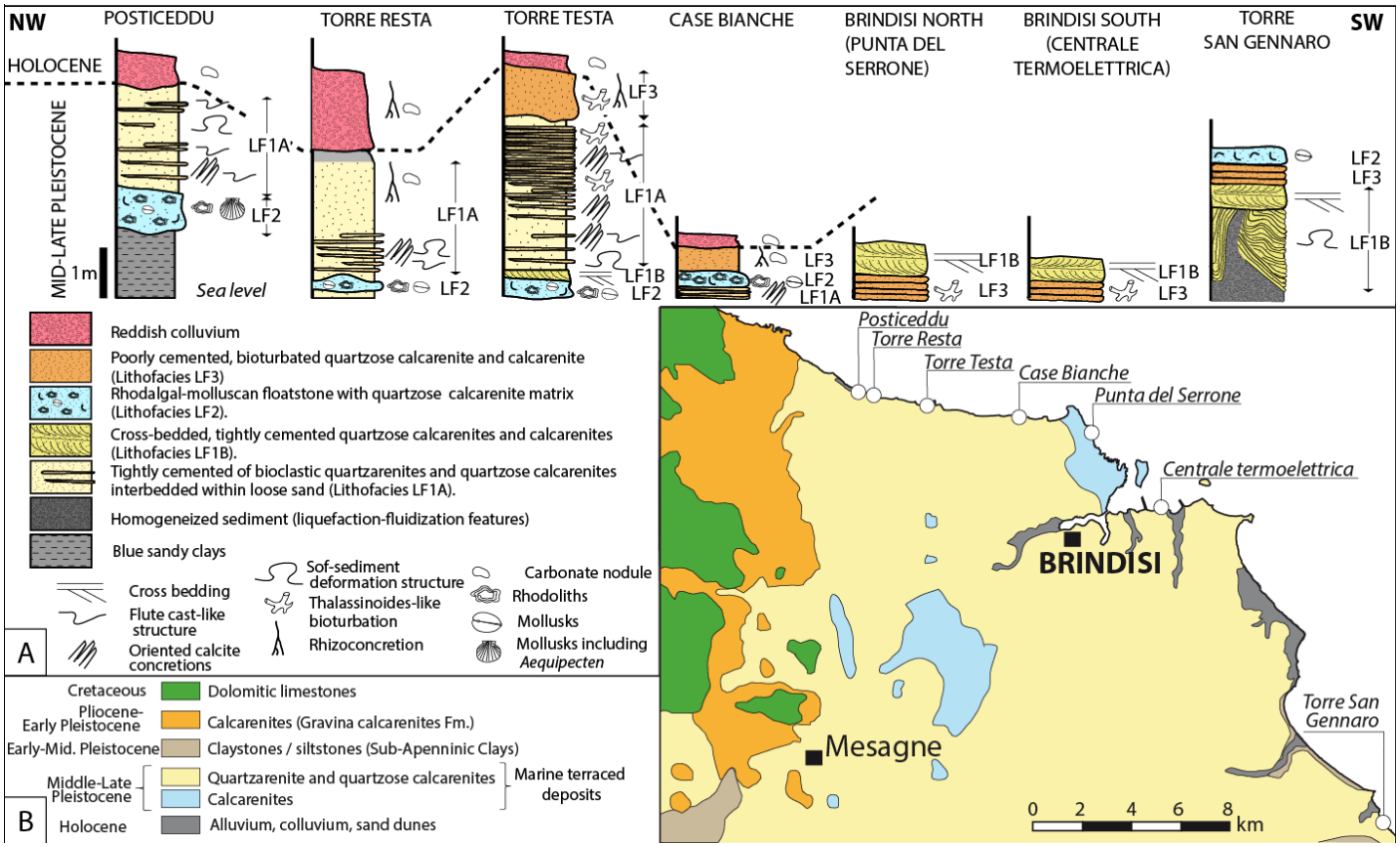

Figure 13: The Brindisi basin: **A:** lithologic and sedimentologic log sections for selected coastal outcrops; **B:** Simplified geological map of the Brindisi basin (modified after Cotecchia, 2014; and Pastore *et al*., 2023).

Figure 14

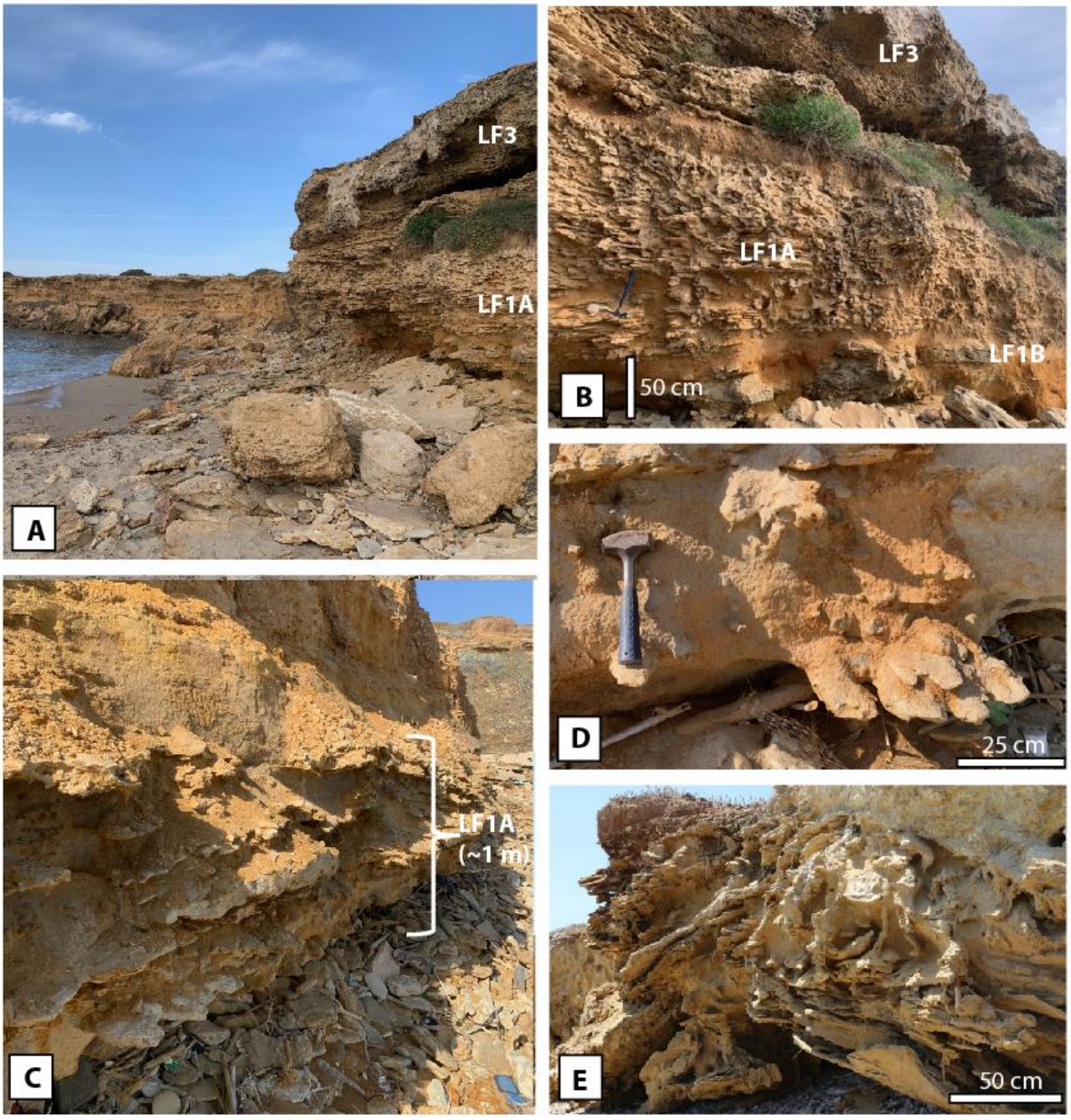

Figure 14: Photographs of coastal outcrops from the Brindisi Basin (see location on Fig.4A). **A:** Torre Testa section showing the vertical succession of lithofacies LF1 (quartzose grainstones and quartzarenites with oriented calcite concretions) and LF3 (massive, weakly cemented quartzose grainstones and grainstones). A mixture of boulders with angular edges (lithofacies LF3) fallen from the top the cliff and rolled pebbles/cobbles (LF1 and LF2 lithofacies dominantly) resulting from the marine erosion of the cliff, lie on the beach and at the foot of the cliff. **B:** closer view of Torre Testa section showing in the lower part of the cliff the oriented calcite concretions within LF1A lithofacies. **C:** Torre Resta cliff showing in its lower part lenses of tightly cemented quartzose grainstones (LF1 lithofacies) embedded within very-fine grained loose sand. **D:** Torre Resta: detail of a cemented quartzose grainstone lens showing elongated, oriented structures (oriented calcite concretions). **E:** Torre San Gennaro: macro-scale soft-sediment deformation structures affecting partly cemented quartzose grainstones (LF1B).

LITHOFACIES	Microfacies				Macro-scale features						
	MF1	MF2	MF3	MF4	flute-cast-like structures	Oriented calcite concretions	soft-sediment deformation features	mollusk accumulations	rhodoliths	bioturbations	cross-bedding
LF1A: Tightly cemented bioclastic quartzarenite and quartzose calcarenite with oriented calcite concretions	X	X			X	X	X			X	
LF1B: Cross-bedded, tightly cemented quartzose calcarenite and calcarenite		X		X			X				X
LF2: Rhodalgal-molluscan floatstone with quartzose calcarenite matrix			X					X	X		
LF3: Poorly cemented, bioturbated quartzose calcarenite and calcarenite		X		X						X	

Table 1: Depositional and diagenetic features of lithofacies LF1, LF2 and LF3

	Ilovik-Parzine ballast stones	Terraced deposits of the Brindisi Basin
Age	Planktic foraminiferal biostratigraphy: Pleistocene (after 1,28 Ma) to Holocene" Sr isotope stratigraphy: younger than 500 ka (Middle Pleistocene to Holocene)	Middle to Late Pleistocene (Ciaranfi et al., 1988; Margiotta et al., 2010; Mastronuzzi et al., 2011)
Lithofacies association	LF1A: Tightly cemented bioclastic quartzarenite and quartzose calcarenite with oriented calcite concretions (80% of the studied ballast) LF2: Rhodalgal-molluscan floatstone with quartzose calcarenite matrix (5% of the studied ballast) LF3: Poorly cemented, bioturbated quartzose calcarenite and calcarenite (11% of the studied ballast) LF4: quartzose calcisistite (<1% of the studied ballast). LF5: conglomerates with quartzose calcarenite matrix (likely to be formed locally) (~1% of the studied ballast). LF6: tight, fractured limestones (Local limestones) (~1% of the studied ballast).	LF1A: Tightly cemented bioclastic quartzarenite and quartzose calcarenite with oriented calcite concretions (Middle to Upper Pleistocene) LF1B: Cross-bedded, tightly cemented quartzose calcarenite and calcarenite (Middle to Upper Pleistocene) LF2: Rhodalgal-molluscan floatstone with quartzose calcarenite matrix (Middle to Upper Pleistocene) LF3: Poorly cemented, bioturbated quartzose calcarenite and calcarenite (Middle to Upper Pleistocene and Holocene)
Sedimentary / diagenetic structures	Bioturbations, elongated-oriented calcite concretions	Bioturbations, cross bedding, elongated-oriented calcite concretions
Macrofauna	Occurrence of *Aequipecten*	Occurrence of *Aequipecten* in Posticeddu section (this study) and San Gennaro (Coppa et al., 2001)
Microfacies (in LF1, LF2 and LF3 lithofacies)	MF1: bioclastic quartzarenite; MF2: bioclastic quartzose grainstone; Microfacies MF3: rhodalgal-molluscan floatstone with quartz-rich bioclastic packstone-grainstone matrix; Microfacies MF4: bioclastic grainstone	MF1: bioclastic quartzarenite; MF2: bioclastic quartzose grainstone; Microfacies MF3: rhodalgal-molluscan floatstone with quartz-rich bioclastic packstone-grainstone matrix; Microfacies MF4: bioclastic grainstone
Morphology of quartz sand	angular to sub-angular	angular to sub-angular
Quartz grain size	very fine to fine-grained (63 to 250 µm) in MF1 and MF3; fine to medium-grained (125 to 500 µm) in MF2; medium to coarse-grained (250 µm to 1 mm) in MF4	Fine to medium-grained (125 to 500 µm) in MF1 and MF2; fine grained (125 to 250 µm) in MF3; medium to coarse-grained (250 µm to 1 mm) in MF4.
Benthic foraminiferal association	Dominated by *Elphidium* (*E. macellum* and *E. paraskevaidisi*) and *Neoconorbina terquemi*.	Dominated by *Elphidium* (*E. macellum* and *E. paraskevaidisi*) and *Neoconorbina terquemi*.
Nature of cement	Equant sparry to microsparry calcite	Equant sparry to microsparry calcite
Carbon and oxygen isotope composition	$\delta^{18}O$: from -5.51 to -3.02‰ $\delta^{13}C$: from -8.93 to -0.95‰	$\delta^{18}O$: from -5.55 to -3.65‰ $\delta^{13}C$: from -8.85 to -1.55‰

Table 2: Comparison of the geological and geochemical characteristics of the Ilovik-Paržine 1 ballast stones with the Pleistocene terraced deposits of the Brindisi Basin.

Figure 1

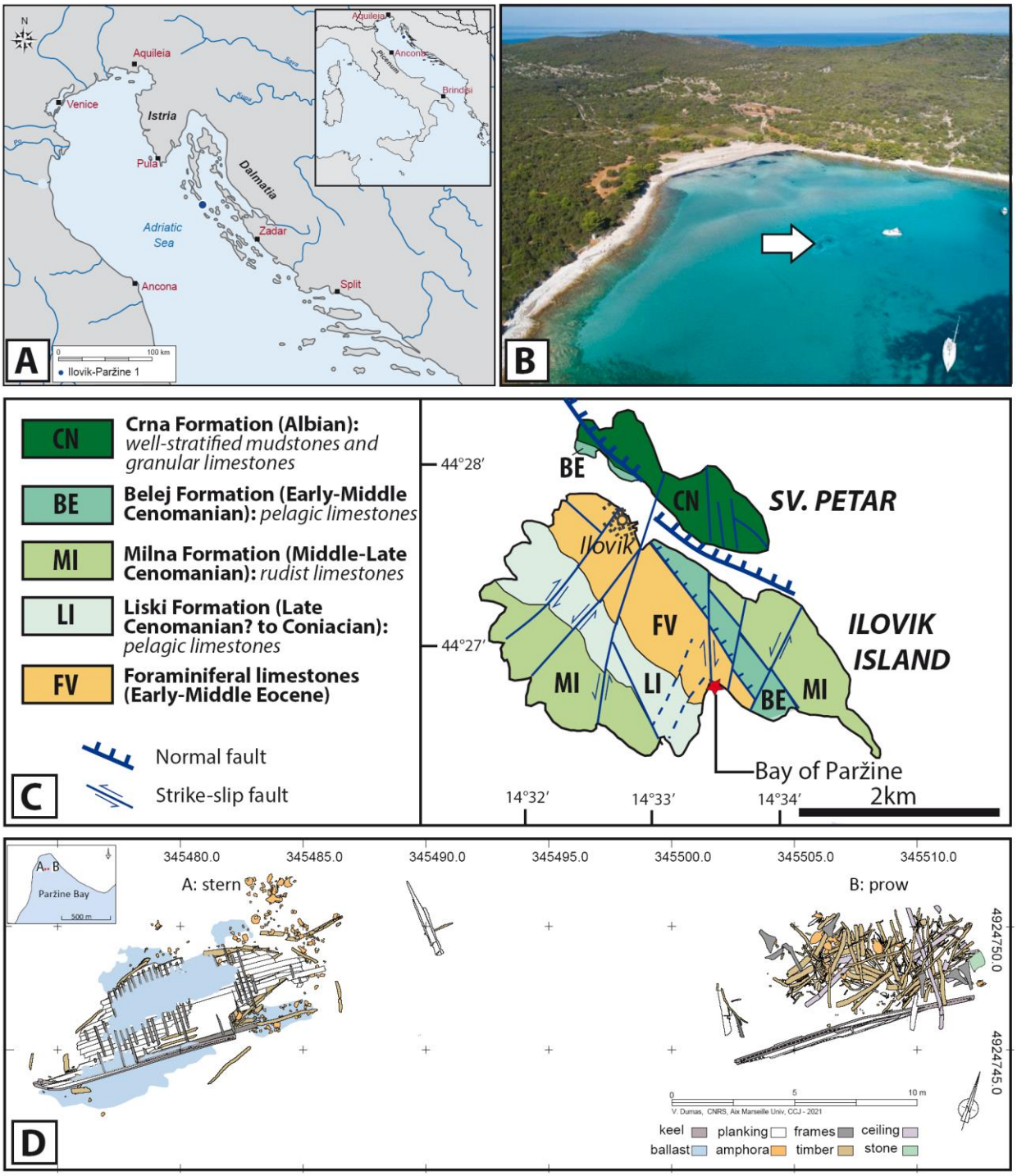

Figure 1: A: Location map of the Ilovik island (drawing: V. Dumas CNRS/CCJ)**; B:** Aerial view of the Bay of Paržine; the white arrow indicates the location of the shipwreck (photograph: L. Damelet CNRS/CCJ); **C:** Geological map of the Ilovik island (modified from Fuček *et al*. (2018) and location of the Bay of Paržine; **D**: Location map of the stern and prow of the Ilovik-Paržine 1 wreck (drawing: V. Dumas CNRS/CCJ).

Figure 2

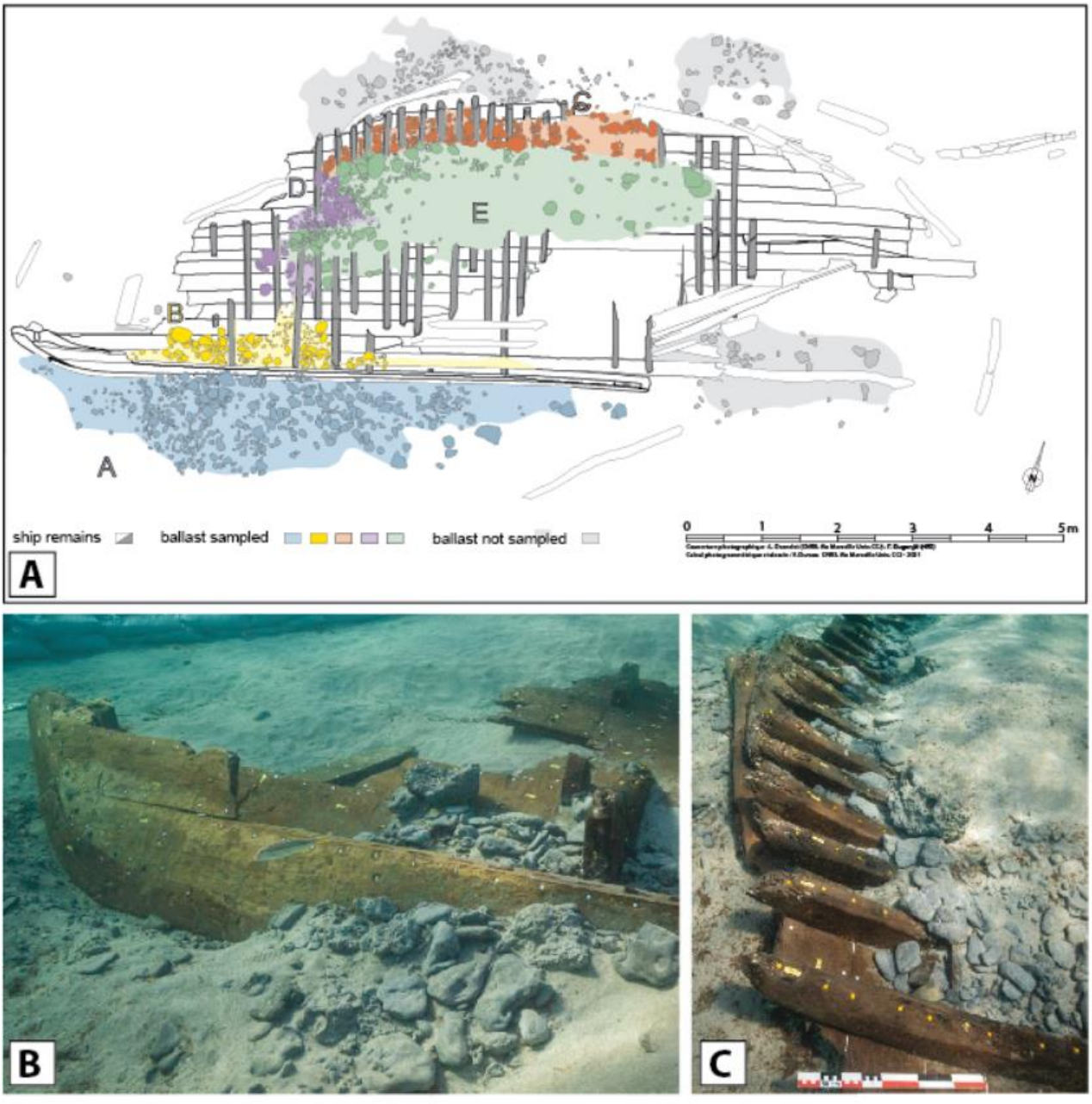

Figure 2: A: Plan of the stern area of the ship with the position of the ballast (drawing: V. Dumas CNRS/CCJ); **B:** View of the ballast spilled out around the sternpost area; **C:** view of the ballast in place between the frames of the port side (photographs: L. Damelet, CCJ-CNRS).

Figure 3

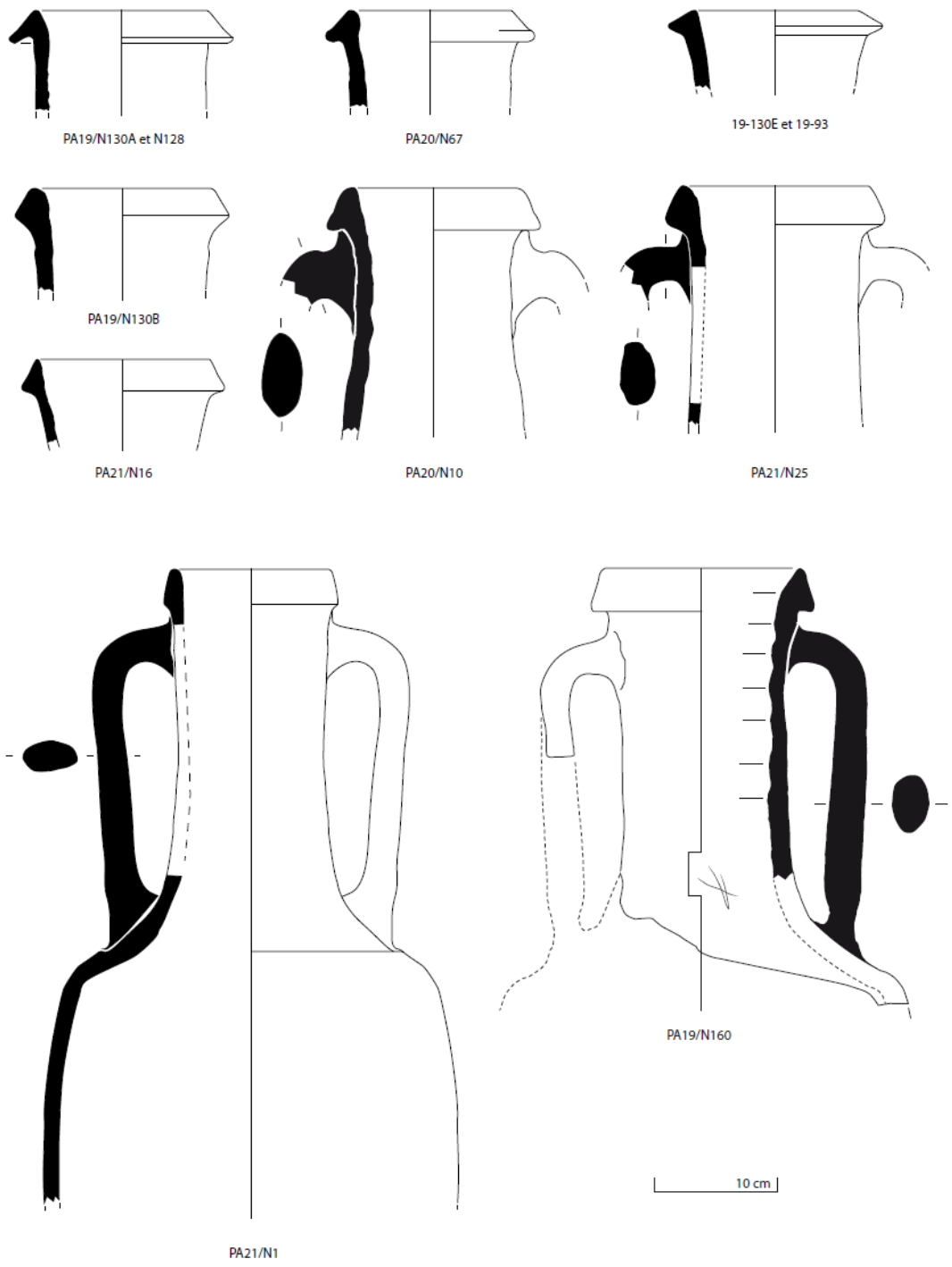

Figure 3: Ilovik-Paržine 1 shipwreck. Greco-Italic amphoras (drawings: L. Cavassa, V. Dumas CNRS/CCJ).

Figure 4

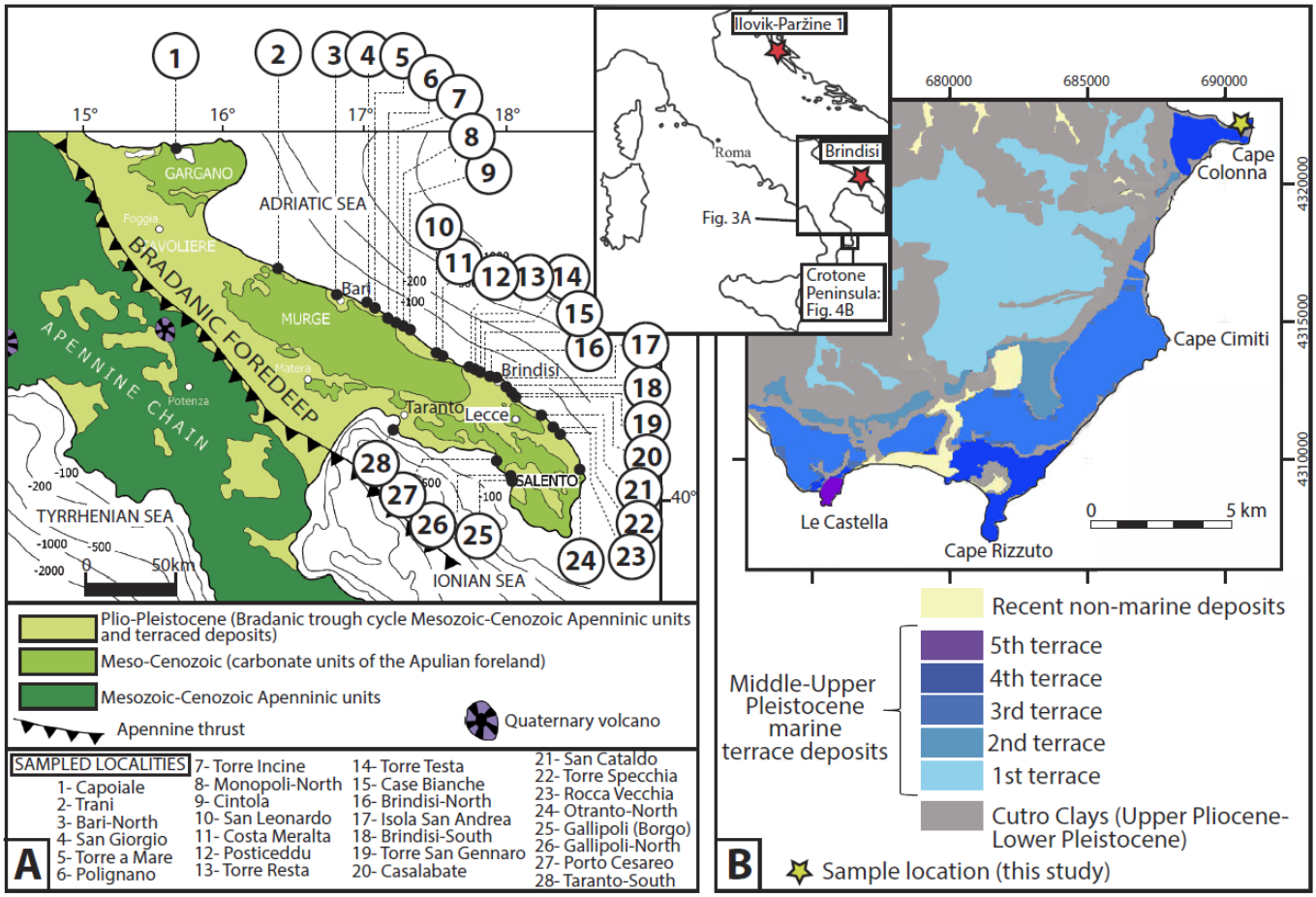

Figure 4: **A:** Simplified geological map of southern Italy (modified from Milli *et al*., 2017) and location of studied outcrops; **B:** Geological map of the southern Crotone Peninsula (modified from Bracchi *et al*., 2014) showing the distinct Pleistocene marine terraces; the yellow star indicates the location of the rock samples analysed in the present work.

Figure 5

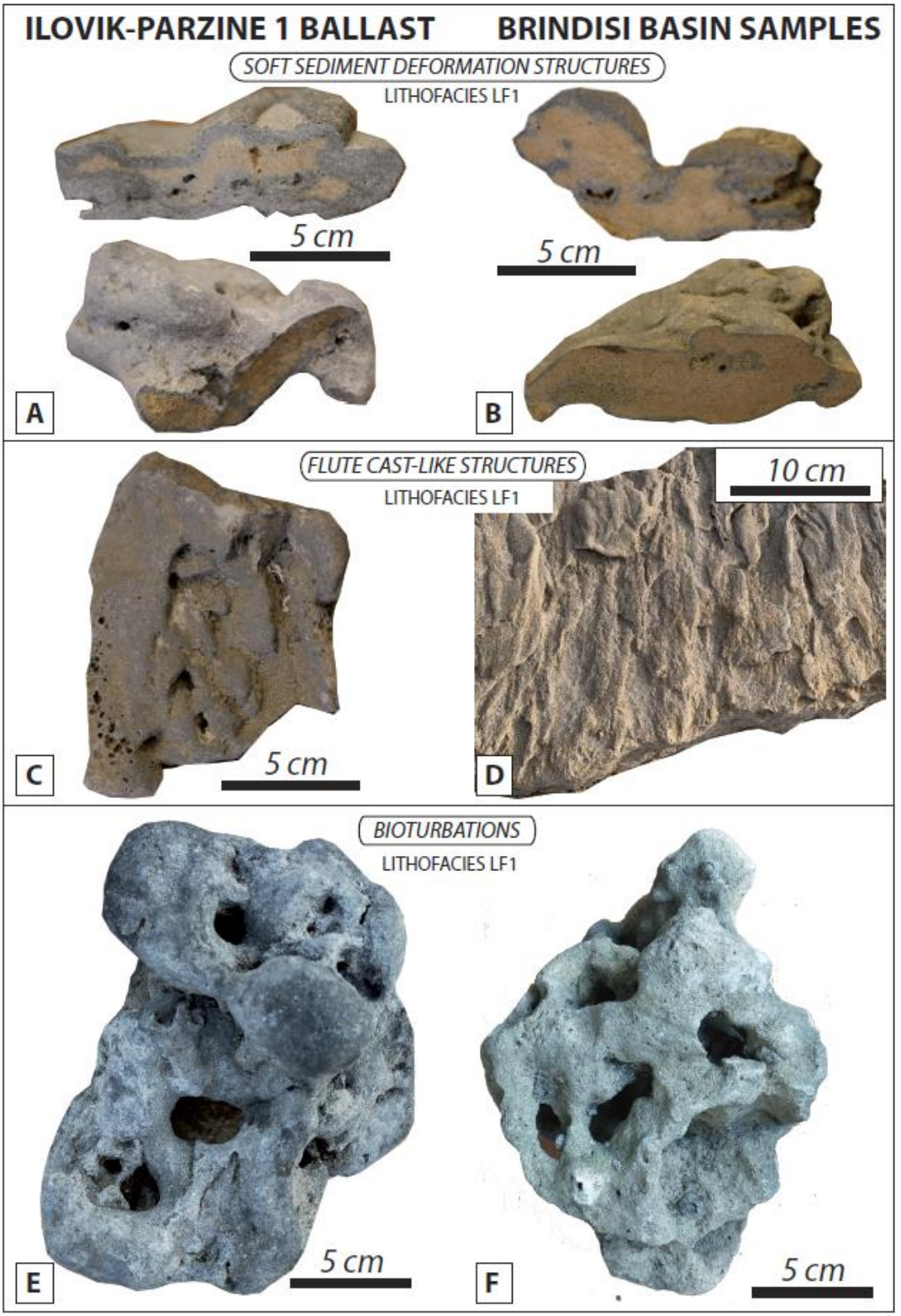

Figure 5: Comparison of depositional, diagenetic and deformation features evidenced in tightly cemented quartzose grainstones (lithofacies LF1) from the Ilovik-Paržine 1 ballast stones and Middle-Upper Pleistocene deposits from the Brindisi basin. **A** and **B**: Soft sediment deformation structures from a ballast stone (**A**) and from Torre San Gennaro (**B**); **C** and **D**: Coalescent oriented concretions (fluid circulation-related cementation features) from the ballast (**C**) and from Torre Testa section (**D**); **E** and **F**: bioturbations from the ballast (**E**) and from Case Bianche (**F**). The location of sampled localities is given in **Fig. 2A**.

Figure 6

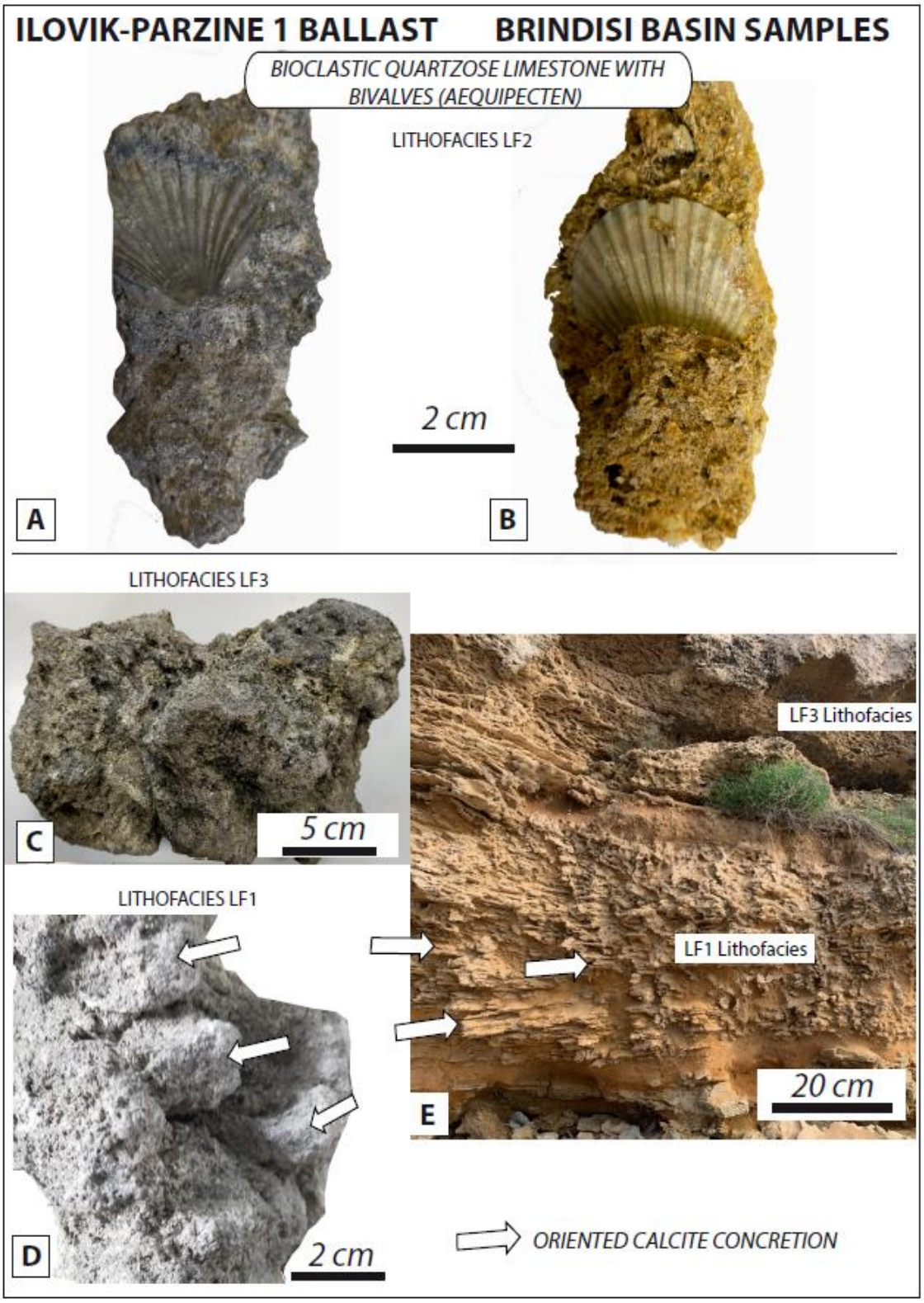

Figure 6: Comparison of rock samples from the Ilovik-Paržine 1 ballast stones and Middle-Upper Pleistocene deposits from the Brindisi basin. **A** and **B**: samples of bioclastic floatstones (lithofacies LF2) showing valves of Aequipecten from the ballast (**A**) and Case Bianche section (**B**); **C**: ballast stone of massive, weakly cemented quartzose grainstone (lithofacies LF3); **D**: ballast stone of tightly cemented quartzose grainstone (LF1) showing elongated, oriented calcite cementation features; **E**: view of the Torre Testa section showing in the lower part quartzose grainstone (LF1) with elongated, oriented calcite cementation features (white arrow) and in the upper part massive, quartzose grainstones and grainstones (LF3). The location of sampled localities is given in **Fig. 2A.**

Figure 7

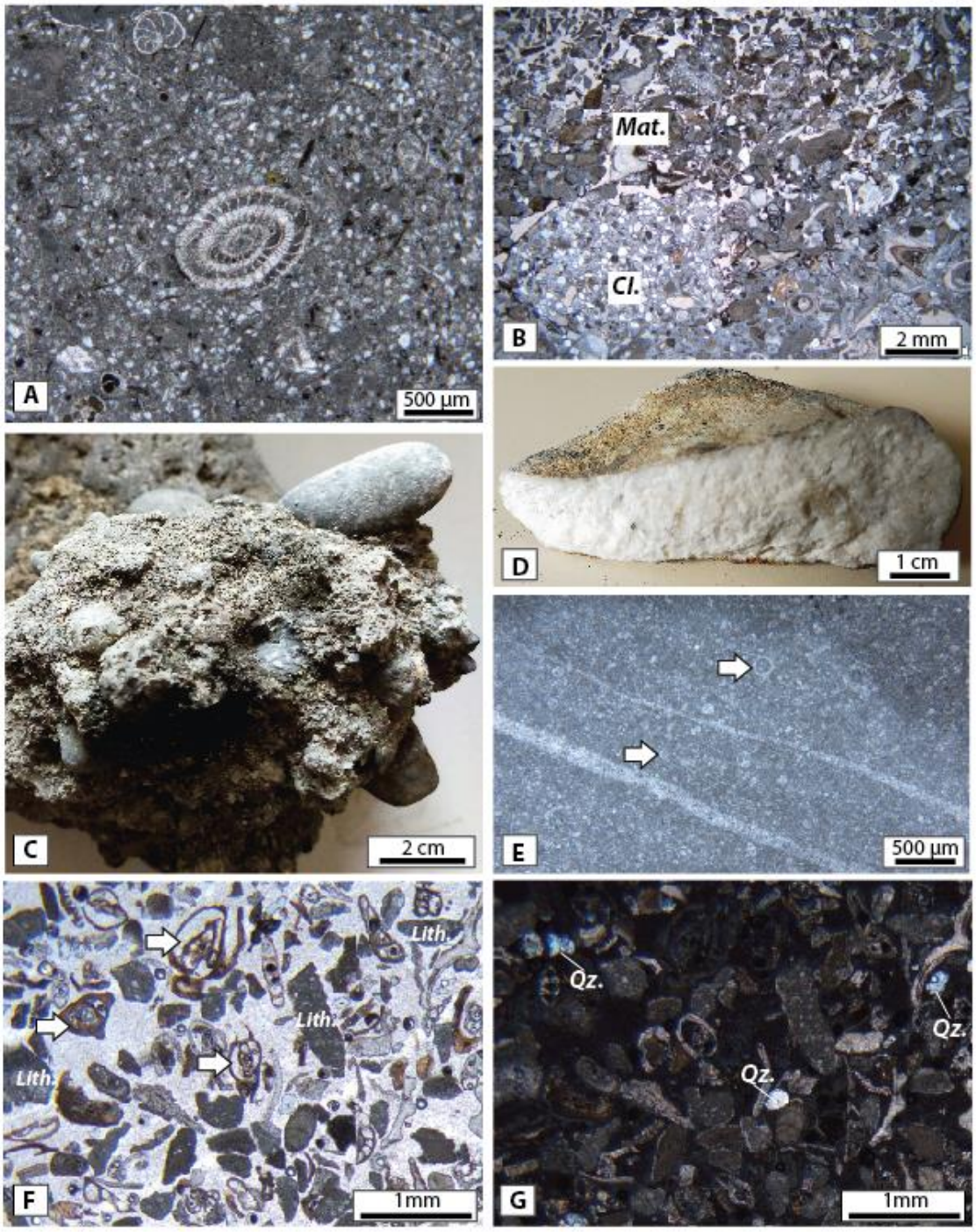

Figure 7: A: Thin-section micro-photograph of a quartzose foraminiferal wackestone-packstone (microfacies MF5) from a ballast stone of lithofacies LF4; **B**: Thin-section micro-photograph of the conglomerate LF5 showing a tightly cemented clast of quarztose grainstone (*Cl.*) encased in a porous, weakly indurated coralline algal and foraminiferal sand matrix (*Mat*.); **C:** Ballast stone of a conglomerate showing LF1 dark pebbles set in weakly indurated sand matrix (lithofacies LF5); **D**: Piece of white limestone samples among the ballast, of probable local origin (lithofacies LF6); note the beige-orange patina (top side of sample) contrasting with the blackish patina of dominant elements of the ballast.; **E**: Thin-section micro-photograph of a LF6 limestone showing a fractured calcispheres-rich (white arrow) wackestone-packstone (MF6 microfacies); **F** and **G**: Thin-section micro-photograph under polarized-light (**F**) and polarized-analysed light (**G**) of a local sand sampled underwater at the vicinity of the wreckship; the sediment is characterized by abundant miliolids (white arrows) and by the scarcity of quartz grains (*Qz*.).

Figure 8

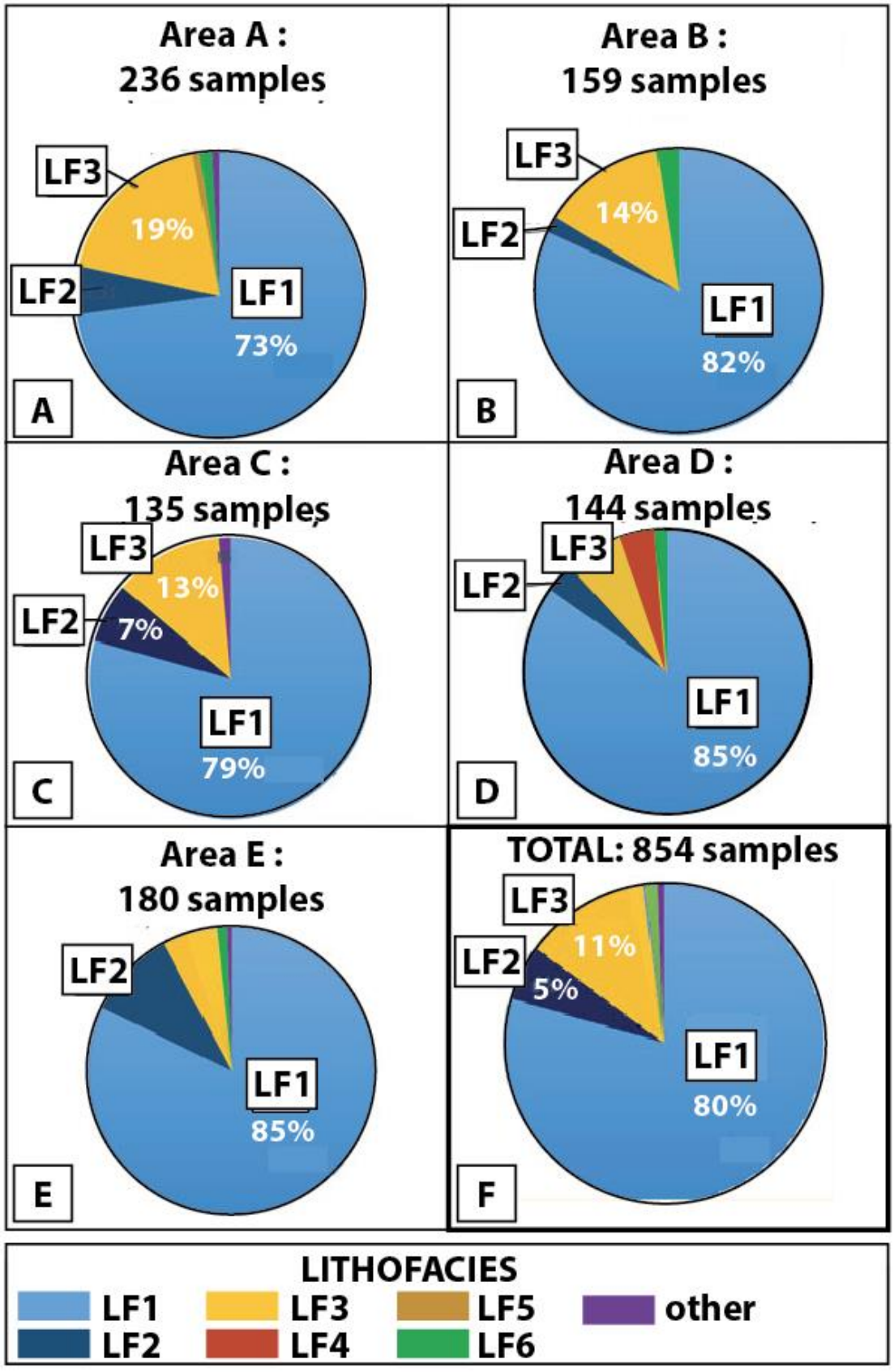

Figure 8: Lithofacies composition of the ballast as a function of the area of sampling (**A-E**) and lithofacies composition of all sampled ballast stones (**F**). The different areas of sampling are indicated in **Fig 2A**.

Figure 9

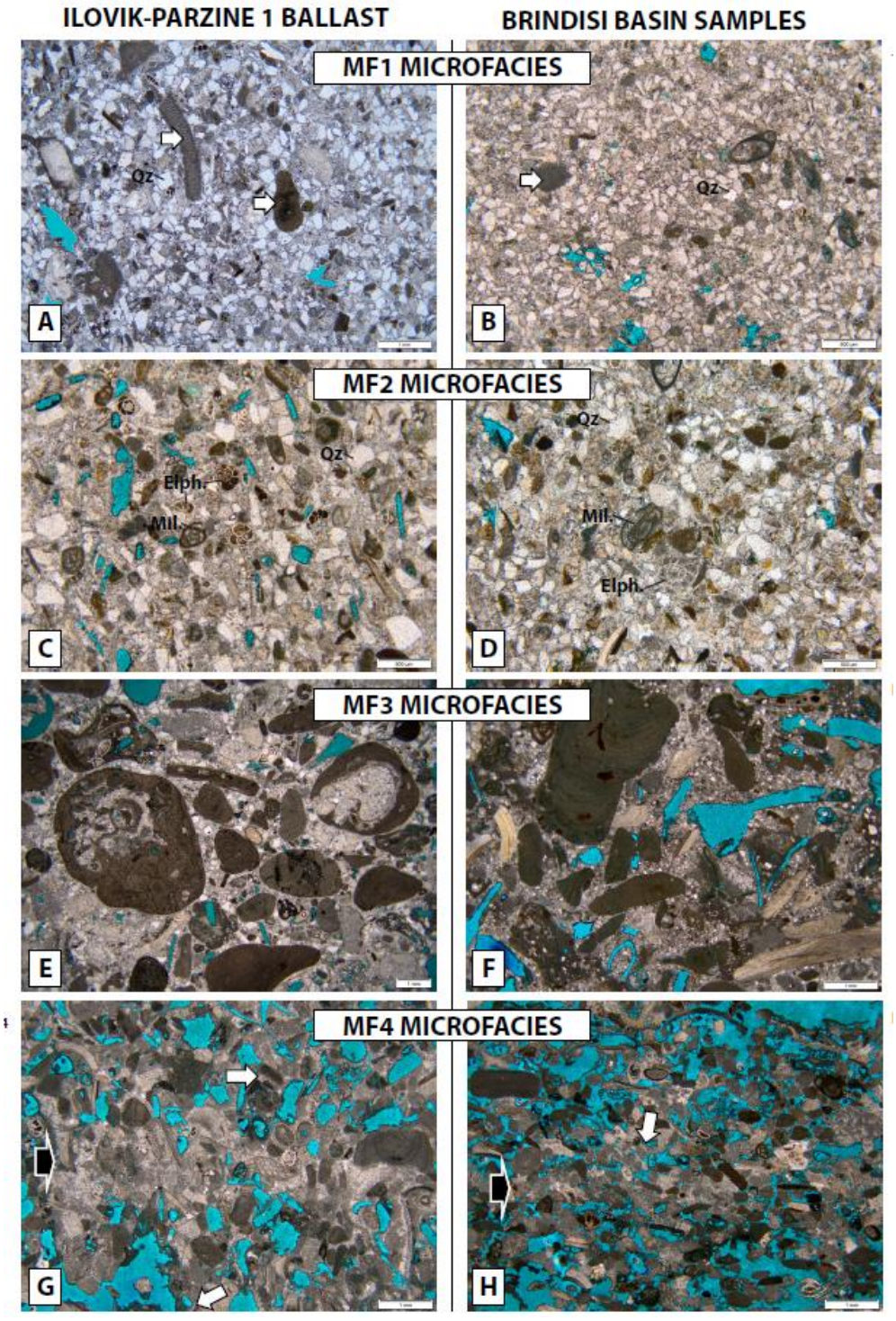

Figure 9: Thin-section micro-photographs of microfacies from LF1, LF2 and LF3 lithofacies of the ballast stones and of the Middle to Upper Pleistocene terrace deposits from the Brindisi basin. Blue areas represent macropores (methylene blue staining of the resin). **A** and **B**: bioclastic quartzarenite (microfacies MF1) with a dominance of angular quartz grains (*Qz*) together with fragments of bioclasts including coralline algae (white arrow); the intergranular space is occupied by a fine mosaic of equant sparry to microsparry calcite cements; **A**: sample KI_4 from the ballast; **B**: sample TR_TST_6 from Torre Testa section. C and D: bioclastic quartzose grainstone (microfacies MF2) with angular to subangular quartz grains (*Qz*), benthic foraminifers including miliolids (*Mil*) and Elphidium (*Elph*.), coralline algae (*Cor*.); the intergranular space is occupied by a fine mosaic of equant sparry to microsparry calcite cements. C: sample 2020C from the ballast; **D**: sample POD_2 from Posticeddu section. **E** and **F**: Rhodolithic-molluscan floatstone with quartz-rich bioclastic packstone-grainstone matrix (microfacies MF3); Cor.: coralline algae. **E**: sample AC_6 from the ballast; **F**: sample POD_1 from Posticeddu section. **G** and **H**: bioclastic grainstone (microfacies MF4) with coralline algae (*Cor*.), benthic foraminifers including Elphidium (*Elph*.). A fine mosaic of sparry calcite cements occludes the intergranular pore space along selected laminae (black arrow) or around grain contacts (meniscus cements: white arrow). **G**: sample KI_14 from the ballast; **H**: sample BR_N_1 from Brindisi North (Punta del Serrone) section.

Figure 10

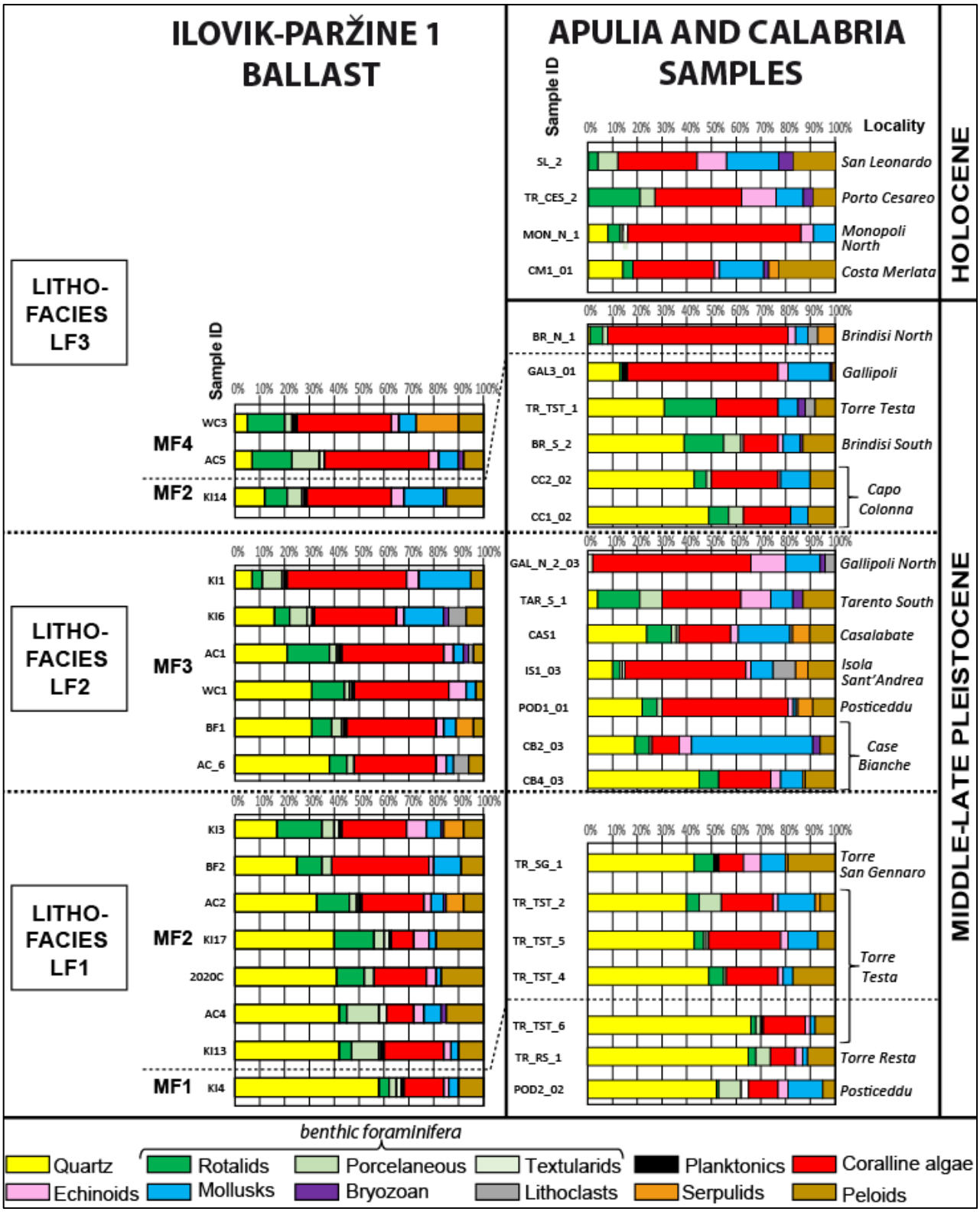

Figure 10: Composition of sand-sized (63 µm – 2 mm) grains in lithofacies LF1, LF2 and LF3 from the Ilovik-Paržine 1 ballast and from Middle to Upper terrace deposits from various outcrops of Adriatic and Ionian Apulia and Ionian Calabria.

Figure 11

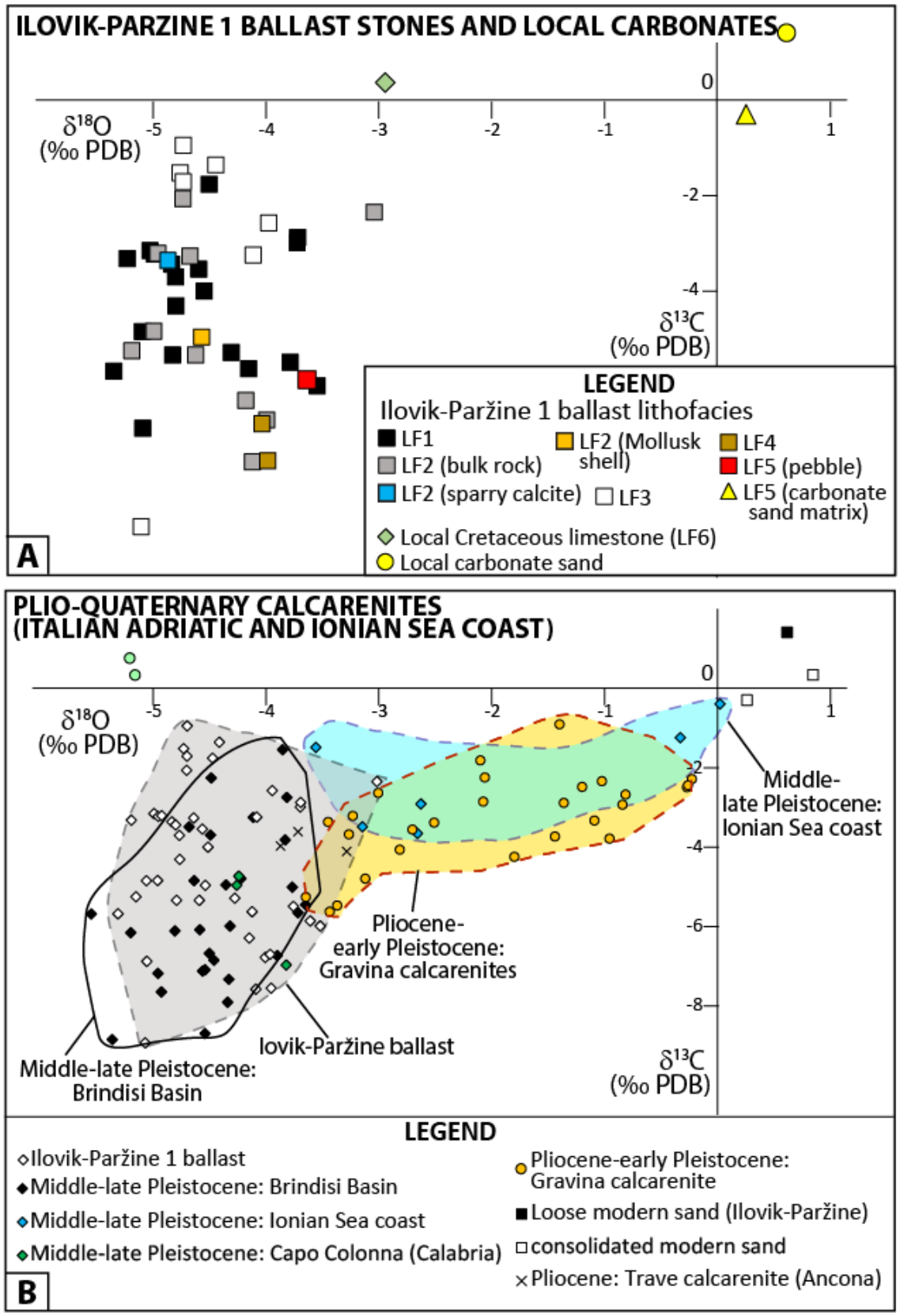

Figure 11: Carbon and oxygen isotope signatures of carbonates the Ilovik-Paržine 1 ballast stones and from various Plio-Quaternary carbonate rocks from Adriatic and Ionian Apulia and Ionian Calabria. **A**: $d^{13}C$ vs $d^{18}O$ crossplot for the Ilovik-Paržine 1 ballast stones with measurements of local carbonate sand and Cretaceous limestone. . **B**: $d^{13}C$ vs $d^{18}O$ crossplot for Plio-Quaternary calcarenitic deposits from the Italian coast of the Adriatic and Ionian seas, superimposed with values from the Ilovik-Paržine 1 ballast.

Figure 12

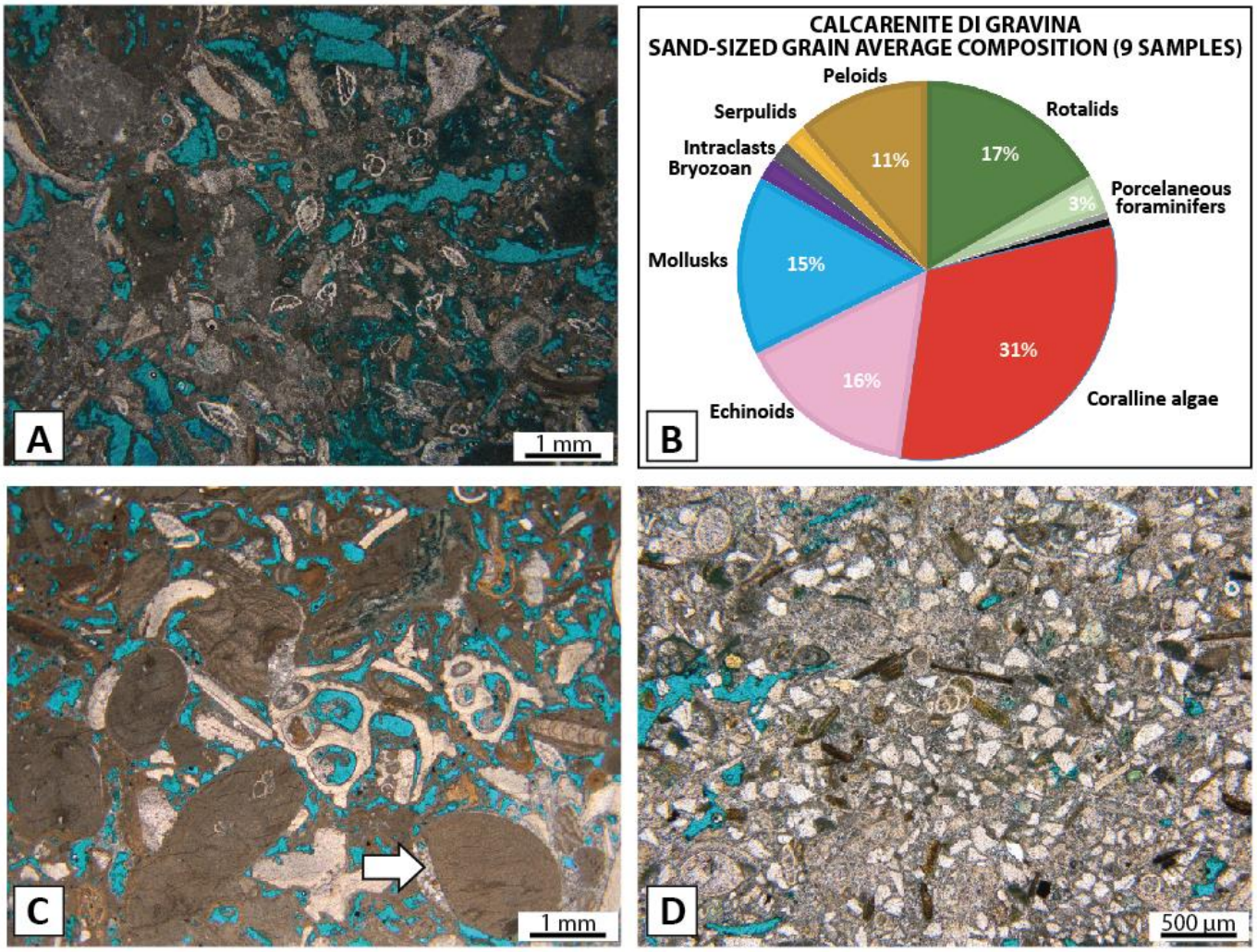

Figure 12: A: Thin-section micro-photographs of an Upper Pliocene to Lower Pleistocene grainstone (Calcarenite di Gravina formation) from the Adriatic Apulian coast (Torre Incine section); **B:** Sand-sized grain average composition of the samples from the Calcarenite di Gravina formation formation analysed in the present work (9 samples). **C:** Thin-section micro-photographs of a coralline algal-molluscan floatstone-rudstone from Middle to Upper Pleistocene terrace deposits of Ionian Apulia (Gallipoli-North section). **D:** tightly cemented quartzose grainstone with coralline algal fragments and benthic foraminifers (microfacies MF2) from Middle to Upper Pleistocene terrace deposits of the Crotone Peninsula, Cape Colonna.

Figure 13

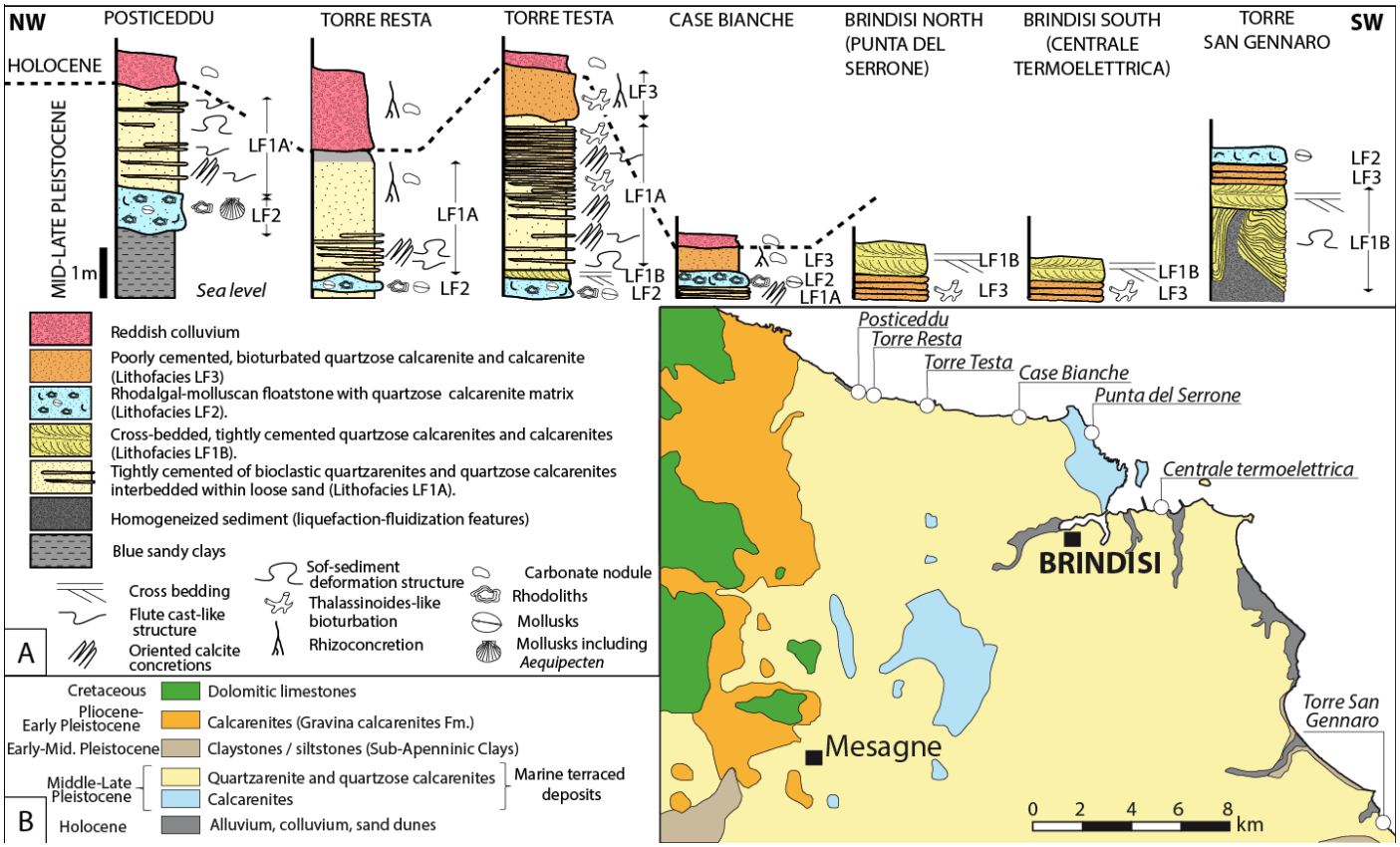

Figure 13: The Brindisi basin: **A:** lithologic and sedimentologic log sections for selected coastal outcrops; **B:** Simplified geological map of the Brindisi basin (modified after Cotecchia, 2014; and Pastore *et al*., 2023).

Figure 14

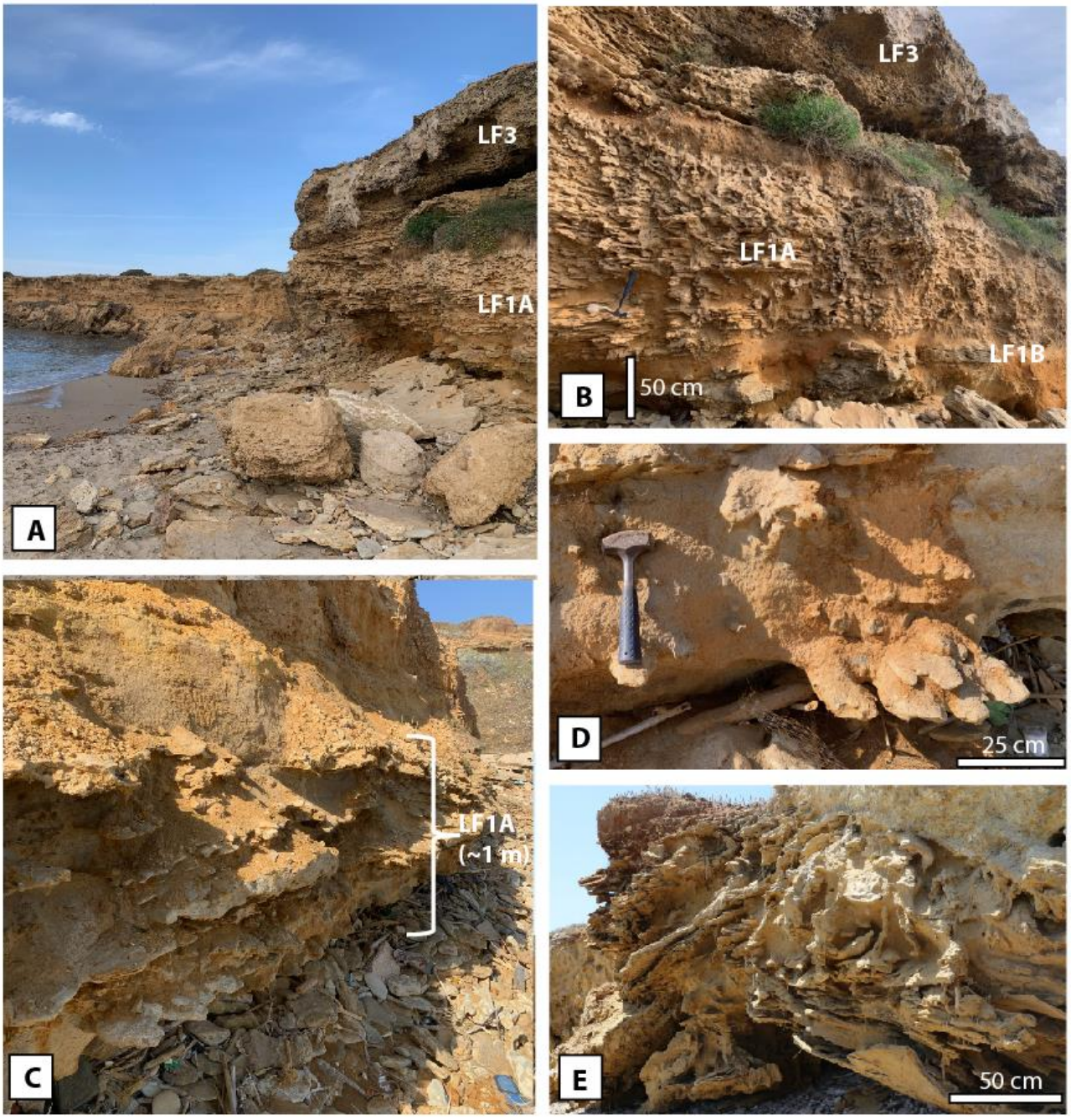

Figure 14: Photographs of coastal outcrops from the Brindisi Basin (see location on Fig.4A). **A:** Torre Testa section showing the vertical succession of lithofacies LF1 (quartzose grainstones and quartzarenites with oriented calcite concretions) and LF3 (massive, weakly cemented quartzose grainstones and grainstones). A mixture of boulders with angular edges (lithofacies LF3) fallen from the top the cliff and rolled pebbles/cobbles (LF1 and LF2 lithofacies dominantly) resulting from the marine erosion of the cliff, lie on the beach and at the foot of the cliff. **B:** closer view of Torre Testa section showing in the lower part of the cliff the oriented calcite concretions within LF1A lithofacies. **C:** Torre Resta cliff showing in its lower part lenses of tightly cemented quartzose grainstones (LF1 lithofacies) embedded within very-fine grained loose sand. **D:** Torre Resta: detail of a cemented quartzose grainstone lens showing elongated, oriented structures (oriented calcite concretions). **E:** Torre San Gennaro: macro-scale soft-sediment deformation structures affecting partly cemented quartzose grainstones (LF1B).

LITHOFACIES	Microfacies				Macro-scale features						
	MF1	MF2	MF3	MF4	flute-cast-like structures	Oriented calcite concretions	soft-sediment deformation features	mollusk accumulations	rhodoliths	bioturbations	cross-bedding
LF1A: Tightly cemented bioclastic quartzarenite and quartzose calcarenite with oriented calcite concretions	X	X			X	X	X			X	
LF1B: Cross-bedded, tightly cemented quartzose calcarenite and calcarenite		X		X			X				X
LF2: Rhodalgal-molluscan floatstone with quartzose calcarenite matrix			X					X	X		
LF3: Poorly cemented, bioturbated quartzose calcarenite and calcarenite		X		X						X	

Table 1: Depositional and diagenetic features of lithofacies LF1, LF2 and LF3

	Ilovik-Parzine ballast stones	Terraced deposits of the Brindisi Basin
Age	Planktic foraminiferal biostratigraphy: Pleistocene (after 1,28 Ma) to Holocene" Sr isotope stratigraphy: younger than 500 ka (Middle Pleistocene to Holocene)	Middle to Late Pleistocene (Ciaranfi et al., 1988; Margiotta et al., 2010; Mastronuzzi et al., 2011)
Lithofacies association	LF1A: Tightly cemented bioclastic quartzarenite and quartzose calcarenite with oriented calcite concretions (80% of the studied ballast) LF2: Rhodalgal-molluscan floatstone with quartzose calcarenite matrix (5% of the studied ballast) LF3: Poorly cemented, bioturbated quartzose calcarenite and calcarenite (11% of the studied ballast) LF4: quartzose calcisistite (<1% of the studied ballast). LF5: conglomerates with quartzose calcarenite matrix (likely to be formed locally) (~1% of the studied ballast). LF6: tight, fractured limestones (Local limestones) (~1% of the studied ballast).	LF1A: Tightly cemented bioclastic quartzarenite and quartzose calcarenite with oriented calcite concretions (Middle to Upper Pleistocene) LF1B: Cross-bedded, tightly cemented quartzose calcarenite and calcarenite (Middle to Upper Pleistocene) LF2: Rhodalgal-molluscan floatstone with quartzose calcarenite matrix (Middle to Upper Pleistocene) LF3: Poorly cemented, bioturbated quartzose calcarenite and calcarenite (Middle to Upper Pleistocene and Holocene)
Sedimentary / diagenetic structures	Bioturbations, elongated-oriented calcite concretions	Bioturbations, cross bedding, elongated-oriented calcite concretions
Macrofauna	Occurrence of *Aequipecten*	Occurrence of *Aequipecten* in Posticeddu section (this study) and San Gennaro (Coppa et al., 2001)
Microfacies (in LF1, LF2 and LF3 lithofacies)	MF1: bioclastic quartzarenite; MF2: bioclastic quartzose grainstone; Microfacies MF3: rhodalgal-molluscan floatstone with quartz-rich bioclastic packstone-grainstone matrix; Microfacies MF4: bioclastic grainstone	MF1: bioclastic quartzarenite; MF2: bioclastic quartzose grainstone; Microfacies MF3: rhodalgal-molluscan floatstone with quartz-rich bioclastic packstone-grainstone matrix; Microfacies MF4: bioclastic grainstone
Morphology of quartz sand	angular to sub-angular	angular to sub-angular
Quartz grain size	very fine to fine-grained (63 to 250 µm) in MF1 and MF3; fine to medium-grained (125 to 500 µm) in MF2; medium to coarse-grained (250 µm to 1 mm) in MF4	Fine to medium-grained (125 to 500 µm) in MF1 and MF2; fine grained (125 to 250 µm) in MF3; medium to coarse-grained (250 µm to 1 mm) in MF4.
Benthic foraminiferal association	Dominated by *Elphidium* (*E. macellum* and *E. paraskevaidisi*) and *Neoconorbina terquemi*.	Dominated by *Elphidium* (*E. macellum* and *E. paraskevaidisi*) and *Neoconorbina terquemi*.
Nature of cement	Equant sparry to microsparry calcite	Equant sparry to microsparry calcite
Carbon and oxygen isotope composition	$\delta^{18}O$: from -5.51 to -3.02‰ $\delta^{13}C$: from -8.93 to -0.95‰	$\delta^{18}O$: from -5.55 to -3.65‰ $\delta^{13}C$: from -8.85 to -1.55‰

Table 2: Comparison of the geological and geochemical characteristics of the Ilovik-Paržine 1 ballast stones with the Pleistocene terraced deposits of the Brindisi Basin.